Carbon dioxide and climate impulse response functions for the computation of greenhouse gas metrics: A multi-model analysis

Fortunat Joos[1,2], Raphael Roth[1,2], Jan S. Fuglestvedt[3], Glen P. Peters[3], Ian G. Enting[4], Werner von Bloh[5], Victor Brovkin[6], Eleanor J. Burke[7], Michael Eby[8], Neil R. Edwards[9], Tobias Friedrich[10], Thomas L. Frölicher[11,1], Paul R. Halloran[7], Philip B. Holden[9], Chris Jones[7], Thomas Kleinen[6], Fred Mackenzie[12], Katsumi Matsumoto[13], Malte Meinshausen[5,14], Gian-Kasper Plattner[1], Andy Reisinger[15], Joachim Segschneider[6], Gary Shaffer[16,17], Marco Steinacher[1,2], Kuno Strassmann[1,2], Katsumasa Tanaka[18], Axel Timmermann[10], Andrew J. Weaver[8]

[1]{Climate and Environmental Physics, Physics Institute, University of Bern, Bern, Switzerland}

[2]{Oeschger Centre for Climate Change Research, University of Bern, Bern, Switzerland}

[3]{ Center for International Climate and Environmental Research – Oslo (CICERO), PO Box 1129 Blindern, 0318 Oslo, Norway}

[4]{ MASCOS, 139 Barry St, The University of Melbourne, Vic 3010, Australia}

[5]{Potsdam-Institute for Climate, Impact Research, Telegraphenberg A31, 14473 Potsdam, Germany}

[6]{Max Planck Institute for Meteorology, Bundesstr. 53, 20146 Hamburg, Germany}

[7]{Met Office Hadley Centre, FitzRoy Road, Exeter, EX1 3PB, UK}

[8]{School of Earth and Ocean Sciences, University of Victoria, Victoria, British Columbia, Canada}

[9]{The Open University, Milton Keynes, United Kingdom}

[10]{International Pacific Research Center, School of Ocean and Earth Science and Technology, University of Hawaii, 1680 East-West Rd. Honolulu, HI, USA}

[11]{AOS Program, Princeton University, Princeton, NJ, USA}

[12]{ Department of Oceanography, School of Ocean and Earth Science and Technology, University of Hawaii, Honolulu, Hawaii, 96822, USA }

[13]{Department of Earth Sciences, University of Minnesota, Minneapolis,, MN, USA}

[14]{School of Earth Sciences, The University of Melbourne, VIC, Australia}

[15]{New Zealand Agricultural Greenhouse Gas Research Centre, Palmerston North 4442, New Zealand}
[16]{Department of Geophysics, University of Concepcion, Chile}
[17]{Niels Bohr Institute, University of Copenhagen, Copenhagen, Denmark}
[18]{Institute for Atmospheric and Climate Science, ETH Zurich, Zurich, Switzerland}

Correspondence to: F. Joos (joos@climate.unibe.ch)

Abstract

The responses of carbon dioxide (CO_2) and other climate variables to an emission pulse of CO_2 into the atmosphere are often used to compute the Global Warming Potential (GWP) and Global Temperature change Potential (GTP), to characterize the response time-scales of Earth System models, and to build reduced-form models. In this carbon cycle-climate model intercomparison project, which spans the full model hierarchy, we quantify responses to emission pulses of different magnitudes injected under different conditions. The CO_2 response shows the known rapid decline in the first few decades followed by a millennium-scale tail. For a 100 Gt-C emission pulse added to a constant CO_2 concentration of 389 ppm, 254±109% is still found in the atmosphere after 1000 years; the ocean has absorbed 6059±128% and the land the remainder (16±14%). The response in global mean surface air temperature is an increase by 0.2019±0.120°C within the first twenty years; thereafter and until year 1000, temperature decreases only slightly, whereas ocean heat content and sea level continue to rise. Our best estimate for the Absolute Global Warming Potential, given by the time-integrated response in CO_2 at year 100 times multiplied by its radiative efficiency, is 92.7×10^{-15} yr W m^{-2} per kg-CO_2. This value very likely (5 to 95% confidence) lies within the range of (70 68 to 1175)$\times10^{-15}$ yr W m^{-2} per kg-CO_2. Estimates for time-integrated response in CO_2 published in the IPCC First, Second, and Fourth Assessment and our multi-model best estimate all agree within 15% during the first 100 years. The integrated CO_2 response, normalized by the pulse size, is lower for pre-industrial conditions, compared to present day, and lower for smaller pulses than larger pulses. In contrast, the response in temperature, sea level and ocean heat content is less sensitive to these choices. Although, -choices in pulse

Formatted: Not Highlight

Formatted: Not Highlight

Formatted: Not Highlight

size, background concentration, and model lead to uncertainties, the most important and subjective choice to determine AGWP of CO_2 and GWP is the time horizon.

1 Introduction

Emissions of different greenhouse gases (GHGs) and other agents that force the climate to change are often compared by simplified metrics in economic frameworks, emission trading and mitigation schemes, and climate policy assessments. The Global Warming Potential (GWP) introduced by the Intergovernmental Panel on Climate Change (IPCC) in 1990 (Shine et al., 1990), is the most widely used emission metric. GWPs are applied for emission reporting under the United Nations Framework Convention on Climate Change (UNFCCC, 2002) and in the emission basket approach of the legally-binding Kyoto Protocol (UNFCCC, 1998) to compare emissions of different GHGs ~~carbon dioxide (CO_2), methane (CH_4), nitrous oxide (N_2O), sulphur hexafluoride (SF_6), hydrofluorocarbons (HCFs) and perfluorocarbons (PFCs)~~ and to compute the so called "CO_2-equivalent" emissions. The initial Kyoto Protocol covered emissions of carbon dioxide (CO_2), methane (CH_4), nitrous oxide (N_2O), sulphur hexafluoride (SF_6), hydrofluorocarbons (HCFs) and perfluorocarbons (PFCs) in the first commitment period (2008-2012). The Doha Amendment to the Kyoto Protocol covers emissions in a second commitment period of 2013-2020 and nitrogen trifluoride (NF_3) is added to the basket of greenhouse gases. The GWP compares the radiative forcing (Forster et al., 2007) integrated over a time period caused by the emission of 1 kg of an agent relative to the integrated forcing caused by the emissions of 1 kg CO_2. As CO_2 is used as a reference gas in the GWP definition, any changes in the computation of the radiative influence of CO_2 affect the GWP of any other agent.

The purpose of this study is to compute the response in atmospheric CO_2, in ocean and land carbon, global mean surface air temperature, ocean heat uptake and sea level change to a pulse-like (i.e., instantaneous) emission of CO_2 into the atmosphere. Best estimates for the mean and the 5 to 95% confidence range are provided for the Absolute Global Warming Potential (AGWP) and the Absolute Global Temperature change Potential (AGTP) introduced by (Shine et al., 2005). We analyse the responses of fifteen carbon cycle-climate models, covering the full model hierarchy, and including two large ensembles of simulations by two of the models constrained with observations as well as an ensemble of runs of a box model substituting for a suite of more complex models. This allows us to address model-related

Formatted: English (U.S.)

Formatted: English (U.S.)

Formatted: English (U.S.)

Formatted: English (U.S.)

Formatted: English (U.S.), Subscript

Formatted: English (U.S.)

Formatted: English (U.S.)

uncertainties by investigating within-model and between-model differences. Uncertainties related to the size of the emission pulse, the atmospheric and climatic background conditions or the choice of the future scenario, and the carbon cycle-climate feedback are assessed in sensitivity simulations. Results are also compared to CO_2 response functions as published in the IPCC First (FAR) (Shine et al., 1990), Second (SAR) (Schimel et al., 1996), and Fourth Assessment Report (AR4) (Forster et al., 2007).

A reevaluation of the CO_2 response appears timely as (i) past GWP calculations applied results from a single model and (ii) the atmospheric and climatic conditions influencing the CO_2 response continue to change with time. The GWP adopted for the first commitment period of the Kyoto protocol (2008-2012) (UNFCCC, 1997, 1998) and used for reporting under the UNFCCC (UNFCCC, 2002) are given by the SAR (Schimel et al., 1996) and based on the CO_2 response of the Bern model (Bern-SAR), an early generation reduced-form carbon cycle model (Joos et al., 1996). Its behaviour was compared to other carbon cycle models in Enting et al. (1994) and it was found to be a middle of the range model. The GWP provided in the AR4 (Forster et al., 2007) relies on the CO_2 response from the Bern2.5CC (here Bern2.5D-LPJ) Earth System Model of Intermediate Complexity (EMIC) (Plattner et al., 2008). More recently, the Conference of the Parties serving as the meeting of the Parties to the Kyoto Protocol decided (UNFCCC, 2011a, b) that the GWP from the AR4 should be used for the second commitment period of the Kyoto Protocol and the Conference also noted in its decision that metrics are still being assessed by IPCC in the context of its Fifth Assessment Report (AR5). A much broader set of models covering the whole model hierarchy from reduced-form models, to EMICs, to comprehensive Earth System Models (ESMs) are now available.

The redistribution of additional CO_2 emissions among the major carbon reservoirs in the Earth System depends on previous emissions and on climate. In addition, radiative forcing of CO_2 depends logarithmically on its own concentration. The response functions are calculated by modelling the response to a pulse emission added to a given concentration and climate state, but these background conditions have changed and will continue to change. For example, the concentration of atmospheric CO_2 continued to increase from 354 ppm in 1990, to 378 ppm at the time of the preparation of the IPCC AR4 report to 389 ppm in 2010 (Conway and Tans, 2012). Such changes in the background concentration cause both the

Formatted: English (U.S.)

radiative forcing and the response function to change, but the changes partially cancel leading to smaller changes in the AGWP (Caldeira and Kasting, 1993;Reisinger et al., 2011).

Additional uncertainties are of a fundamental nature as any metric to compare greenhouse gas emissions represents a crude simplification. Different forcing agents are distinct and have distinct impacts on climate and the Earth system. Differences include different atmospheric perturbation lifetimes ranging from weeks to many millennia, different regional and vertical distributions within the atmosphere and thus different influences on the energy fluxes within the atmosphere and to the Earth's surface, different indirect effects such as confounding impacts on the lifetimes of other GHGs (Prather and Hsu, 2010).

A complication is the complex and regionally and temporally distinct relationship between anthropogenic emissions, atmospheric abundances, radiative forcing, climate change and impacts and damages on socio-economic and natural systems. Other metrics have been proposed in addition to GWP such as global temperature change potential (GTP) (Shine et al., 2005;Fuglestvedt et al., 2010), the integrated temperature change potential (iGTP) (Peters et al., 2011;Azar and Johansson, 2012;Gillett and Matthews, 2010), the TEMPerature proxy index (TEMP) (Tanaka et al., 2009a), global damage potentials (GDP) (Kandlikar, 1995), global cost potentials (GCP) (Tol et al., 2012;Manne and Richels, 2001) and the Cost-Effective Temperature Potential (CETP) (Johansson, 2012). These metrics compare, for equal mass emissions of two GHGs, the global average surface air temperature change at a given point in time (GTP), the relative damages (GDP), or the ratio of the shadow price of a gas to the shadow price of CO_2~~the relative marginal abatement costs for two gases~~ when a given climate change target is achieved at least cost (GCP). TEMP is defined so that it provides a best fit to the temperature ~~projection~~ trajectory of a given period and CETP is based on an approximation of the GCP. Uncertainties generally increase along the cause-effect chain from emissions to impacts (Prather et al., 2009) and there is a trade-off for the selection of metrics between completeness and complexity versus simplicity and transparency, implying ~~and~~ the necessity of subjective judgments (Fuglestvedt et al., 2003;Plattner et al., 2009;Tanaka et al., 2010).

Formatted: Subscript

While the GWP is a proxy for climate impacts, non-climatic effects are not captured by the GWP or similar metrics. Air pollutants, such as ozone, aerosols, nitrogen oxides, carbon monoxide, or volatile organic compounds, influence human health and ecosystems directly. Anthropogenic CO_2 emissions cause not only global warming, but also ocean acidification by

the uptake of excess CO_2 (Orr et al., 2005;Joos et al., 2011;Friedrich et al., 2012) – a threat to coral reefs, marine ecosystems, and related economic sectors (Gattuso et al., 2011).

The different perturbation ~~lifetimes~~ timescales imply that near-term effects of short-lived agents must be compared with the persistent effects of long-lived agents if a metric is to be defined. Attempts involve the restriction to a distinct time horizon for the numerical evaluation of the metric (traditionally 20, 100 or 500 years for GWP) or the application of discounting rates, typically giving little weight to effects in the more distant future. In summary, any metric used to compare emissions of GHGs and other agents involves subjective choices and value judgments and represents a considerable simplification (e.g., (Tanaka et al., 2010;Fuglestvedt et al., 2003;Boucher, 2012).

2 Emission Metrics and Impulse Response Functions

2.1 Global Warming Potential

The Global Warming Potential is based on the time-integrated radiative forcing due to a *pulse* emission of a unit mass of gas at nominal time, $t=0$. It can be given as an Absolute Global Warming Potential for gas x ($AGWP_x$) or as a dimensionless value by dividing the $AGWP_x$ by the AGWP of a reference gas, usually CO_2. The GWP is thus defined as:

$$GWP_x(TH) = \frac{AGWP_x(TH)}{AGWP_{CO_2}(TH)} \qquad (1)$$

and the *AGWP* by:

$$AGWP_x(TH) = \int_0^{TH} RF_x(t)\, dt = \int_0^{TH} A_x \cdot IRF_x(t)\, dt\,, \qquad (2)$$

where $RF_x(t)$ is the radiative forcing at time t caused by the emission pulse released at time t=0. *TH* is the time horizon of choice over which the radiative forcing is integrated. For the GWP used by the UNFCCC and in the Kyoto Protocol, a time horizon *TH* of 100 years is applied, though this choice lacks a scientific basis (Shine et al., 1990).

Forster et al., 2007 ~~(Forster et al., 2007)~~(Table 2.14, page 212) report the GWP of many gases and for different time horizons. A problem related to reporting GWP only is that each update

Formatted: Font: Not Italic

Formatted: Font: Not Italic

Formatted: Font: Not Italic

Formatted: Font: Not Italic

Formatted: English (U.S.)

Formatted: English (U.S.)

Formatted: English (U.S.)

Formatted: English (U.S.)

in $AGWP_{CO2}$ affects the reported GWP values of all other gases. This could be easily avoided by reporting Absolute Global Warming Potentials in addition to GWP.

The radiative forcing, RF_{x}, of gas x can be written as the product of its radiative efficiency, A_{x}, and the perturbation in its abundance or burden, IRF_{x}. A_{x} is defined as the radiative forcing per kg increase in atmospheric ~~abundance~~ burden of gas x. $IRF_{x}(t)$ is the impulse response function (IRF) or Green's function. IRF_{x} represents the time-dependent abundance of gas x caused by the additional emission of one kg of gas x at time 0. In other words, the $IRF_{x}(t)$ is the fraction of the enhancement in concentration due to the added emission pulse ~~additional emission pulse~~ remaining in the atmosphere at time t. For sufficiently small emissions and approximately constant background conditions the radiative efficiency, A_{x}, can be approximated as time-invariant.

The radiative forcing by a perturbation in the atmospheric burden of CO_2, ΔN_{CO2}, relative to a reference burden , $N_{CO2,0}$, is parameterized following (Myhre et al., 1998):

$$RF_{CO2}(\Delta N_{CO2}) = 5.35\ \mathrm{W\ m^{-2}} \ln\left(\frac{N_{CO2,0} + \Delta N_{CO2}}{N_{CO2,0}}\right) . \quad (3)$$

This yields for small perturbations:

$$RF_{CO2}(\Delta CO_2(t)) = 5.35\ \mathrm{W\ m^{-2}} \frac{\Delta N_{CO2}}{N_{CO2,0}} = A_{CO2} \cdot \Delta N_{CO2} \quad \text{for } \Delta N_{CO2} \rightarrow 0 \quad (4)$$

Thus in the limit of a small perturbation, the radiative efficiency of CO_2 is 5.35 W m^{-2} divided by the constant reference burden and is thus itself a constant and time-invariant.

It is convenient to describe the IRF_x by exponential functions (Prather, 2007;Maier-Reimer and Hasselmann, 1987;Aamaas et al., 2012).

$$IRF_x(t) = \sum_{i=0}^{n} a_{x,i} \cdot \exp\left(\frac{-t}{\tau_{x,i}}\right) \quad \text{for } t \geq 0. \quad (5)$$

The unitless coefficients $a_{x,i}$ represent a fraction that is associated with a certain nominal timescale $\tau_{x,i}$ and their sum equals 1. In turn the AGWP for gas x is:

$$AGWP_x(t) = A_x \sum_{i=0}^{n} a_{x,i} \cdot \tau_{x,i} \left(1 - \exp\left(\frac{-TH}{\tau_{x,i}}\right)\right). \quad (6)$$

Formatted: Font: Italic
Formatted: Subscript
Formatted: Do not check spelling or grammar
Formatted: Font: Italic
Formatted: Subscript
Formatted: Subscript
Formatted: Font: Italic
Formatted: Subscript
Formatted: Subscript
Formatted: Lowered by 17 pt
Formatted: Font: Not Italic, Subscript
Formatted: Lowered by 18 pt

~~It is convenient to describe the IRF_x by exponential functions. Many agents, although not CO_2, are removed from the atmosphere with an approximately constant decay rate, 1/τ, and thus their removal can be represented by exponential decay. In this case, the IRF is:~~

$$\cancel{IRF_x(t) = \exp\frac{-t}{\tau_x}, \qquad (3)}$$

~~where τ_x is the mean perturbation lifetime of agent x. Then, the integrated radiative forcing up to TH is given by:~~

$$\cancel{AGWP_x(TH) = A_x \cdot \tau_x \cdot \left(1 - \exp\left(\frac{-TH}{\tau_x}\right)\right). \qquad (4)}$$

AGWP increases with increasing time horizon *TH* to finally approach a constant value for *TH* several times larger than the largest perturbation timescale of gas x~~τ_x~~. The AGWP becomes the product of the ~~mean~~ "steady-state" life time of a perturbation, $\tau_{x,SS}$, (Prather, 2007) and the radiative efficiency, i.e., $AGWP_x = A_x \cdot \tau_{x,SS}$. The steady-state perturbation lifetime is the weighted sum over all timescales ($\tau_{x,SS} = \sum a_{x,i} \cdot \tau_{x,i}$)~~, i.e., $AGWP_x = A_x \cdot \tau_x$~~. This implies that a change in the integration horizon from, for example, 100 years to 1000 years has no impact on the AGWP of gases with up to decadal perturbation ~~life~~timescales~~s~~ such as methane, but AGWP continues to increase~~s~~ with TH for long-lived gases such as CO_2, N_2O, or SF_6. Consequently, the GWP of gases with a short -life time generally decreases with increasing time horizon and the variation in GWP values with time horizon only reflects properties of the reference gas CO_2. For instance, the GWP values for CH_4, ~~(~~which has an adjustment time of approximately 12 years,~~)~~ decrease with increasing time horizon (except for time horizons of a few years only), since GWP is defined with the (increasing) integrated *RF* of CO_2 in the denominator. As *TH* increases past the adjustment time of CH_4, the development in GWP_{CH4} with time horizon is purely controlled by the development in $AGWP_{CO2}$ (Aamaas et al., 2012). For long-lived gases (e.g. N_2O, SF_6) the development in GWP is controlled by both the increasing integrals of the ~~SF_6 and CO_2~~ radiative forcing by the long-lived gas and CO_2. In conclusion, the GWP depends strongly on the behavior of the reference gas and sensitively on the (subjective) choice of the time horizon (see e.g., (Shine, 2009)).

Most GHGs are involved in complex chemical reactions in the atmosphere and are transported within the atmosphere. A local perturbation in one species invokes perturbations elsewhere on a range of timescales and often involving many other species. The chemistry-

Formatted: Font: Symbol

Formatted: Font: Italic

Formatted: Not Superscript/ Subscript

transport system can be linearized and represented with the help of eigenvalue decomposition following Prather, 2007. Then, it becomes clear that the perturbation timescales $\tau_{x,i}$ represent the (negative inverse) eigenvalues characterizing the leading chemical modes of gas x.

CO_2 is, unlike most other agents, not destroyed by chemical reactions in the atmosphere or deposited on the earth surface, but redistributed within the major carbon reservoirs atmosphere, ocean, land biosphere involving multiple timescales for exchange among and for overturning within these reservoirs. A substantial fraction of the initial perturbation by the emission pulse~~s~~ remains ~~airborne~~ in the atmosphere and the ocean for millennia. This fraction is only removed by ocean-sediment interactions and interactions with the weathering and burial cycle of carbon involving timescales from many millennia to hundred thousand years (Archer et al., 2009).

~~The IRF for CO_2 is commonly approximated by a sum of exponentials:~~

$$\cancel{IRF_{CO_2}(t) = \sum_{i=0}^{n} a_i \cdot \exp\left(\frac{-t}{\tau_i}\right) \quad (5)}$$

~~The unitless coefficients a_i represent a fraction that is associated with a certain nominal lifetime τ_i and their sum equals 1. In turn the AGWP for CO_2 is:~~

$$\cancel{AGWP_{CO_2}(t) = A_{CO_2} \sum_{i=0}^{n} a_i \cdot \tau_i \left(1 - \exp\left(\frac{-TH}{\tau_i}\right)\right)}.$$

The continuum of timescales involved in the redistribution of CO_2 can be approximated in practice by a few timescales only. It is usually sufficient to consider three to four terms in the sum in equation (5). ~~Generally~~ Then the coefficients $a_{CO2,i}$ and $\tau_{CO2,i}$ have no direct process-based meaning, but are fitting parameters chosen to represent a given model-based IRF_{CO2}. The IRF of a model is normally computed by calculating the response to a pulse-like perturbation. In our case, the IRF for atmospheric CO_2 is computed within the suite of carbon cycle-climate models by monitoring the simulated decrease of an initial atmospheric CO_2 perturbation due to a pulse-like CO_2 release into the model atmosphere. Similarly, IRFs for surface temperature, ocean heat uptake, sea level rise or any other variable of interest are obtained by monitoring its simulated evolution after the initial perturbation.

The IRFs or Green's functions computed in this study are also useful to characterize the carbon cycle-climate models. The theoretical justification is that IRFs represent a complete characterization of the response of a linear system to an external perturbation. For CO_2, the

Formatted: Subscript

Formatted: Font: Italic, Subscript

value of the IRF at any particular time is the fraction of the initially added carbon which is still found in the atmosphere. In a linear approximation, the change in atmospheric CO_2 inventory at time *t* can be represented as the sum of earlier anthropogenic emissions, *e*, at time *t'* multiplied by the fraction still remaining airborne after time *t-t'*, $IRF_{CO2}(t-t')$:

$$CO_2(t) = \int_{t_0}^{t} e(t') \cdot IRF_{CO_2}(t-t')\, dt' + CO_2(t_0) \ , \qquad (7\cancel{7})$$

where $CO_2(t_0)$ is the atmospheric CO_2 inventory at a time when the system was in (approximate) ~~equilibrium~~steady state. The IRF is thus a first-order approximation how excess anthropogenic carbon is removed from the atmosphere by a particular model.

Non-linearities in the carbon cycle-climate system, however, limit the accuracy of the above equation substantially. The IRF_{CO2} is not an invariant function, but depends on the magnitude of the carbon emissions (Maier-Reimer and Hasselmann, 1987). Non-linearities arise from the non-linearity of the carbonate chemistry in the ocean, from changes in ocean circulation with global warming that affect the surface-to-deep transport of excess anthropogenic CO_2 as well as from other effects such as non-linear dependencies of terrestrial productivity or soil overturning rates on climate and atmospheric CO_2. It has been shown that the atmospheric response, as simulated with a comprehensive model, is better approximated using oceanic and terrestrial impulse response functions that include major non-linearities of the carbon cycle (Joos et al., 1996;Meyer et al., 1999). In conclusion, the IRF and thus also the AGWP for CO_2 depends on the details of the experimental setup (background concentration, pulse size) as well as on the characteristics of the carbon cycle-climate model used for its determination.

2.2 Global Temperature change Potential

The GWP has been critiqued from several angles (e.g,(Shine, 2009;O'Neill, 2000))~~, but~~ and an important critique is that the AGWP does not directly translate into a well-known climate response. The Global Temperature change Potential (GTP) was developed as an alternative (Shine et al., 2005). The Absolute Global Temperature change Potential (AGTP) is the change in global mean surface temperature, ΔT, at time *TH* in response to a pulse emission, *e*, of one unit of agent ~~*x~~x at time *t*=0. It corresponds to $IRF_{T,\cancel{x}x}$, the impulse response of temperature, *T*, to a unit emission of agent ~~*x~~x:

$$AGTP_x(TH) = \frac{\Delta T(TH)}{e_x(t=0)} \,. \qquad (8\cancel{8})$$

The Global Temperature change Potential, GTP_x, is the AGTP of ~~x~~x compared to that of CO_2:

$$GTP_x(TH) = \frac{AGTP_x(TH)}{AGTP_{CO_2}(TH)} \qquad (9\cancel{9})$$

The AGTP is often written as convolution integral of the radiative forcing:

$$AGTP_x(TH) = \int_0^{TH} RF_x(t) \cdot R(TH - t)\, dt \,, \qquad (10\cancel{0})$$

where *R(t)* is the temporally displaced response in *T* to a ~~unit~~ δ-function change in radiative forcing at time t=0. ~~and not to be confused with $IRF_{T,x}$~~x. *R* is influenced by the uncertain properties of the global climate system such as the climate sensitivity, the heat capacity of the lower atmosphere-earth surface system, and by the rate of ocean heat uptake.

Formatted: Font: Symbol

~~While the AGWP is an integrated metric, the AGTP is an instantaneous (end-point) metric.~~ In most previous work (Fuglestevedt et al 2010), the AGTP has been estimated from the convolution of the RF_{x} with R_T (Eq. (10)), where the RF_{x} and R_T often come from different models that are likely not consistent in terms of ocean heat and carbon uptake (for example, the RF_{CO2} is from the Bern-SAR model and the R_T is from HadCM3). It is also possible to estimate $AGTP_{CO2}$ and $IRF_{T,CO2}$ directly from a climate-carbon cycle model in response to a pulse emission. This is done in this study with the suite of carbon-cycle climate models. Apart from the box models, these models feature a consistent treatment of heat and carbon transport. Following similar logic, it is possible to derive similar expressions for the time-integrated GTP, ocean heat content, and sea level rise. Recent research has shown that the GWP and the time-integrated GTP are numerically similar over a range of time horizons, other than for very short lived species like black carbon (Peters et al., 2011;Azar and Johansson, 2012).

3 Model description and experimental setup

An open call was directed to the carbon cycle-climate modelling community to participate in this IRF_{CO2} intercomparison project (Joos et al., 2012). A common protocol defines model setup, ~~and~~ requested simulations (Table 1), and output ~~and~~ and it is given as supporting online information (SI). The procedure corresponds to that for the calculation of the IRF_{CO2} for the IPCC SAR (Enting et al., 1994) and the IPCC AR4. In addition, output was also requested

for the change in global mean surface air temperature as well as ocean heat content, and steric sea level rise. This allows us to derive the impulse response functions for temperature, ocean heat content and steric sea level rise to an emission pulse of CO_2 and correspondingly the AGWP and AGTP for CO_2 and similar metrics for ocean heat content and steric sea level rise.

Results from fifteen models were submitted (Tables 2 and 3) and these are briefly described and referenced in the Appendix A. The models include three comprehensive Earth System Models (~~NCAR CSM1.4,~~ HADGEM2-ES, MPIM-ESM, NCAR CSM1.4), seven Earth System Models of Intermediate Complexity (EMICs), and four box-type models (ACC2, Bern-SAR, MAGICC, TOTEM). Many of these EMICs also participated in three model intercomparsion project~~sed~~ targeted to study the evolution of the climate and the carbon cycle over the historical period (Eby et al., 2012) and under different future scenarios (Zickfeld et al., 2012) and to explore the evolution of the North Atlantic Meridional Overturning Circulation scenarios (Weaver et al., 2012). The EMICs are of varying complexity and include either a 3-dimensional dynamic ocean (Bern3D-LPJ, GENIE, LOVECLIM, MESMO, Uvic-2.9), a 2-dimensional dynamic ocean (Bern2.5D-LPJ, Climber2.4-LPJmL), or a box-type ocean (DCESS). Nine models include a Dynamic Global Vegetation Model (HADGEM2-ES, MPI-ESM, Bern2.5-LPJ, Bern3D-LPJ, Climber2.4-LPJmL, GENIE, LOVECLIM, MESMO, UVic-2.9), one model a spatially-resolved terrestrial carbon cycle with prescribed vegetation distribution (NCAR CSM1.4) and five models (ACC2, Bern-SAR, DCESS, MAGGIC6, TOTEM) a box-type biosphere with a simple logarithmic dependency of NPP on CO_2. Land use and land use changes and their impacts on the carbon cycle and biophysical forcing are explicitly included as internal part of the model in five models (HADGEM2-ES, MPI-ESM, Bern3D-LPJ, GENIE, UVic-2.9). One model (Bern3D-LPJ, ensemble version) also includes a representation of peatlands and permafrost processes and corresponding carbon stocks (Tarnocai et al., 2009). The equilibrium climate sensitivity of the models ranges between 1.5 to 5.7^{o}C for a nominal doubling of atmospheric CO_2. Eight models include an ocean-sediment and weathering/burial module to address long-term (multi-millennial) carbon cycle changes. However, here we restrict the time horizon to 1000 years and do not provide results for the multi-millennial CO_2 evolution. The models used to compute IRF_{CO2} for the SAR (Bern-SAR) and for the AR4 (Bern2.5-LPJ) as used by the UNFCCC are included for traceability of results.

The "standard" setup corresponds to a pulse input of 100 GtC added to a constant background concentration of 389 ppm~~v~~. The emission pulse is equivalent to a mean atmospheric change of 47.10 ppm~~v~~ when using a unit conversion factor of 2.123 GtC/ppm~~v~~ (Enting et al., 1994). Recently, the factor to convert ppm into mol was slightly revised to 0.1765 (±5%) Pmol/ppm (Prather et al., 2012); this yields a conversion factor of 2.120 GtC/ppm (0.1765 Pmol/ppm x 12.01 gC/mol) when assuming that CO_2 is distributed evenly in the atmosphere as done here. For current emissions, the increase in the stratosphere lags the tropospheric increase and a 1 ppm change in the troposphere may corresponds to a mean atmospheric change that is about 1 to 2% lower. In the following these uncertainties of order 2% are neglected. Three simulations are performed to determine the "standard" *IRF* from individual models. An example figure showing results from these three simulations in terms of atmospheric CO_2 can be found in the protocol added in the SI.

Formatted: Font: Not Bold

In run 1, a model is forced with historical concentration up to a reference year (here t_{ref}=2010) and then concentration is kept fixed thereafter at a constant value (here $CO_{2,ref}$=389 ppm). A data file with the reconstructed distribution of atmospheric CO_2 over the period 850 to 2010 AD was distributed to all groups. The model emissions, that are compatible with the prescribed CO_2 evolution, are diagnosed from the simulated change in total carbon inventory (prescribed atmospheric change plus modelled ocean and terrestrial carbon uptake and any imbalance in the weathering/burial cycle).

In run 2, a model is forced with the diagnosed emissions obtained from run 1 with the same model. Run 2 serves for control purposes only and was not provided for the MPI-ESM and NCAR CSM1.4 model as CPU time was lacking. In run 3, the same forcing and setup as in run 2 is applied, but in addition 100 GtC are added instantaneously to the atmosphere five years after the reference year (here in 2015.0). The normalised IRF is then approximately:

$$IRF_{CO2}(t=t_{model}-2015.0) = (CO_2(t_{model})-CO_{2,ref})/(100\ \text{GtC}/2.123\text{GtC/ppm}) \text{ for } t_{model} \geq 2015$$

The general advice in the protocol was to include non-CO_2 forcing and land use area changes to the extent possible. Non-CO_2 forcing as well as land use area are kept constant at 2010 level after 2010. While the total radiative forcing is kept constant in run 1 and 2 after 2010, the climate is evolving freely. The response to a 100 GtC pulse obtained from run 1 to 3 for a present day (PD) background is also termed "PD100" and represents our standard case.

In addition to these standard experiments, groups were also asked to provide results for emissions pulses of 100 GtC (run 5, case PI100) and 5000 GtC (run 6, PI5000) added to a

preindustrial (PI) background. A preindustrial control simulation with constant boundary conditions and freely evolving CO_2 was also requested (run 4). 5000 GtC is of the same order as available conventional (coal, oil, gas) fossil carbon resources and has been used in past pulse experiments (e.g., (Archer et al., 2009;Eby et al., 2009)). This experiment is thus indicative of the long-term consequences for burning all conventional fossil resources. The influence of different background CO_2 concentrations is quantified by comparing the standard run with the 100 GtC pulse added to the preindustrial CO_2 concentration.

Sensitivity simulations with one model (Bern3D-LPJ, see figures in protocol in SI) for PD100 suggest that the simulated response is insensitive to the inclusion of non-CO_2 forcing and whether the emissions pulse is released at the beginning of the year or distributed over one year. On the other hand, the simulated IRF_{CO2} is about 0.02 higher if anthropogenic land use is explicitly included compared to a simulation with natural vegetation only as less carbon is taken up on the converted land.

Three of the participating modeling groups delivered results from an ensemble of simulations. The GENIE group reported results from an ensemble with 69 members where model parameters where varied within uncertainties. The 69-member ensemble was derived from a set of around 1500 simulations combined with a statistical modelling and filtering procedure applying eight preindustrial climatic constraints (Holden et al., 2012). The 69 member ensemble was reduced to 20 members by requiring a plausible present-day CO_2 concentration in an emission–forced simulation over the industrial period and beyond. Here, median and 5% to 95% intervals from these 20 different model setups are reported.

The 69-member ensemble has an ensemble-averaged CO_2 concentration of 404±50ppm (mean±1 sdv) at 2000AD, compared to 370 ppm measured at Mauna Loa. CO_2 is on average lowered to 364±14ppm at 2000 AD in the reduced set. The cases that give the better agreement with observed CO_2 have the larger land uptake through the model's CO_2 fertilization mechanism. Gross primary productivity in GENIE increases by 27±18% (mean±1 sdv) in the full set and by 39±17% in the reduced set for a doubling of the atmospheric CO_2 concentration and considering fertilization only.

The MAGICC model version 6.3 has been run in 171 different parameter settings that emulate 19 AOGCMs and 9 coupled climate-carbon cycle models from the Coupled Model Intercomparison Project Three (CMIP3) and the Coupled Carbon Cycle Climate Model

Intercomparison Project (C4MIP). The application of this model to simulate IRFs has been described in (Reisinger et al., 2010).

The Bern3D-LPJ model was run in 1069 different setups selected from a 5000-member ensemble following a Bayesian approach. Nineteen key model parameters are varied. These are related to terrestrial and ocean carbon and heat exchange, uncertainties in anthropogenic radiative forcing, and the transient and equilibrium climate sensitivity of the model. The 5000 member ensemble is constrained by a large set of observation-based data including estimates for surface air temperature change, ocean heat uptake, atmospheric CO_2 change and ocean and land carbon uptake rates, seven physical and biogeochemical 3-d ocean tracer fields, and land carbon stocks and fluxes.

Additional sensitivity simulations were carried out with the standard setup of the Bern3D-LPJ model. These include a series of runs with emission pulses ranging from 10 to 10,000 GtC added to a preindustrial background. These simulations are used to demonstrate the dependency of the *IRF* on the magnitude of emissions. The model was also run in a mode where climate was kept constant for emission pulses of 100 and 5000 GtC. These simulations allow us to quantify the impact of carbon-cycle climate feedbacks on the IRF_{CO2} within the Bern3D-LPJ model.

The pulse size of 100 GtC applied in the standard simulation (run 3) is larger than the pulse size of 10 GtC applied to determine the IRF_{CO2} in the Bern-SAR model for the SAR and the pulse of 40 GtC applied in the Bern2.5D-LPJ for the AR4. The choice of the larger pulse size is to improve signal-to-noise ratio in the simulated response. The simple Bern-SAR model does not feature any internal variability and so a small pulse size still permits us to compute its response reliably. In contrast, the Bern2.5d-LPJ used in the AR4 and even more the ESM used in this study feature considerable internal variability in atmospheric CO_2 and climate that would mask the response to a small emission pulse.

Model output was smoothed to remove short-term variability using a spline-fit method (Enting, 1987). A cut-off period is chosen as input parameter to the spline routine such that the amplitude of a sine wave with this period is attenuated by 50%. ~~Results from the control simulations from the models with a dynamic atmosphere (NCAR-CSM1.4, HadGEM2-ES, MPIM-ESM, and LOVECLIM) are smoothed with a cut-off period of 30 years during nominal year 0 to 30 after the pulse emission; afterwards a cut-off period of 200 years was applied. This choice of cut-off periods yields the removal of interannual-to-decadal~~

~~variability, while still following the initial adjustment of the system after the trend in atmospheric CO_2 is abruptly changed five years before the emission pulse release in year 2010. Smoothing was not applied for the control runs of the other models.~~ The results from run 3 are subtracted from the ~~(smoothed)~~ control run (run 2; run 1 for MPIM-ESM and NCAR CSM1.4). The resulting response is smoothed using cut-off periods of 4, 20, 50, 250, and 500 years for the periods from year 0 to 10, from year 10 to 50, from year 50 to 100, from year 100 to 300 and year 300 to 1000, respectively. The response of all models to the 100 GtC pulse added to a 389 ppm background was smoothed in this way for consistency. This treatment has virtually no effect on results from box-models and from EMICs with small or absent internal variability and on the integrated IRF_{CO2} that is used to compute the AGWP and GWP.

The multi-model mean IRF_{CO2} and responses in other quantities are fitted by a sum of exponentials:

$$IRF_{CO2}(t) = a_0 + \sum_{i=1}^{3} a_i \cdot \exp\left(\frac{-t}{\tau_i}\right) \qquad \text{for } 0 \le t \le 1000 \text{ years} \qquad (11)$$

For IRF_{CO2} the conditions is applied that the sum of the coefficients a_i equals 1 and for the other variables that the sum equals zero. We suggest to use numerical values as obtained by these fits for the multi-model mean in future studies. Note that the fits only apply for the period from 0 to 1000 year. We use the values from the fit as our best estimates.

The responses as simulated by individual models were also fitted using equation 11. The coefficients (a_i, τ_i) are tabulated in the supplementary information for all models and for the responses in CO_2. Results of the fits are compared with the model output in a complementary figure in the supplementary information.

4 Results

4.1 Impulse Response Functions and Absolute Global Warming Potentials for CO_2

The evolution of the IRF_{CO2} (Figure 1a) shows a rapid decrease in the first few years after the emission pulse and then a continued but slow decline. It reaches a fraction of 0.60±0.14 (±two sdv) at year 20 and 0.41±0.13 at year hundred. In other words, while 40% of the initial

atmospheric CO_2 perturbation is on model-average removed from the atmosphere within 20 years, it takes additional 80 years to mitigate the next 19% of the perturbation. At year 1000, more than 25~~4~~% (± 9~~10~~%) of the perturbation is still airborne. This evolution is consistent with earlier model results (Maier-Reimer and Hasselmann, 1987;Cao et al., 2009;Siegenthaler and Joos, 1992;Sarmiento et al., 1992;Enting et al., 1994;Archer et al., 2009;Eby et al., 2009). It is also consistent with our understanding of the carbon cycle as two-way transfers of carbon between reservoirs with different timescales (Prentice et al., 2001;Denman et al., 2007;Oeschger et al., 1975;Broecker et al., 1980).

The time-integrated IRF_{CO2} (Figure 1b), and thus $AGWP_{CO2}$, increases continuously with time and there is no sign of approaching ~~an equilibrium~~a steady state value at year 1000. The time-integrated IRF_{CO2} for the individual models is tabulated in Table 4. The multi-model mean increases from 14.3±1.8 years (mean±2 sdv) ~~–~~at year 20, to 30.2±5.6~~7~~ at year 50, to 52.4±11.3~~7~~ at year 100, to 185.6±48~~7~~ at year 500, and to 308±94~~5~~ at year 1000.

The multi-model mean IRF_{CO2} over the first 1000 years is fitted by a sum of exponentials and ~~and the conditions that the sum of the coefficients a_i equals 1:~~

$$\cancel{IRF_{CO2}(t) = a_0 + \sum_{i=1}^{3} a_i \cdot \exp\left(\frac{-t}{\tau_i}\right) \qquad \text{for } 0 \le t \le 1000 \text{ years} \qquad (11)}$$

t~~T~~he coefficients for IRF_{CO2} and for other responses are ~~-~~given in Table 5 ~~a_0 = 0.21787, a_1 = 0.22896 , a_2 = 0.28454, a_3 = 0.26863 and the time scales τ_1= 381.33 yr, τ_2= 34.785 yr, and τ_3= 4.1237 yr~~. We note that the time-integrated IRF_{CO2} as calculated with this fit is the same for a time horizon of 100 years and slightly different for the time horizons of 20, 50, 500, and 1000 years than those given in T~~t~~able 4. (the values from the fit are: 14.2 yr, 30.3 yr, 52.4 yr, 184 yr, 310 yr). We use these values from the fit as our best estimates in Table 4.

Uncertainty ranges across models and from model ensembles: There are uncertainties in the IRF_{CO2} and the $AGWP_{CO2}$. The range in integrated IRF_{CO2} across all models is 40~~5~~ to 65~~7~~ years at year hundred. This is comparable to the 5-95% interval ranging from 40 to 64 years for the MAGICC6 ensemble that emulates a number of carbon-climate models. The 5-95% confidence interval for the Bern3D-LPJ ensemble, constrained with a broad set of observations, is 49 to 65 years at year 100 and somewhat smaller than the model range. The ensemble interval from the GENIE model is larger than the other ranges at year 100; the time-dependence of this ensemble was constrained only by preindustrial to modern CO_2 change. At

Formatted: Font color: Yellow

Formatted: Font color: Auto

Formatted: Font: Italic

year 20 and 50, the situation with regard to uncertainties ranges is qualitatively similar as for year 100. However, the 5-95% confidence range for the MAGICC6 ensemble is smaller than the range across all models at year 500, whereas the width of the confidence range is larger than that of the model range for the observation-constrained Bern3D-LPJ and GENIE ensembles. This may suggest that observational-constraints as applied in the Bern3D-LPJ narrow the uncertainty range for a time horizon of up to 100 years.

An alternative, linear programming approach: An alternative approach is to constrain the uncertainty in IRF_{CO2} by assuming a linear carbon system and constraining the IRF_{CO2} with estimates of the 20th century airborne fraction of CO_2. If we consider the uncertainty in the integrated response, then clearly if IRF_{CO2} lies between 0 and 1, the integral to time *TH* will lie between 0 and *TH*, regardless of the form of the function IRF_{CO2}. However not all functions have physically reasonable behaviour and not all functions will be consistent with the 20th century pattern of emissions and concentrations. Including such considerations can narrow the range of possible values of the integrated response. Finding the maximum and minimum possible values of the integral (and the functions that give these extrema) is a problem in mathematical optimisation that can be analysed using the calculus of variations. If the constraints are linear, then the discretised form of the optimisation can be expressed as a problem in linear programming for which well-established computational techniques are available (Press et al., 1986). Such an approach to analysing the carbon cycle response was introduced earlier (Enting and Mansbridge, 1987).

For the present study we consider functions with $IRF_{CO2}(t=0) = 1$, $IRF_{CO2}(t) \geq 0$, $d/dt\, IRF_{CO2}(t) \leq 0$, and $d^2/dt^2\, IRF_{CO2}(t) \geq 0$, and which give behavior consistent with observations for the 20th century. This last condition is expressed in terms of the 20th century cumulative airborne fraction γ. If we take γ as known precisely then we find that for *TH* =100, the integrated response is constrained to lie in the range 39.7 to 52.4 years. The implication is that regardless of the model structure, no linear model that exhibits the dissipative behaviour expressed by the constraints on the derivatives, can have an integrated response that lies outside this range. This range of 13 years is thus an upper bound on the amount of uncertainty that can arise from differences in model structure (and termed "structural uncertainty" (Enting et al., 2012)).

If, however, it is acknowledged that the 20th century cumulative airborne fraction is not known precisely, mainly because of uncertainties in land-use emissions (Stocker et al., 2011), then a wider class of response functions and a wider range of integrals is possible.

Formatted: Superscript

Constraining the airborne fraction to lie in the range 0.5±0.05 gives the range 33.6 to 57.6 years -for possible values of the integral for *TH*=100. This expanded range of uncertainty is a combination of the "structural uncertainty" described above, and a "calibration uncertainty" arising from uncertainties in the calibration data (Enting et al., 2012).

Since we are primarily concerned with the range rather than the specific value, the 20th century constraint has been approximated in terms of carbon emissions that grew exponentially over 150 years with a time–scale of 50 years (emissions are proportional to exp(*t*/(50 years))). This is a truncation of the expression for the airborne fraction in terms of the Laplace transform of the response (Enting, 1990). In principle, the same approach can be used for *TH*=20 years but because the 20 year time-scale is less representative of 20th century changes, the "calibration" constraint does little to constrain the range of uncertainty for the integral.

5-95% confidence range: In conclusion, different approaches to estimate the uncertainty in the integrated IRF_{CO2} for a time horizon of 100 years yield comparable results. Taken together, these approaches yield an average uncertainty range of 26 years or of 49% for the 100-yr integrated response (Table 4). We assume that this average range represents approximately a 5-95% confidence range and that it is symmetrically distributed around the multi-model mean to arrive at our best estimates for the mean and 5-95% confidence range for the time-integrated IRF_{CO2}.

The MAGICC and Bern3D-LPJ ensemble ranges are roughly symmetrically distributed around the median for time horizons of 20, 50, and 100 years and skewed, but in different directions, for 500 year. These results tend to support the assumption that the uncertainty range is symmetric around the best estimate, though the ensemble range from the GENIE model is skewed towards high values.

Absolute Global Warming Potential: Multiplying the time-integrated IRF_{CO2} with the radiative efficiency of CO_2, A_{CO2}, yields the Absolute Global Warming Potential, $AGWP_{CO2}$. Here, A_{CO2} is computed for an atmospheric background of 389 ppm and in the limit of a small perturbation by using the derivative of the simplified radiative forcing expression of (Myhre et al., 1998) (Equation (3) and (4) and converting ppm into kg- CO_2): A_{CO2} =5.35 W m^{-2} (389 ppm)$^{-1}$ × (2.123×10^{12} kg-C/ppm)$^{-1}$ × (12 kg-C / 44 kg-CO_2) = 1.77 10^{-15} W m^{-2} kg-CO_2^{-1}.

The uncertainty in the radiative efficiency of CO_2 is given as ±10% in the IPCC TAR and AR4 (90% confidence interval; see page 140 of (Forster et al., 2007)) and guided by the

Formatted: Font: Italic

Formatted: Font: Italic

spread in published estimates. An uncertainty of ±10% translates to an uncertainty range of 20%. The overall uncertainty in $AGWP_{CO2}$ is ~~insignificantly~~ only slightly larger than that for IRF_{CO2} as the uncertainty in A_{CO2} is much smaller than that of the time integrated IRF_{CO2}. Assuming quadratic error propagation, the uncertainty range in $AGWP_{CO2}$(TH=100 yr) ~~would be~~is 53~~0~~% (~~sqrt~~ √(0.49^2+0.2~~1~~^{2})=0.53~~0~~) compared to 49% of the integrated IRF_{CO2} (Table 4). ~~Here, we use the same relative uncertainty for $AGWP_{CO2}$ and IRF_{CO2}.~~ Our best estimate for the $AGWP_{CO2}$ is a mean value of 92.5~~7~~ × 10^{-15} yr W m^{-2} kg-CO_2^{-1} and a 5-95% confidence range of (68~~70.1~~ to 117~~5~~) × 10^{-15} yr W m^{-2} kg-CO_2^{-1} for a time horizon of 100 years. In IPCC uncertainty language (Solomon et al., 2007), it is very likely that the $AGWP_{CO2}$ for a time horizon of 100 years is within a range of (~~70~~ 68 to 117~~5~~) × 10^{-15} yr W m^{-2} kg-CO_2^{-1}.

4.2 Response in surface air temperature and AGTP, ocean heat uptake and steric sea level rise

The response in radiative forcing to the 100 GtC pulse (equivalent to 47.1 ppm) corresponds to a step increase by 0.61 W m^{-2} at year 0, followed by a decrease to 0.26 W m^{-2} at year 100 and to 0.16 W m^{-2} at year 1000. ~~as~~ These values are computed from the multi-model mean IRF_{CO2} with the help of ~~–~~equation (3) and for a reference mixing ratio of 389 ppm ($RF(t)$=5.35 W m^{-2} ln((389 ppm + $IRF_{CO2}(t)$ × 47.1 ppm)/389 ppm)). ~~(Myhre et al., 1998) corresponds to a step increase by 0.61 W m^{-2} at year 0, followed by a decrease to 0.26 W m^{-2} at year 100 and to 0.15 W m^{-2} at year 1000.~~ What magnitude in the SAT response is to be expected from this forcing? The equilibrium response in global mean surface air temperature (SAT) to these forcing values are 0.49^{o}C (year 0), 0.21~~2~~^{o}C (year 100) and 0.13~~2~~^{o}C (year 1000) ~~and~~ when assuming for illustrative purposes a typical mid-range climate sensitivity of 3°C for a nominal doubling of CO_2.

The multi-model mean response in SAT to the 100 GtC pulse emission (Figure 2a, Tables 6 and 7~~5~~) is an increase by 0.20~~19~~±0.12~~0~~^{o}C within the first 20 years. Afterwards, SAT remains almost constant until year 100. This evolution is a consequence of the delayed response in SAT to the initial increase in radiative forcing as it takes time to heat the surface layers of the ocean with its large heat capacity and heat exchange with the deep ocean. After year 100, SAT is generally closer to ~~equilibrium~~ steady state with the simulated radiative forcing and decreases slowly to 0.14±0.08~~9~~^{o}C by year 1000. Our best estimates for the mean and 5 to 95% uncertainty ranges in SAT changes and AGTP for CO_2 are tabulated for a range of time horizons in Table 6~~5~~. For a time horizon of 100 years, AGTP of CO_2 is 0.49~~46~~×10^{-15} ^{o}C per

kg-CO_2 and the estimated 5 to 95% confidence range is (0.~~22~~ 05 to 0.~~74~~92)×10^{-15} °C per kg-CO_2.

(Fuglestvedt et al., 2010) applied the analytical response functions for CO_2 as given in the AR4 and the analytical response function for temperature to a change in radiative forcing (*R*) by (Boucher and Reddy, 2008) to estimate $AGTP_{CO2}$ to 0.68, 0.58 and 0.51×10^{-15} °C per kg-CO_2 for time horizons of 20, 100, and 500 years respectively. These values are higher than our best estimates of 0.55~~2~~, 0.55~~46~~ and 0.38×10^{-15} °C per kg-CO_2, but well within the 5 to 95% confidence range (Table 6~~5~~). The different values are explained by the difference in temperature responses and less due to the differences in IRF_{CO2}.

The response in SAT is fairly smooth in most EMICs and box models and the response in SAT is well defined in these models. However, the models that feature a dynamic atmosphere (HadGEM2-ES, MPI-ESM, NCAR CSM1.4, LOVECLIM) show strong interannual-to-decadal variability in SAT of several tenths of a degree Celsius both in the control and in the pulse simulation. We note that the three Earth System Models were run over the first 100 years only. This internal variability of the more comprehensive models makes the extraction of the response in SAT challenging for these models and a well-defined separation of the forced response from the models' internal variability is not achieved when relying on single simulations. For example HadGEM2-ES shows a positive variation in annual SAT values of several tenths of a degree Celsius towards the end of the simulation in the standard pulse experiment. This yields a difference in SAT of about 0.4~~3~~°C between the smoothed HadGEM2-ES response and the multi-model mean response near year 100 (Figure 2). This indicates that it is difficult to extract the temperature response for use in GTP from comprehensive models when they are forced with a pulse of modest size as applied here. Excluding the four models with dynamic atmosphere from the averaging has a relatively small effect on the multi-model mean SAT and deviations are well within the uncertainty range.

The response in ocean heat content (OHC) and steric sea level rise (SSLR) is ~~of~~ on multi-century ~~type~~ timescales (Figure 2b,c, Table 8~~6~~). The responses in these quantities are in general much smoother than for SAT as they mainly reflect the time-integrated, cumulative perturbation in air-sea heat fluxes. Multi-model SSLR is 1.8~~7~~ ±1.7 cm (±2 sdv) at year 100 and 4.6±6.1~~0~~ cm at year 1000 in response to the 100 GtC pulse. The median in SSLR

Formatted: English (U.S.)
Formatted: English (U.S.)
Formatted: English (U.S.)
Formatted: English (U.S.)
Formatted: Font: Italic, English (U.S.)
Formatted: English (U.S.)

response in the Bern3D-LPJ ensemble is close to the multi-model mean at year 100, while the 5 to 95% confidence interval ranges from 0.7 to 2.8 cm and is thus smaller than the multi-model range.

The multi-model response in OHC for the 100 GtC pulse reaches 15~~4~~±13~~1~~×10^{22} J by year 100 and 40±41×10^{22} J by year 1000. The upper and lower extreme cases in the multi-model ensemble are the ESMs: the MPIM and NCAR CSM1.4 on the low side and the HadGEM2-ES on the high side. This indicates that the responses in globally aggregated values do not depend on the type of model, e.g., ESM versus EMIC. The 5 to 95% interval in OHC of the MAGICC ensemble and of the observation-constrained Bern3D-LPJ ensemble is smaller at year 100 and comparable to the model range at year 500.

In conclusion, AGTP of CO_2 varies much less than AGWP for time horizons between 20 and 1000 years. However, relative uncertainties (e.g., in percent of the mean value) in the estimates of AGTP are much larger than those for AGWP, as also inferred with a box model ensemble by (Reisinger et al., 2010), and relative uncertainties in the response in ocean heat content and steric sea level rise are also larger than for AGTP.

4.3 Response in ocean and land carbon

The carbon that is removed from the atmosphere is taken up by the ocean and the land biosphere (Figure 3). In the first decade, both the ocean and the land contribute substantially to removing the atmospheric carbon perturbation. Land and ocean absorb on multi-model mean close to 20 GtC during the first 20 years after the emission. The ocean continues to absorb carbon from the atmosphere and the multi-model perturbation in the ocean carbon inventory is ~~19~~20±7~~8~~ GtC by year 20, 33~~2~~±12~~5~~ GtC by year 100 and 59~~60~~±12~~8~~ GtC by year 1000. In other words, ~~60~~59% of the emission pulse (multi-model average) has been transferred to the ocean by year 1000 (Figure 3a)

In contrast, the land perturbation remains fairly constant after a few decades up to year 100 and decreases thereafter in most models. On multi-model average, the land has sequestered 19~~8~~±16 GtC by year 20, 23~~2~~±20~~1~~ GtC by year 100 and 16~~7~~±14~~8~~ GtC by year 1000. It is interesting to note that the three ensembles include also cases where the land loses carbon to the atmosphere in response to the 100 GtC emission pulse (Figure 3b). In these model realizations, the climate change resulting from an emission pulse forces a carbon loss from land ecosystems that is larger than the positive impacts of elevated atmospheric CO_2. This

loss is likely predominantly driven by accelerated turnover of soil and litter carbon in response to warming (Joos et al., 2001).

The response in ocean carbon inventory to an emission pulse is relatively well understood. Ocean uptake is mainly driven by physico-chemical processes and uptake rates are governed by the quantitatively well-understood carbonate chemistry in surface waters and by the rates of surface-to-deep transport. The latter are constrained by the distribution of transient tracers such as CFCs and bomb-produced radiocarbon in the thermocline (Key et al., 2004). In early generation carbon cycle models such as the Bern-SAR model only these physico-chemical processes were included. This first-order response is modified by other processes such as ocean warming and changes in ocean circulation and marine biogeochemistry (Plattner et al., 2001;Sarmiento et al., 1998;Joos et al., 1999).

The response of the land biosphere carbon inventory is associated with considerable uncertainties. It is currently not clear whether the land will continue to act as a strong carbon sink or whether climate change will lead to a loss of land carbon that overwhelms the potentially positive influence of elevated atmospheric CO_2 and nitrogen input on net primary productivity and carbon stocks. This limited understanding is reflected in the large uncertainty range. We estimate the 5 to 95% confidence range for the response in land carbon inventory to 45 GtC at year 100. For comparison, the corresponding uncertainty range for the ocean inventory is 29 GtC.

In conclusion, carbon uptake by the land biosphere is about equally important for the evolution of IRF_{CO2} as uptake by the ocean during the first two decades after the release. Subsequently, the ocean becomes the dominant carbon sink. The uncertainty range of the terrestrial and oceanic carbon inventories remain substantial over the 1000 year analysis period.

Formatted: English (U.S.)

4.4 Influence of background conditions, pulse size, and carbon cycle-climate feedback

4.4.1 Background conditions

The response in atmospheric CO_2 and cumulative air-to-sea and air-to-land carbon fluxes depends sensitively on the background conditions (Figure 4). Ten out of fifteen models were also used to run the simulations where a 100 GtC emission pulse is added to preindustrial (PI) in addition to present day (PD) conditions. For these models, the time integrated IRF_{CO2} at year 100 ranges between 34 and 47 years for the PI100 case and between 45 and 62 years for the PD100 case. The lower CO_2 perturbation for PI100 is generally due to a higher uptake by both the ocean and the land biosphere and is consistently lower for PI than PD conditions for all individual models.

The responses in SAT, OHC, and SSLR are similar for PI100 and PD100. This is due to two compensating effects (Caldeira and Kasting, 1993;Wuebbles et al., 1995;Reisinger et al., 2011). The time-integrated CO_2 response decreases by roughly 23~~5~~% from PD to PI conditions. On the other hand, the radiative forcing per unit change in atmospheric CO_2 increases by 39% from PD to PI conditions. The range in time-integrated forcing at year 100 is then almost identical (32~~0~~ to 43~~2~~ yr W m^{-2} for PI100 versus 29 to 40 yr W m^{-2} for PD100).

The ocean uptake capacity regulated by the carbonate chemistry decreases with increasing CO_2 and warmer climate conditions are generally associated with a lower solubility of CO_2 and a more sluggish surface-to-deep transport (Joos et al., 1999;Roy et al., 2011). As expected, the model range in cumulative air-to-sea flux is smaller for PD (24 to 40 GtC) than for PI (32 to 47 GtC) conditions and at year 100. The ocean carbon uptake is consistently lower for PD than PI conditions in all models during the first hundred years. In the long-run, the time-integrated ocean uptake becomes larger for PD100 than PI100 in the Bern3D-LPJ model. This is likely related to the large difference in the land carbon responses (~26~~7~~ GtC at year 500) between the PI100 and PD100 cases in this model.

The land carbon uptake in the model depends on factors such as the spatio-temporal evolution of net primary productivity (NPP) under changing CO_2 and climate and the change in soil and litter carbon turnover rates with changing climate conditions. It is beyond the scope of this paper to discuss the processes affecting land carbon stocks in detail for the range of models.~~.~~ The response in land carbon inventory to changes in CO_2 and climate is complex and

regionally distinct. Generally, the models react with an increase in NPP to increasing atmospheric CO_2. Temperature and precipitation changes can have both positive and negative effects on NPP, while most models assume that soil and litter turnover rates increase approximately exponentially with increasing temperatures.

The response in land carbon inventory at year 100 ranges between 21~~2~~ and 36~~5~~ GtC for PI100 compared to 10 to 42 GtC for PD100. The model spread is thus considerably smaller for the PI100 than for the PD100 case. The response is not consistent among models. LOVECLIM shows a higher land carbon uptake under PD than PI conditions, NCAR CSM1.4 and DCESS show similar changes, whereas most models simulate a reduced land uptake for PD100 compared to PI100.

The response for temporally varying background conditions is in addition explored with one model (Bern3D-LPJ) for illustrative purposes. Emissions of CO_2 and non-CO_2 agents are prescribed to follow those from the Representative Concentration Pathways RCP2.6, RCP4.5, RCP6.0 and RCP8.5 in the control setup. The same procedure was applied to determine the IRF as in the standard setup. However, forcing (CO_2, non-CO_2, aerosoles,landuse area) was extended based on the RCPs until year 2300 as described in (Zickfeld et al., 2012). After year 2300, the forcing is extended until year 3010 by using 2300 values. The pulse was released in year 2010 instead of 2015 as in the 389 ppm background scenario. The evolution of IRF_{CO2} (Figure 5a) is relatively similar between the standard case (389 ppm background) and RCP2.6, but very different for the three other RCP cases. IRF_{CO2} decreases in all cases to about 70% in the first two decades after the pulse. Then, it continues to decrease for the standard and the RCP2.6 cases, whereas IRF_{CO2} increases again in the other cases as atmospheric CO_2 and global warming continues to rise in these scenarios. For RCP8.5, the pulse fraction remaining airborne is still well above 80% at year 1000. The time-integrated IRF_{CO2} evaluated at year 100 is 62 years for the 389 ppm background and 66, 68, 69 and 75 years for RCP2.6, RCP4.5, RCP6.0, and RCP8.5, respectively. The resulting perturbation in radiative forcing is evaluated as difference in forcing between the control without pulse and the corresponding pulse run and using the non-linear equation (3). AGWP range between 105 and 85 × 10^{-15} yr W m^{-2} kg-CO_2^{-1} for the five cases and at year 100. The RCP8.5 case, although featuring the largest time-integrated IRF_{CO2}, has the smallest AGWP of the five cases as the radiative efficiency decreases with higher CO_2 concentration.

Formatted: Indent: Hanging: 0.02 cm
Formatted: English (U.S.)
Formatted: English (U.S.)
Formatted: English (U.S.), Subscript
Formatted: English (U.S.)
Formatted: English (U.S.), Subscript
Formatted: English (U.S.)
Formatted: English (U.S.)
Formatted: Font: Italic
Formatted: Font: Italic
Formatted: Font: Italic
Formatted: Font: Italic
Formatted: English (U.S.)

4.4.2 Pulse size

We next turn to the case where 5000 GtC were released into the atmosphere (PI5000) (Figure 6~~5~~). The 5000 GtC pulse run was carried out with 10 models. With this higher input, a considerably greater proportion of CO_2 remains in the atmosphere, compared to the release of 100 GtC (PI100). For the PI5000 simulation, the integral of IRF_{CO2} through to year 100 is about double that from the PI100 simulation. In other words, the time integrated IRF_{CO2} depends sensitively on the pulse size. In particular the ocean uptake of carbon per unit carbon emitted is substantially smaller for the PI5000 than PI100 case.

As for pulse sizes of 100 GtC, the SAT increases rapidly within the first two decades after the pulse and remains high for the centuries to follow, while ocean heat content and steric sea level rise increase more gradually. The simulated SAT at year 100 per unit carbon emission is roughly 40% smaller in the PI5000 than the PI100 case (0.05~~2.6~~ to ~~8.6~~1.7 °C versus ~~4~~ 0.08 to 0.3~~15~~°C per ~~50~~100 GtC). Similarly, the responses in ocean heat content and steric sea level rise are smaller per unit emission for the larger pulse. This smaller climate response per unit emission is a consequence of the smaller time-integrated forcing per unit emissions for larger pulses. The time-integrated radiative forcing at year 100 is smaller by 39% for PI5000 than for PI100. The decrease in radiative efficiency (Equation 3) more than compensates for the larger time-integrated IRF_{CO2} in PI5000 than PI100.

Next, the influence of the pulse size on the Absolute Global Warming Potential of CO_2 at year 100 is investigated in more detail (Figure 5b). Specifically, we ask how representative is the $AGWP_{CO2}$ as determined with a pulse input of 100 GtC in our standard setup for the limiting case of an infinitely small pulse. The pulse size was varied between 1 GtC and 5000 GtC in the Bern3D-LPJ both for constant background conditions of 389 ppm as well as for the RCP6.0 case. $AGWP_{CO2}(t=100\text{ yr})$ is plotted versus pulse size in Figure 5b. A polynomial fit through the data points yields a continuous relationship between pulse size and AGWP over the range from 0 to 5000 GtC. The results show that $AGWP_{CO2}(t=100\text{ yr})$ for an infinitely small pulse is only about 1.2% higher than for a pulse size of 100 GtC. Results also show that internal climate variability affect the computed $AGWP_{CO2}$ significantly for small pulses of a few GtC only in the Bern3D-LPX. This is evidenced by the scatter in results for small pulses. In conclusion, the $AGWP_{CO2}$ values tabulated in Table 4 are a good approximation for the limiting case of infinitely small carbon additions or removals to the atmosphere.

Formatted: Not Highlight

Formatted: Font: Italic

Formatted: Font color: Auto, Not Highlight

Formatted: Font color: Auto

Formatted: Not Highlight

~~4.4.2~~ 4.4.3 Carbon Cycle-Climate Feedbacks

The influence of the carbon cycle-climate feedbacks is investigated with the Bern3D-LPJ model for emission pulses of 100 and 5000 GtC added to preindustrial conditions (Figure 7~~6~~). Results are compared between a setup where climate varies in response to an emission pulse and a setup where climate is kept invariant at preindustrial conditions and for a range of pulse sizes. The time-integrated IRF_{CO2} at year 20, 50, 100, 500, and 1000 is 5%, 10%, 13%, 13%, 8% lower for the 100 and 4%, 9%, 15%, 33%, 40% lower for the 5000 GtC ~~around 13% and 15% lower for the 100 and 5000 GtC~~ pulses if the carbon cycle-climate feedback is suppressed. ~~At year 1000, the reduction is similar for the small pulse, but about 40% for the 5000 GtC pulse.~~ The reductions in the time-integrated IRF_{CO2} due to the carbon cycle-climate feedback are similar to the effects of reducing the pulse size from 5000 GtC to about 2000 GtC and from 100 GtC to 10 GtC, respectively (Figure 7~~6~~).

In summary, IRF_{CO2} and its time integral is lower for preindustrial than present day background conditions and for smaller compared to larger emission pulses. On the other hand, the ocean uptake per unit emission decreases with increasing background CO_2 concentrations (and related warmer climate conditions) and increasing pulse sizes. The responses in SAT, ocean heat content and steric sea level rise show little differences between the two 100 GtC cases and a smaller response per unit emission for larger pulse sizes. The time-integrated IRF_{CO2} and thus the AGWP depend also on the carbon cycle-climate feedback. However, the most important factor that determines the time-integrated IRF_{CO2} and AGWP is the choice of time horizon.

5 Discussion and Conclusion

We have reassessed the response of the coupled carbon cycle-climate system to an emission pulse of carbon for present day CO_2 and climate conditions using a suite of models of various complexity. The multi-model mean response in atmospheric CO_2 was fitted by an analytical function (sum of exponentials) for easy use by others. A novel element of the study is a thorough assessment of uncertainties in the simulated responses based on the spread of the multi-model ensemble and of three ensembles with individual models as well as using a linear programming approach constrained by observations. These different approaches to estimate the uncertainty in the integrated IRF_{CO2} yield comparable results. We also quantified the sensitivity of the responses to the magnitude of the emission pulse and the atmospheric and

Formatted: No bullets or numbering

Formatted: English (U.S.)

Formatted: English (U.S.)

climatic background conditions. The influence of the climate-carbon cycle feedback on results was investigated within one model. A recent study investigates how differences among the IRFs impact the estimates of GWP and GTP (Olivie and Peters, 2012).

It is important to update the AGWP and AGTP of CO_2 and to assess their uncertainty since CO_2 is the reference gas in GWP and GTP calculations. It therefore exerts a significant control on the GWP and GTP of any other gas. We find that that the absolute global warming potential (AGWP) of CO_2 for a time horizon of 100 year is 92.7×10^{-15} yr W m^{-2} per kg-CO_2 with a 5 to 95% confidence range of (~~70~~ 68 to 11~~5~~) × 10^{-15} yr W m^{-2} per kg-CO_2 (Table 4). Although, the ocean absorbs most of the emission pulse, the uncertainty in the perturbation of the land carbon inventory (in absolute units) is larger than for the perturbation in the ocean carbon inventory. This is related to different responses of the land biosphere models to changes in atmospheric CO_2 and climate and reflects our incomplete knowledge on these terrestrial processes.

There are also uncertainties related to the experimental setup. The time-integrated CO_2 impulse response at year 100 is about twice as large for an emission pulse of 5000 GtC compared to our standard pulse size of 100 GtC. An emission of 5000 GtC is an extreme case in the context of Global Warming Potential (GWP), though within reach when burning all fossil resources. Such large pulses are also used in other studies to assess the evolution in the CO_2 perturbation over several centuries and up to 10 000 years (Archer et al., 2009;Eby et al., 2009). These studies also find a long-lasting perturbation in atmospheric CO_2. A more modest~~n~~ increase of the pulse size from 100 GtC to 1000 GtC yields an increase in the time-integrated CO_2 impulse response, used to compute AGWP and GWP, by one third. The influence of the carbon-cycle climate feedback is found to be of order 10% to 20% on the time integrated CO_2 impulse response and the AGWP of CO_2. The magnitude of this effect varies across models (Friedlingstein et al., 2006;Gillett and Matthews, 2010). The carbon-cycle climate feedback was not included in the IRF of CO_2 derived with the Bern-SAR model, but is included in the Bern model versions as used in the TAR and AR4 and corresponding IRFs. A potential inconsistency in GWP can arise if climate feedbacks are included in the calculation of IRF_{CO2} and $AGWP_{CO2}$, but not in the calculation of the gas under consideration. Although, choices in pulse size, background concentration, and model lead to considerable uncertainties in AGWP and GWP, the most important variable is the time horizon (Table 9~~7~~).

Formatted: Subscript

Formatted: Font: Italic

The subjective choice of the time horizon ~~dominates uncertainties in~~has a much larger influence on the range in absolute global warming potential of CO_2 and ~~related uncertainties in~~in the global warming potential of most other agents than uncertainties associated with the computation of these values for a given time horizon. The uncertainty in AGWP (in units of yr W m^{-2} per kg-CO_2) can be mapped to a range~~n uncertainty~~ in the time horizon (in units of year). For a time horizon of 100 years, the lower and upper bound of the 5-95% confidence range of the AGWP for CO_2 correspond to the multi-model mean value of AGWP evaluated at the time horizon of 68~~70~~ years and 135~~2~~ years. This ~~uncertainty~~ range of 67~~2~~ years, steming from uncertainties in the carbon cycle-climate model response, is much smaller than the differences resulting from the subjective choice of alternative time horizons; in the AR4 IPCC report (Table 2.14, page 212 in (Forster et al., 2007)) GWP are tabulated for illustrative time horizons of 20, 100, and 500 years. Table 9~~7~~ illustrates how the GWP of methane, nitrous oxide, and sulphur hexafluoride calculated with a single e-fold decay ~~with perturbation life times~~ of 12 years, 114 years and 3200 years changes with the choice of time horizon. For example, one could select a time horizon of 1000 years instead of 100 years in the UNFCCC process and thereby account somewhat more explicitly for the long -time-scales involved in the Earth System. In this case, the GWP for methane would be more than 5 times smaller and only 17% (13 to 24~~5~~%; 5 to 95% confidence range considering uncertainty in ~~*IRF*~~$_{CO2}$ only) of that for 100 years. The GWP for N_2O would be more than 3 times smaller and only 29% (23~~2~~ to 41~~2~~%) of that for 100 years, whereas the GWP for SF_6 would be about 48% (15~~3~~% to 110~~4~~%) larger than that for a time horizon of 100 years. On the other hand, selecting a time horizon of 20 years instead of 100 years yields a three times larger GWP for methane. A strong influence of the time horizon is also found for GTP and time-integrated GTP (Peters et al., 2011).

The IPCC presented impulse response functions of CO_2, IRF_{CO2}, in its major assessment reports. Figure 8~~7~~ shows how IRF_{CO2} has changed from the IPCC First Assessement Report (FAR), to the Second Assessment Report (SAR), to the Fourth Assessement Report (AR4) and compares these responses with the results of this study. IRF_{CO2} was not updated in the Third Assessment Report. Differences in the IRF_{CO2} are relatively small. The higher initial airborne fraction published in the FAR is related to the application of an atmosphere-ocean model with a neutral land biosphere, whereas in subsequent reports the land biosphere model absorbs a considerable fraction of the initial emission pulse during the first few decades. The responses published in the SAR and the AR4 are lower than the multi-model model mean

Formatted: Font: Italic

response of this study. This is predominant~~e~~ly due to the smaller pulse size and lower CO_2 background in the SAR and AR4 setup. The time-integrated IRF_{CO2} for the AR4 (Bern2.5D-LPJ) and SAR (Bern-SAR) models under the setup of this study (Table 4) are with 49 and 51 years only slightly lower than the multi-model mean of 52 years at year 100. We do not find indications that there are systematic differences in IRF_{CO2} between models of different complexities such as EMICs and comprehensive Earth System Models.

In addition to the Absolute Global Warming Potential, we have also quantified the Absolute Global Temperature change Potential and corresponding responses in ocean heat content and steric sea level rise by directly applying the suite of carbon cycle-climate models. The uncertainty in these responses is much larger than the uncertainty in the IRF_{CO2} and the AGWP of CO_2. This is mainly a consequence of the large range in the climate sensitivity of the different models (Table 2) and their ocean heat uptake efficiency. More general, uncertainties increase along the cause-effect chain from emissions to atmospheric abundance to radiative forcing to climate change (Steinacher et al., 2012). In addition, it is difficult to extract the temperature signal from a relatively small CO_2 emission pulse from results of comprehensive ESM as these models feature considerable interannual-to-decadal temperature variability. Larger pulse sizes and/or running ensembles instead of single simulations would improve signal-to-noise ratio. Intercomparison studies~~y~~ that look~~s~~ into the responses of non-CO_2 agents might further improve the quantification of metrics and their uncertainties. Yet fundamental issues will remain. Different forcing agents are distinct and any simple metric intended to compare forcing agents relies on subjective choices.

CO_2 continues to dominate ~~man-made~~anthropogenic ~~-~~warming. For the current crop of emission scenarios from the integrated assessment community (Weyant et al., 2006;Van Vuuren et al., 2008), the contribution of CO_2 to the anthropogenic warming by 2100 is estimated using an emission-driven climate model to be 58 to 76% of that of all greenhouse gases together (Strassmann et al., 2009). Independent from the choice of emission metric, the long life time of the anthropogenic CO_2 perturbation implies that anthropogenic emissions of CO_2 must be reduced if greenhouse gas forcing and anthropogenic climate change are to be stabilized (Siegenthaler and Oeschger, 1978).

Appendix A: Model Descriptions

ACC2: The Aggregated Carbon Cycle, Atmospheric Chemistry and Climate model (ACC2) (Tanaka et al., 2007;Tanaka, 2008) consists of a box model of the global carbon cycle, simple parameterizations of the atmospheric chemistry, and a land-ocean energy balance model. Most relevant to this study is the carbon cycle component, which is a four-layer atmosphere-ocean box model coupled with a four-reservoir land biosphere box model (Section 2.1 of (Tanaka, 2008)). The saturation of the ocean CO_2 uptake under rising atmospheric CO_2 concentration is dynamically reproduced by the thermodynamic equilibrium for carbonate species. The CO_2 fertilization effect is parameterized by the β factor. The temperature sensitivity of the soil respiration is modeled through the Q10 parameter. The land and ocean CO_2 uptake is influenced by the temperature change. Values of uncertain parameters (including the β factor and the Q10 parameter) are estimated based on an inverse estimation setup (Section 3 of (Tanaka, 2008)), in which a large number of parameters are simultaneously optimized by using associated historical observations and prior parameter estimates including their uncertainties from year 1750 to 2000 (Tables 3.1 and 3.2 of (Tanaka, 2008)). Parameter values estimated through the inverse estimation are consistently used in projections beyond 2000. The simplified process representations in ACC2 allow one to perform a sensitivity analysis for the CO_2 response under various sets of assumptions. ACC2 has been applied to several studies (Tanaka et al., 2009a;Tanaka et al., 2009b;Tanaka et al., 2012).

Field Code Changed

Bern-SAR: This model was applied to calculate the CO_2 impulse response function as used for the Global Warming Potentials of IPCC 1994 report on Radiative Forcing, the IPCC Second Assessment Report and the Kyoto Protocol. The Bern model (Siegenthaler and Joos, 1992;Joos et al., 1996) is designed to compute the uptake of anthropogenic carbon by land and ocean. It links a well-mixed atmosphere with the High-Latitude Exchange/Interior Diffusion-Advection(HILDA) ocean model and a 4-box representation of the land biosphere (Siegenthaler and Oeschger, 1987). Model parameters of the box-diffusion-type ocean model were determined such that the model reproduces the oceanic distribution of natural and bomb-produced radiocarbon. Net primary production on land increases with the natural logarithm of CO_2 and the scaling factor (β=0.27) was chosen in order to close the atmospheric CO_2 budget in the early nineties.

Bern2.5D-LPJ: This model was used to calculate the CO_2 impulse response function for the IPCC AR4 report (Forster et al., 2007) (p.213). Here, the same code version as in the AR4

was used and subsequent updates of the land biosphere component (LPJ) are not included. The Bern2.5D-LPJ (or Bern2.5CC in (Plattner et al., 2008)) reduced complexity climate model includes components describing 1) the physical climate system, 2) the cycling of carbon and related elements, and 3) a module to calculate concentrations of non-CO2 greenhouse gases and radiative forcing by atmospheric CO_2, non-CO_2 greenhouse gases, and aerosols (Plattner et al., 2008). The ocean physical component is the zonally averaged, three-basin circulation model of (Stocker et al., 1992), coupled to a zonally and vertically averaged atmospheric energy balance model, including an active hydrological cycle (Schmittner and Stocker, 1999). The ocean biogeochemical component includes a simple prognostic description of the cycles of carbon, carbon isotopes, oxygen, and carbon-related tracers (Marchal et al., 1998;Joos et al., 1999;Plattner et al., 2001). The terrestrial biosphere component is the Lund–Potsdam–Jena (LPJ) dynamic global vegetation model at 3.75° x2.5° resolution as used by (Joos et al., 2001;Gerber et al., 2003) and described in detail by (Sitch et al., 2003). Vegetation is represented by nine plant functional types. Fertilization of plants by increasing atmospheric CO_2 concentrations is modeled according to a modified Farquhar scheme (Farquhar et al., 1980;Haxeltine and Prentice, 1996). The module designed to calculate radiative forcing by atmospheric CO_2, non-CO_2 greenhouse gases, and aerosols is based on work summarized in (Fuglestvedt and Berntsen, 1999) and (Joos et al., 2001).The climate sensitivity is 3.2 K for a nominal doubling of CO_2.

Bern3D-LPJ: Bern3D-LPJ is an Earth System Model of Intermediate Complexity with a fully coupled carbon cycle and components that represent the ocean and sea ice, ocean sediments, the atmosphere, and the terrestrial biosphere. The ocean component is a seasonally forced three-dimensional frictional geostrophic global ocean model (Edwards et al., 1998) with a resolution of 36 × 36 boxes in the horizontal direction and 32 vertical layers (Müller et al., 2006). Marine biogeochemical cycles are implemented following OCMIP-2 (Najjar and Orr, 1999;Orr et al., 1999;Najjar et al., 2007) with the addition of prognostic formulations for biological productivity and the cycling of iron, silica, ^{13}C and ^{14}C (Parekh et al., 2008;Tschumi et al., 2008), as well as a sedimentary component (Tschumi et al., 2011;Gehlen et al., 2006;Heinze et al., 1999). The atmosphere is represented by a single-layer energy and moisture balance model with the same horizontal resolution as the ocean component (Ritz et al., 2011). The CO_2 forcing is calculated after (Myhre et al., 1998) and the model is tuned to simulate an equilibrium climate sensitivity of 3°C. Other greenhouse gases and volcanic

aerosols are prescribed as global radiative forcing, while tropospheric sulphate aerosols are taken into account by changing the surface albedo locally (Steinacher, 2011;Reader and Boer, 1998). The climate sensitivity is 3 K for a nominal doubling of CO_2. The terrestrial biosphere component is based on the Lund-Potsdam-Jena (LPJ) Dynamic Global Vegetation Model at $3.75^{\circ} \times 2.5^{\circ}$ resolution (Joos et al., 2001;Sitch et al., 2003). Vegetation is represented by 12 plant functional types and CO_2 fertilization is modeled according to the modified Farquhar scheme (Farquhar et al., 1980;Haxeltine and Prentice, 1996). The model has recently been extended with modules to account for land use (Strassmann et al., 2008;Stocker et al., 2011), peatlands and permafrost dynamics (Gerten et al., 2004;Wania et al., 2009a, b), and land surface albedo (Steinacher, 2011). The LPJ component is driven by global mean CO_2 concentrations and changes in surface air temperature relative to a reference period by scaling global mean surface temperature change simulated by the Bern3D with spatial patterns of precipitation and temperature (Steinacher, 2011;Stocker et al., 2011).

CLIMBER2-LPJmL: CLIMBER2-LPJml (Kleinen et al., 2010) consists of the Earth System Model of Intermediate Complexity (EMIC) CLIMBER2, coupled to the dynamic global vegetation model (DGVM) LPJmL. CLIMBER2 (Petoukhov et al., 2005) consists of a 2.5-dimensional statistical-dynamical atmosphere with a resolution of roughly 51° (longitude) by 10° (latitude), a zonally averaged ocean resolving three basins with a latitudinal resolution of 2.5°, and a sea ice model. CLIMBER2 also contains oceanic biogeochemistry, a model for marine biota, and a sediment model (Archer, 1996;Brovkin et al., 2002;Brovkin et al., 2007). Weathering rates scale to runoff from the land surface. To this EMIC we have coupled the DGVM LPJmL (Sitch et al., 2003;Bondeau et al., 2007;Fader et al., 2010;Portmann et al., 2008) in order to investigate land surface processes at a significantly higher resolution of 0.5x0.5°. Agricultural land use is included in this version of LPJ. Monthly anomalies from the climatology of the climate fields are passed to LPJ, where they are added to climate patterns based on the Climatic Research Unit CRU-TS climate data set (New et al., 2000). The carbon flux between atmosphere and land surface is determined from the annual change in the LPJ carbon pools, and employed in CLIMBER2 to determine the CO_2 concentration. Biogeochemical feedbacks are thus determined by the combination of CLIMBER2 and LPJmL, while biogeophysical effects are solely determined by CLIMBER2. The climate sensitivity is 3 K.

DCESS: The DCESS model consists of fully coupled modules for the atmosphere, ocean,

ocean sediment, land biosphere and lithosphere (Shaffer et al., 2008). The model geometry consists of one hemisphere, divided into two 360° x 52° zones. Long term climate sensitivity has been calibrated to 3˚C. The atmosphere component considers radiation balance, heat and gas exchanges with other modules, and meridional transport of heat and water vapor between low-mid latitude and high latitude zones. The ocean component is 270° wide and extends from the equator to 70° latitude. Both ocean sectors are divided into 55 layers with 100 m vertical resolution. Each layer is assigned an ocean sediment section, with width determined from observed ocean depth distributions. Sea ice and snow cover are diagnosed from estimated atmospheric temperature profiles. Circulation and mixing are prescribed, with values calibrated from observations as in the HILDA model (Shaffer and Sarmiento, 1995). Biogenic production of particulate organic matter in the ocean surface layer depends on phosphate availability but with lower efficiency in the high latitude zone. The calcite to organic carbon rain ratio depends on surface layer temperature. The ocean sediment component considers calcium carbonate dissolution as well as oxic-anoxic organic matter remineralisation. The land biosphere component includes leaves, wood, litter and soil. Here, it has been modified to include prescribed land use change carbon losses, distributed in proportion to the initial inventory sizes of the module components. With this change, the model CO_2 fertilization factor, originally 0.65, has been recalibrated to 0.37. Finally, the lithosphere component considers outgassing and climate-dependent weathering of carbonate and silicate rocks, as well as rocks containing old organic carbon and phosphorus. The atmospheric methane module was not used here.

GENIE: The GENIE-1 physical model comprises the 3D frictional geostrophic ocean model GOLDSTEIN, with a resolution of 36 × 36 boxes in the horizontal direction and 16 vertical levels, coupled to a 2D energy moisture balance atmosphere and a thermodynamic-dynamic sea-ice model (Edwards and Marsh, 2005). Recent developments (Marsh et al., 2011)(Marsh et al. 2011) include the incorporation of stratification-dependent mixing, a more general equation of state through a parameterization of thermobaricity, and improvements to the representation of fixed wind forcing. The land surface component is ENTS, a dynamic model of terrestrial carbon storage (Williamson et al., 2006) with a relatively simple implementation of spatiotemporal land use change. Ocean chemistry is modeled with BIOGEM (Ridgwell et al., 2007), including iron limitation (Annan and Hargreaves, 2010), and is coupled to the sediment model SEDGEM with fixed weathering, diagnosed during the model spin-up to simulated observed ocean alkalinity (Ridgwell and Hargreaves, 2007). All GENIE results are

derived from ensembles applying the same 20-member parameter set. The selected parameters were filtered from a 100-member, 28-parameter pre-calibrated ensemble, constrained for plausible present-day CO_2 concentrations.

HadGEM2-ES: HadGEM2-ES (Collins et al., 2011) couples interactive ocean biogeochemistry, terrestrial biogeochemistry and dust, interactive tropospheric chemistry and aerosol components into an update of the physical model HadGEM1. The physical model contains a 40 level 1x1 degree, moving to 1/3rd degree at the equator ocean, and a 38 level 1.875 x 1.25 atmosphere (Martin et al., 2011). HadGEM2-ES has been set-up and used to perform all of the CMIP5 simulations as described by (Jones et al., 2011). The ocean biogeochemistry uses the Diat-HadOCC model (Totterdell and Halloran in prep), an update of HadOCC (Palmer and Totterdell, 2001), now simulating diatom and non-diatom phytoplankton functional types, a single zooplankton, and cycling of nitrogen, silica and iron. Diat-HadOCC is coupled to other earth system components through the model's physics, iron supplied through dust, air-sea exchange of CO_2 and oceanic emission of dimethylsulphide. The terrestrial carbon cycle is represented by the MOSES2 land surface scheme (Essery et al., 2003) which simulates exchange of water, energy and carbon between the land surface and the atmosphere, and the TRIFFID dynamic global vegetation model (Cox, 2001) which simulates the coverage and competition between 5 plant functional types (broadleaf tree, needleleaf tree, C3 and C4 grass and shrub) and 4 non-vegetated surface types (bare soil, urban, lakes and land-ice).

LOVECLIM: The Earth system model of intermediate complexity LOVECLIM (version 1.1) (Menviel et al., 2008) links the ECBilt atmosphere, the CLIO sea-ice ocean model and a bucket model for land hydrology with the VECODE dynamic vegetation model and the LOCH ocean carbon model. The atmosphere model (ECBilt) is a spectral T21 model, based on quasigeostrophic equations with 3 vertical levels and a horizontal resolution of about 5.625x5.625 degree. Ageostrophic forcing terms are estimated from the vertical motion field and added to the prognostic vorticity equation and thermodynamic equation.

The sea ice-ocean component (CLIO) (Goosse et al., 1999) consists of a primitive equation ocean general circulation model with 3x3 degree resolution on a partly rotated grid in the North Atlantic. CLIO uses a free surface and is coupled to a thermodynamic-dynamic sea ice model (Fichefet and Maqueda, 1997). In the vertical there are 20 unevenly spaced levels . Mixing along isopycnals, diapycnal mixing, as well as the effect of mesoscale eddies on transports and mixing and downsloping currents at the bottom of continental shelves are

parameterized (Goosse et al., 2011). The ocean, atmosphere and sea ice components model are coupled by exchange of momentum, heat and freshwater fluxes. The hydrological cycle over land is closed by a bucket model for soil moisture and simple river runoff scheme. The global dynamic terrestrial vegetation is modeled using VECODE (Brovkin et al., 1997). Annual mean values of precipitation and temperature are communicated to the vegetation from the atmospheric model. On the basis of these mean values the evolution of the vegetation cover described as a fractional distribution of desert, tree, and grass in each land grid cell is calculated once a year. In the current version, only land albedo (as seen by the atmospheric model) outside the ice sheets is changed by VECODE. LOCH is a three-dimensional global model of the oceanic carbon cycle with prognostic equations for dissolved inorganic carbon, total alkalinity, phosphate, dissolved and particulate organic matter, oxygen and silicates (Goosse et al., 2011;Menviel et al., 2008). The phytoplankton growth is a function of temperature, light and phosphate concentration. The sink term depends on grazing and mortality. Although phytoplankton biomass is a prognostic variable it is not subject to advective transports. Remineralization below the euphotic zone (0-120 m) is a function of oxygen concentrations. Anoxic remineralization can occur in oxygen-depleted areas but is less efficient. The export production is accompanied by the export of opal assuming a constant silicate-to-phosphate ratio. Furthermore CaCO3 (calcite and aragonite) shells are formed as a function of phytoplankton growth. The dissolution of shells occurs in the deepest ocean layer. LOCH is coupled to CLIO, using the same time step. Biogeochemical tracers that are subject to advection and mixing are advected and mixed using the same circulation field and mixing parameters respectively as in CLIO.

MAGICC6: MAGICC is a reduced-complexity climate model with an upwelling-diffusive-entrainment ocean and is coupled to a simple carbon cycle model including CO_2 fertilization and temperature feedback parameterizations of the terrestrial biosphere and oceanic uptake. MAGICC version 6 has been calibrated to AOGCMs (Meehl et al., 2007) and carbon cycle models (Friedlingstein et al., 2006) used in the Fourth IPCC Assessment Report (see (Meinshausen et al., 2011b;Meinshausen et al., 2011a) for details). Varying the parameters in MAGICC to emulate AOGCM/C4MIP model combinations allows to explore the climate response space in terms of concentrations, radiative forcing, and hemispheric land/ocean surface air temperatures spanned by the range of complex climate models. This version of MAGICC6 was also used to produce harmonized GHG concentrations for the new set of Representative Concentration Pathways (Meinshausen et al., 2011b). For this

intercomparison, we used a set of 19 AOGCM calibrations and 9 coupled climate-carbon cycle model calibrations.

MESMO: MESMO version 1 (Matsumoto et al., 2008) is based on the C-GOLDSTEIN ocean model (Edwards and Marsh, 2005). It consists of a frictional geostrophic 3-D ocean circulation model coupled to a dynamic-thermodynamic sea ice model and atmospheric model of energy and moisture balance. Ocean production is based on prognostic nutrient uptake kinetics of phosphate and nitrate with dependence on light, mixed layer depth, temperature, and biomass. Interior ocean ventilation is well calibrated against natural radiocarbon on centennial timescale and against transient anthropogenic tracers on decadal time-scales. Here MESMO1 is coupled to a simple prognostic land biosphere model (Williamson et al., 2006) that calculates energy, moisture, and carbon exchanges between the land and the atmosphere. Prognostic variables include vegetation and soil carbon as well as land surface albedo and temperature.

MPI-ESM: The fully comprehensive Earth System Model MPI-ESM of the Max-Planck-Institute for Meteorology in Hamburg, Germany consists of the atmospheric model ECHAM6 (here in T63L47 resolution) with land surface model JSBACH, (Raddatz et al., 2007). Each land grid cell is divided into tiles covered with 8 natural and 4 anthropogenic PFTs; vegetation model in JSBACH includes an efficient module for vegetation dynamics (Brovkin et al., 2009). Anthropogenic land use is predetermined. The physical ocean model is MPIOM, which further includes a sea-ice model (Marsland et al., 2003) on a nominal 1.5^{o} grid with higher resolution in the North Atlantic. Marine biogeochemistry is represented by the Hamburg Ocean carbon cycle HAMOCC 5.1 which operates on the same grid as MPIOM and includes the full carbonate chemistry and a NPZD type model of the biological pump (Maier-Reimer et al., 2005;Maier-Reimer, 1993). MPI-ESM is used here in the same version that is employed for the CMIP5 experiments 'MPI-ESM-LR'. CO_2 is allowed to float freely between the model's carbon reservoirs (i.e., atmosphere, land, and ocean) depending on the state of the compartments and climate-carbon cycle feedbacks are simulated by the model.

NCAR CSM1.4: The physical core of the Climate System Model of the National Centre for Atmospheric Research (NCAR CSM1.4-carbon) (Doney et al., 2006;Fung et al., 2005) is a modified version of the NCAR CSM1.4 coupled physical model, consisting of ocean, atmosphere, land and sea ice components integrated via a flux coupler without flux adjustments. Atmospheric CO_2 is treated as a prognostic variable whose balance is determined by exchange fluxes with the land and ocean. The ocean model includes a derivate

of the OCMIP-2 (Ocean Carbon-Cycle Model Intercomparison Project Phase 2) ocean biogeochemistry model (Najjar et al., 2007) with prognostic formulations for marine biological production. The main processes of the organic and inorganic carbon cycle within the ocean and air-sea CO_2 flux are included. A parameterization of the marine iron cycle (Doney et al., 2006) considers atmospheric dust deposition/iron dissolution, biological uptake, vertical particle transport and scavenging. Prognostic variables in the ocean include phosphate, dissolved inorganic carbon, alkalinity, oxygen, and dissolved organic phosphorus. The land carbon module combines the NCAR Land Surface Model with a modified version of the terrestrial biogeochemical Carnegie-Ames-Stanford Approach (CASA; (Randerson et al., 1997)) providing full coupling of energy (via dynamic leaf phenology and hence albedo), water (via transpiration), and carbon cycles of the atmosphere and land. CASA follows the life cycles of plant functional types from carbon assimilation via photosynthesis, to mortality and decomposition, and the return of CO_2 to the atmosphere via respiration. NPP is allocated to leafs, roots, and wood with preferred allocation to roots during water-limited conditions and to wood/leaves during light-limited conditions. There are nine soil carbon pools. The transfer rates between them and to the atmosphere are sensitive to soil temperature and soil moisture saturation. The land model does not include other land surface processes that affect atmosphere-biosphere interactions such as an explicit nitrogen cycle, fires and other disturbances, herbivory, dynamic vegetation cover, or anthropogenic land cover change.

TOTEM2: TOTEM2 (Ver et al., 1999;Mackenzie et al., 2011) is a global biogeochemical model of the life-essential elements carbon, nitrogen, and phosphorus. The model comprises thirteen reservoirs: the atmosphere; six terrestrial reservoirs (living biota, humus, inorganic soil, continental soilwater, shallow groundwater, and lakes); three coastal-zone reservoirs (organic matter, water, and sediments); and three open ocean reservoirs (organic matter, surface water, and deep water). The coupling of the individual cycles is achieved by the average C:N:P ratios associated with oceanic and terrestrial photosynthesis (Redfield ratios), autorespiration on land and in ocean waters, humus formation, and sedimentation of organic matter in the coastal zone and open ocean. We make a simplifying assumption that these biologically mediated coupling processes apply over many different species and environments, and occur with the same global mean elemental ratios on the decadal to century time-scale. All the transfer processes between the model reservoirs are represented by linear or nonlinear equations describing reaction mechanisms and physical transport processes. The

model has been shown to reproduce well the atmospheric CO_2 concentration for the past 300 years (Ver et al., 1999).

UVic ESCM: The UVic ESCM version 2.9 (Eby et al., 2009) consists of a primitive equation 3-D ocean general circulation model coupled to a dynamic-thermodynamic sea-ice model and an atmospheric energy-moisture balance model with dynamical feedbacks (Weaver et al., 2001). The model conserves heat, moisture, and carbon between components to machine precision without flux adjustments. The land surface and terrestrial vegetation components are represented by a simplified version of the Hadley Centre's MOSES land-surface scheme coupled to the dynamic vegetation model TRIFFID (Meissner et al., 2003). Land carbon fluxes are calculated within MOSES and are allocated to vegetation and soil carbon pools (Matthews et al., 2004). Ocean carbon is simulated by means of an OCMIP-type inorganic carbon-cycle model and a NPZD marine ecosystem model with two nutrients (PO_4 and NO_3), two phytoplankton classes, and prognostic denitrification (Schmittner and Galbraith, 2008) . Sediment processes are represented using an oxic-only model of sediment respiration (Archer, 1996). Terrestrial weathering is diagnosed from the net sediment flux during spin-up and held fixed at the ~~equilibrium~~ steady state pre-industrial value for transient simulations. The model was spun up with boundary conditions from the year 1800 for more than 10,000 years.

Acknowledgements

This project was funded by the Swiss National Science Foundation and the EU FP7 project CARBOCHANGE ”Changes in carbon uptake and emissions by oceans in a changing climate” which received funding from the European Community’s Seventh Framework Programme under grant agreement no. 264879. Met Office authors were supported by the Joint DECC/Defra Met Office Hadley Centre Climate Programme (GA01101). K.Tanaka is supported by the Marie Curie Intra-European Fellowship within the seventh European Community. NRE and PBH acknowledge support from EU FP7 ERMITAGE grant no. 265170. T.F. and A.T. are grateful to Anne Mouchet for providing the LOCH carbon cycle component for the LOVECLIM model. TLF is supported by the Carbon Mitigation Initiative (CMI) project at Princeton University, sponsored by BP.

Formatted: English (U.S.)

References

Aamaas, B., Peters, G. P., and Fuglestvedt, J. S.: A synthesis of climate-based emission metrics with applications, Earth Syst. Dynam. Discuss., 3, 871-934, 10.5194/esdd-3-871-2012, 2012.

Annan, J. D., and Hargreaves, J. C.: Efficient identification of ocean thermodynamics in a physical/biogeochemical ocean model with an iterative Importance Sampling method, Ocean Modelling, 32, 205-215, 10.1016/j.ocemod.2010.02.003, 2010.

Archer, D.: A data-driven model of the global calcite lysocline, Global Biogeochem. Cycles, 10, 511-526, 10.1029/96gb01521, 1996.

Archer, D., Eby, M., Brovkin, V., Ridgwell, A., Cao, L., Mikolajewicz, U., Caldeira, K., Matsumoto, K., Munhoven, G., Montenegro, A., and Tokos, K.: Atmospheric Lifetime of Fossil Fuel Carbon Dioxide, Annu. Rev. Earth Planet. Sci., 37, 117-134, 10.1146/annurev.earth.031208.100206, 2009.

Azar, C., and Johansson, D. J. A.: On the relationship between metrics to compare greenhouse gases – the case of IGTP, GWP and SGTP, Earth Syst. Dynam. , 3, 139-147, 10.5194/esd-3-139-2012, 2012.

Bondeau, A., Smith, P. C., Zaehle, S., Schaphoff, S., Lucht, W., Cramer, W., Gerten, D., Lotze-Campen, H., MÜLler, C., Reichstein, M., and Smith, B.: Modelling the role of agriculture for the 20th century global terrestrial carbon balance, Global Change Biology, 13, 679-706, 2007.

Boucher, O., and Reddy, M. S.: Climate trade-off between black carbon and carbon dioxide emissions, Energy Policy, 36, 193-200, 2008.

Boucher, O.: Comparison of physically- and economically-based CO_2-equivalences for methane, Earth Syst. Dynam., 3, 49-61, 2012.

Broecker, W. S., Peng, T.-H., and Engh, R.: Modelling the carbon system, Radiocarbon, 22, 565-598, 1980.

Brovkin, V., Ganopolski, A., and Svirezhev, Y.: A continuous climate-vegetation classification for use in climate-biosphere studies, Ecological Modelling, 101, 251-261, 10.1016/s0304-3800(97)00049-5, 1997.

Brovkin, V., Bendtsen, J., Claussen, M., Ganopolski, A., Kubatzki, C., Petoukhov, V., and Andreev, A.: Carbon cycle, vegetation, and climate dynamics in the Holocene: Experiments with the CLIMBER-2 model, Global Biogeochem. Cycles, 16, 1139, 1131-1113, 10.1029/2001GB001662, 2002.

Brovkin, V., Ganopolski, A., Archer, D., and Rahmstorf, S.: Lowering of glacial atmospheric CO2 in response to changes in oceanic circulation and marine biogeochemistry, Paleoceanography, 22, PA4202, 10.1029/2006pa001380, 2007.

Brovkin, V., Raddatz, T., Reick, C. H., Claussen, M., and Gayler, V.: Global biogeophysical interactions between forest and climate, Geophys. Res. Lett., 36, L07405, 10.1029/2009gl037543, 2009.

Caldeira, K., and Kasting, J. F.: Insensitivity of global warming potentials to carbon dioxide emission scenarios, Nature, 366, 251-253, 1993.

Cao, L., Eby, M., Ridgwell, A., Caldeira, K., Archer, D., Ishida, A., Joos, F., Matsumoto, K., Mikolajewicz, U., Mouchet, A., Orr, J. C., Plattner, G. K., Schlitzer, R., Tokos, K., Totterdell, I., Tschumi, T., Yamanaka, Y., and Yool, A.: The role of ocean transport in the uptake of anthropogenic CO_2, Biogeosciences, 6, 375-390, 2009.

Collins, W. J., Bellouin, N., Doutriaux-Boucher, M., Gedney, N., Halloran, P., Hinton, T., Hughes, J., Jones, C. D., Joshi, M., Liddicoat, S., Martin, G., O'Connor, F., Rae, J., Senior, C., Sitch, S., Totterdell, I., Wiltshire, A., and Woodward, S.: Development and evaluation of an Earth-System model - HadGEM2, Geosci. Model Dev., 4, 1051-1075, 10.5194/gmd-4-1051-2011, 2011.

Conway, T. and Tans, P. P. Globally averaged marine surface annual mean data. NOAA/ESRL www.esrl.noaa.gov/gmd/ccgg/trends/, 2012.

Cox, P. M.: Description of the TRIFFID dynamic global vegetation model, Met Office, UK, 2001.

Denman, K. L., Brasseur, G., Chidthaisong, A., Ciais, P., Cox , P., Dickinson, R. E., Hauglustaine, D., Heinze, C., Holland, E., Jacob, D., Lohmann, U., Ramachandra, S., da Silva Dias, P. L., Wofsy, S., and Zhang, X.: Couplings between changes in the climate system and biogeochemistry, in: Climate Change 2007: The Physical Science Basis. Contribution of Working Group I to the Fourth Assessment Report of the Intergovernmental Panel on Climate Change, edited by: Solomon, S., Qin, D., Manning, M., Chen, Z., Marquis, M., Averyt, K. B., Tignor, M., and Miller, H. L., Cambridge University Press, Cambridge United Kingdom and New York, NY, USA, 498-587, 2007.

Doney, S. C., Lindsay, K., Fung, I., and John, J.: Natural variability in a stable, 1000-year global coupled climate-carbon cycle simulation, J. Climate, 19, 3033–3054, 2006.

Eby, M., Zickfeld, K., Montenegro, A., Archer, D., Meissner, K. J., and Weaver, A. J.: Lifetime of Anthropogenic Climate Change: Millennial Time Scales of Potential CO2 and Surface Temperature Perturbations, Journal of Climate, 22, 2501-2511, 10.1175/2008jcli2554.1, 2009.

Eby, M., Weaver, A. J., Alexander, A., Zickfeld, K., Abe-Ouchi, A., Cimatoribus, A. A., Crespin, E., Drijfhout, S. S., Edwards, N. R., Eliseev, A. V., Feulner, G., Fichefet, T., Forest, C. E., Goosse, H., Holden, P. B., Joos, F., Kawamiya, M., Kicklighter, D., Kienert, H., Matsumoto, K., Mokhov, I. I., Monier, E., Olsen, S. M., Pedersen, J. O. P., Perrette, M., Philippon-Berthier, G., Ridgwell, A., Schlosser, A., Schneider von Deimling, T., Shaffer, G., Smith, R., Spahni, R., Sokolov, A. P., Steinacher, M., Tachiiri, K., Tokos, K., Yoshimori, M., Zeng, N., and Zhao, F.: Historical and Idealized Climate Model Experiments: An EMIC Intercomparison, Climate of the Past Discussion, 8, 4121-4181, 10.5194/cpd-8-4121-2012, 2012. , 2012.

Edwards, N. R., Willmott, A. J., and Killworth, P. D.: On the role of topography and wind stress on the stability of the thermohaline circulation, J. Physical Oceanography, 28, 756-778, 1998.

Edwards, N. R., and Marsh, R.: Uncertainties due to transport-parameter sensitivity in an efficient 3-D ocean-climate model, Climate Dynamics, 24, 415-433, 10.1007/s00382-004-0508-8, 2005.

Enting, I. G.: On the use of smoothing splines to filter CO_2 data, J. Geophys. Res., 92, 10977-10984, 1987.

Enting, I. G., and Mansbridge, J. V.: The incompatibility of ice-core CO_2 data with reconstructions of biotic CO2 sources, Tellus, 39B, 318-325, 1987.

Enting, I. G.: Ambiguities in the calibration of carbon cycle models, Inverse Problems, 6, L39-L46, 1990.

Enting, I. G., Rayner, P. J., and Ciais, P.: RECCAP uncertainty, Biogeosciences Discuss., 9, 1829-1868, 2012.

Essery, R. L. H., Best, M. J., Betts, R. A., Cox, P. M., and Taylor, C. M.: Explicit representation of subgrid heterogeneity in a GCM land-surface scheme, J. Hydrometeorol., 43, 530-543, 2003.

Fader, M., Rost, S., Müller, C., Bondeau, A., and Gerten, D.: Virtual water content of temperate cereals and maize: Present and potential future patterns, Journal of Hydrology, 384, 218-231, 10.1016/j.jhydrol.2009.12.011, 2010.

Farquhar, G. D., von Caemmerer, S., and Berry, J. A.: A biochemical model of photosynthetic CO_2 assimilation in leaves of C3 species, Planta, 149, 78-90, 1980.

Fichefet, T., and Maqueda, M. A. M.: Sensitivity of a global sea ice model to the treatment of ice thermodynamics and dynamics, J. Geophys. Res., 102, 12609-12646, 10.1029/97jc00480, 1997.

Forster, P., Ramaswamy, V., Artaxo, P., Berntsen, T., Betts, R., Fahey, D. W., Haywood, J., Lean, J., Lowe, D. C., Myhre, G., Nganga, J., Prinn, R., Raga, G., Schulz, M., and Van Doorland, R.: Changes in Atmospheric Constitutents and in Radiative Forcing, in: Climate Change 2007: The Physical Science Basis. Contribution of Working Group I to Fourth Assessment Report of the Intergovernmental Panel on Climate Change, edited by: Solomon, S., Qin, D., Manning, M., Chen, Z., Marquis, M., Averyt, K. B., Tignor, M., and Miller, H. L., Cambridge United Kingdom and New York, NY, USA, New York, NY, USA, 129-234, 2007.

Friedlingstein, P., Cox , P., Betts, R., Bopp, L., von Bloh, W., Brovkin, V., Doney, S., Eby, M., Fung, I., Govindasamy, B., John, J., Jones, C., Joos, F., Kato, T., Kawamiya, M., Knorr, W., Lindsay, K., Matthews, H. D., Raddatz, T., Rayner, R., Reick, C., Roeckner, E., Schnitzler, K.-G., Schnur, R., Strassmann, K., Thompson, S., Weaver, A. J., Yoshikawa, C., and N. Zeng, N.: Climate-carbon cycle feedback analysis, results from the C4MIP model intercomparison., Journal of Climate, 19, 3337-3353, 2006.

Friedrich, T., Timmermann, A., Abe-Ouchi, A., Bates, N. R., Chikamoto, M. O., Church, M. J., Dore, J. E., Gledhill, D. K., Gonzalez-Davila, M., Heinemann, M., Ilyina, T., Jungclaus, J. H., McLeod, E., Mouchet, A., and Santana-Casiano, J. M.: Detecting regional anthropogenic trends in ocean acidification against natural variability, Nature Clim. Change, advance online publication, http://www.nature.com/nclimate/journal/vaop/ncurrent/abs/nclimate1372.html#supplementary-information, 2012.

Fuglestvedt, J., Berntsen, T., Godal, O., and Sausen, R.: Metrics of climate change: Assessing radiative forcing and emission indices, Climatic Change, 267-331, 2003.

Fuglestvedt, J. S., and Berntsen, T.: A simple model for scenario studies of changes in global climate, Working Paper, Center for International Climate and Environmental Research, Oslo, 1999:2, 1999.

Fuglestvedt, J. S., Shine, K. P., Berntsen, T., Cook, J., Lee, D. S., Stenke, A., Skeie, R. B., Velders, G. J. M., and Waitz, I. A.: Transport impacts on atmosphere and climate: Metrics, Atmospheric Environment, 44, 4648-4677, 10.1016/j.atmosenv.2009.04.044, 2010.

Fung, I., Doney, S. C., Lindsay, K., and John, J.: Evolution of carbon sinks in a changing climate, Proceedings of the National Academy of Science, 102, 11201-11206, 2005.

Gattuso, J. P., Bijma, J., Gehlen, M., Riebesell, U., and Turley, C.: Ocean acidification: knowns, unknowns, and perspectives, in: Ocean Acidification, edited by: Gattuso, J. P., and Hansson, L., Oxford University Press, Oxford, 291-311, 2011.

Gehlen, M., Bopp, L., Emprin, N., Aumont, O., Heinze, C., and Ragueneau, O.: Reconciling surface ocean productivity, export fluxes and sediment composition in a global biogeochemical ocean model, Biogeosciences, 3, 521-537, 2006.

Gerber, S., Joos, F., Brugger, P., Stocker, T. F., Mann, M. E., Sitch, S., and Scholze, M.: Constraining temperature variations over the last millennium by comparing simulated and observed atmospheric CO_2, Climate Dynamics, 20, 281-299, 2003.

Gerten, D., Schaphoff, S., Haberlandt, U., Lucht, W., and Sitch, S.: Terrestrial vegetation and water balance - hydrological evaluation of a dynamic global vegetation model, Journal of Hydrology, 286, 249-270, 2004.

Gillett, N. P., and Matthews, H. D.: Accounting for carbon cycle feedbacks in a comparison of the global warming effects of greenhouse gases, Environmental Research Letters, 5, 1-6, 10.1088/1748-9326/5/3/034011, 2010.

Goosse, H., Deleersnijder, E., Fichefet, T., and England, M. H.: Sensitivity of a global coupled ocean-sea ice model to the parameterization of vertical mixing, J. Geophys. Res., 104, 13681-13695, 10.1029/1999jc900099, 1999.

Goosse, H., Brovkin, V., Fichefet, T., Haarsma, R., Huybrechts, P., Jongma, J., Mouchet, A., Selten, F., Barriat, P.-Y., Campin, J.-M., Deleersnijder, E., Driesschaert, E., Goelzer, H., Janssens, I., Loutre, M.-F., Morales Maqueda, M. A., Opsteegh, T., Mathieu, P.-P., Munhoven, G., Pettersson, E. J., Renssen, H., Roche, D. M., Schaeffer, M., Tartinville, B., Timmermann, A., and Weber, S. L.: Description of the Earth system model of intermediate complexity LOVECLIM version 1.2, Geosci. Model Dev., 3, 603-633, 10.5194/gmd-3-603-2010, 2011.

Haxeltine, A., and Prentice, I. C.: A general model for the light use efficiency of primary production, Functional Ecology, 10, 551-561, 1996.

Heinze, C., Maier-Reimer, E., Winguth, A. M. E., and Archer, D.: A global oceanic sediment model for long-term climate studies, Global Biogeochem. Cycles, 13, 221-250, 1999.

Holden, P. B., Edwards, N. R., Gerten, D., and Schaphoff, S.: A model-based constraint of CO_2 fertilisation, Biogeosciences Discuss., 9, 9425-9451, 2012.

Johansson, D.: Economics- and physical-based metrics for comparing greenhouse gases, Climatic Change, 110, 123-141, 10.1007/s10584-011-0072-2, 2012.

Jones, C. D., Hughes, J. K., Bellouin, N., Hardiman, S. C., Jones, G. S., Knight, J., Liddicoat, S., O'Connor, F. M., Andres, R. J., Bell, C., Boo, K.-O., Bozzo, A., Butchart, N., Cadule, P., Corbin, K. D., Doutriaux-Boucher, M., Friedlingstein, P., Gornall, J., Gray, L., Halloran, P. R., Hurtt, G., Ingram, W. J., Lamarque, J.-F., Law, R. M., Meinshausen, M., Osprey, S., Palin, E. J., Parsons Chini, L., Raddatz, T., Sanderson, M. G., Sellar, A. A., Schurer, A., Valdes, P., Wood, N., Woodward, S., Yoshioka, M., and Zerroukat, M.: The HadGEM2-ES

implementation of CMIP5 centennial simulations, Geosci. Model Dev., 4, 543-570, 10.5194/gmd-4-543-2011, 2011.

Joos, F., Bruno, M., Fink, R., Siegenthaler, U., Stocker, T. F., and LeQuere, C.: An efficient and accurate representation of complex oceanic and biospheric models of anthropogenic carbon uptake, Tellus Series B-Chemical and Physical Meteorology, 48, 397-417, 1996.

Joos, F., Plattner, G. K., Stocker, T. F., Marchal, O., and Schmittner, A.: Global warming and marine carbon cycle feedbacks an future atmospheric CO_2, Science, 284, 464-467, 1999.

Joos, F., Prentice, I. C., Sitch, S., Meyer, R., Hooss, G., Plattner, G. K., Gerber, S., and Hasselmann, K.: Global warming feedbacks on terrestrial carbon uptake under the Intergovernmental Panel on Climate Change (IPCC) emission scenarios, Global Biogeochemical Cycles, 15, 891-908, 2001.

Joos, F., Frölicher, T. L., Steinacher, M., and Plattner, G.-K.: Impact of climate change mitigation on ocean acidification projections, in: Ocean Acidification, edited by: Gattuso, J. P., and Hansson, L., Oxford University Press, Oxford, 273-289, 2011.

Joos, F, Roth R. Fuglestvedt, J. S., Peters, G. P.:CO_2 pulse response function for the calculation of Global Warming Potentials:a multi-model analysis: http://www.climate.unibe.ch/~joos/IRF_Intercomparison/, access: 13 July 2012, 2012.

Kandlikar, M.: The relative role of trace gas emissions in greenhouse abatement policies Energy Policy, 23, 879-883, 1995.

Key, R. M., Kozyr, A., Sabine, C. L., Lee, K., Wanninkhof, R., Bullister, J. L., Feely, R. A., Millero, F. J., Mordy, C., and Peng, T. H.: A global ocean carbon climatology: Results from Global Data Analysis Project (GLODAP), Global Biogeochem. Cycles, 18, GB4031, 10.1029/2004GB002247, 2004.

Kleinen, T., Brovkin, V., von Bloh, W., Archer, D., and Munhoven, G.: Holocene carbon cycle dynamics, Geophys. Res. Lett., 37, L02705, 10.1029/2009GL041391., 2010.

Mackenzie, F. T., De Carlo, E. H., and Lerman, A.: Coupled C, N, P, and O biogeochemical cycling at the land-ocean interface, in: Treatise on Estuarine and Coastal Science, edited by: Wolanski, E., and McLusky, D. S., Academic Press, Waltham, 317-342, 2011.

Maier-Reimer, E., and Hasselmann, K.: Transport and storage of CO_2 in the ocean - an inorganic ocean-circulation carbon cycle model, Climate Dynamics, 2, 63-90, 1987.

Maier-Reimer, E.: Geochemical cycles in an ocean general circulation model. Preindustrial tracer distributions, Global Biogeochem. Cycles, 7, 645-677, 10.1029/93gb01355, 1993.

Maier-Reimer, E., Kriest, I., Segschneider, J., and Wetzel, P.: The Hamburg ocean carbon cycle model HAMOCC5.1 Technical description, Release 1.1, Max-Planck-Institut für Meteorologie, Hamburg, 2005.

Manne, A. S., and Richels, R. G.: An alternative approach to establishing trade-offs among greenhouse gases, Nature, 410, 675-677, 2001.

Marchal, O., Stocker, T. F., and Joos, F.: Impact of oceanic reorganizations on the ocean carbon cycle and atmospheric carbon dioxide content, Paleoceanography, 13, 225-244, 1998.

Marsh, R., Müller, S. A., Yool, A., and Edwards, N. R.: Incorporation of the C-GOLDSTEIN efficient climate model into the GENIE framework: "eb_go_gs" configurations of GENIE, Geosci. Model Dev., 4, 957-992, 2011.

Formatted: German (Switzerland)

Marsland, S. J., Haak, H., Jungclaus, J. H., Latif, M., and Röske, F.: The Max-Planck-Institute global ocean/sea ice model with orthogonal curvilinear coordinates, Ocean Modelling, 5, 91-127, 10.1016/s1463-5003(02)00015-x, 2003.

Martin, G. M., Bellouin, N., Collins, W. J., Culverwell, I. D., Halloran, P. R., Hardiman, S. C., Hinton, T. J., Jones, C. D., McDonald, R. E., McLaren, A. J., O'Connor, F. M., Roberts, M. J., Rodriguez, J. M., Woodward, S., Best, M. J., Brooks, M. E., Brown, A. R., Butchart, N., Dearden, C., Derbyshire, S. H., Dharssi, I., Doutriaux-Boucher, M., Edwards, J. M., Falloon, P. D., Gedney, N., Gray, L. J., Hewitt, H. T., Hobson, M., Huddleston, M. R., Hughes, J., Ineson, S., Ingram, W. J., James, P. M., Johns, T. C., Johnson, C. E., Jones, A., Jones, C. P., Joshi, M. M., Keen, A. B., Liddicoat, S., Lock, A. P., Maidens, A. V., Manners, J. C., Milton, S. F., Rae, J. G. L., Ridley, J. K., Sellar, A., Senior, C. A., Totterdell, I. J., Verhoef, A., Vidale, P. L., and Wiltshire, A.: The HadGEM2 family of Met Office Unified Model climate configurations, Geosci. Model Dev., 4, 723-757, 10.5194/gmd-4-723-2011, 2011.

Matsumoto, K., Tokos, K. S., Price, A. R., and Cox, S. J.: First description of the Minnesota Earth System Model for Ocean biogeochemistry (MESMO 1.0), Geosci. Model Dev., 1, 1-15, 10.5194/gmd-1-1-2008, 2008.

Matthews, H. D., Weaver, A. J., Meissner, K. J., Gillett, N. P., and Eby, M.: Natural and anthropogenic climate change: incorporating historical land cover change, vegetation dynamics and the global carbon cycle, Climate Dynamics, 22, 461-479, 10.1007/s00382-004-0392-2, 2004.

Meehl, G. A., Stocker, T. F., Collins, W. D., Friedlingstein, P., Gaye, A. T., Gregory, J. M., Kitoh, A., Knutti, R., Murphy, J. M., Noda, A., Raper, S. C. B., Watterson, I. G., J., W. A., and Zhao, Z.-C.: Global Climate Projections, in: Climate Change 2007: The Physical Science Basis. Contribution of Working Group I to Fourth Assessment Report of the Intergovernmental Panel on Climate Change, edited by: Solomon, S., Qin, D., Manning, M., Chen, Z., Marquis, M., Averyt, K. B., Tignor, M., and Miller, H. L., Cambridge United Kingdom and New York, NY, USA, New York, NY, USA, 747-845, 2007.

Meinshausen, M., Raper, S. C. B., and Wigley, T. M. L.: Emulating coupled atmosphere-ocean and carbon cycle models with a simpler model: — part 1 model description and calibration MAGICC6, Atmospheric Chemistry and Physics, 11, 1417–1456, 10.5194/acp–11–1417–2011, 2011a.

Meinshausen, M., Smith, S. J., Calvin, K., Daniel, J. S., Kainuma, M. L. T., Lamarque, J.-F., Matsumoto, K., Montzka, S. A., Raper, S. C. B., Riahi, K., Thomson, A., Velders, G. J. M., and van Vuuren, D. P. P.: The RCP greenhouse gas concentrations and their extensions from 1765 to 2300, Climatic Change, 10.1007/s10584-011-0156-z, 2011b.

Meissner, K. J., Weaver, A. J., Matthews, H. D., and Cox, P. M.: The role of land surface dynamics in glacial inception: a study with the UVic Earth System Model, Climate Dynamics, 21, 515-537, 10.1007/s00382-003-0352-2, 2003.

Menviel, L., Timmermann, A., Mouchet, A., and Timm, O.: Climate and marine carbon cycle response to changes in the strength of the Southern Hemispheric westerlies, Paleoceanography, 23, PA4201, 10.1029/2008pa001604, 2008.

Meyer, R., Joos, F., Esser, G., Heimann, M., Hooss, G., Kohlmaier, G., Sauf, W., Voss, R., and Wittenberg, U.: The substitution of high-resolution terrestrial biosphere models and

carbon sequestration in response to changing CO_2 and climate, Global Biogeochemical Cycles, 13, 785-802, 1999.

Müller, S. A., Joos, F., Edwards, N. R., and Stocker, T. F.: Water mass distribution and ventilation time scales in a cost-efficient, three-dimensional ocean model., Journal of Climate, 19 5479-5499, doi:10.1175/JCLI3911.1, 2006.

Myhre, G., Highwood, E. J., Shine, K. P., and Stordal, F.: New estimates of radiative forcing due to well mixed greenhouse gases, Geophysical Research Letters, 25, 2715-1718, 1998.

Najjar, R.G., and Orr, J.C.: OCMIP-2 Biotic-HOWTO: http://www.ipsl.jussieu.fr/OCMIP/, 1999.

Najjar, R. G., Jin, X., Louanchi, F., Aumont, O., Caldeira, K., Doney, S. C., Dutay, J. C., Follows, M., Gruber, N., Joos, F., Lindsay, K., Maier-Reimer, E., Matear, R. J., Matsumoto, K., Monfray, P., Mouchet, A., Orr, J. C., Plattner, G. K., Sarmiento, J. L., Schlitzer, R., Slater, R. D., Weirig, M. F., Yamanaka, Y., and Yool, A.: Impact of circulation on export production, dissolved organic matter, and dissolved oxygen in the ocean: Results from Phase II of the Ocean Carbon-cycle Model Intercomparison Project (OCMIP-2), Global Biogeochem. Cycles, GB3007, doi:10.1029/2006GB002857, 2007.

New, M., Hulme, M., and Jones, P.: Representing Twentieth-Century Space–Time Climate Variability. Part II: Development of 1901–96 Monthly Grids of Terrestrial Surface Climate, Journal of Climate, 13, 2217-2238, 10.1175/1520-0442(2000)013<2217:rtcstc>2.0.co;2, 2000.

O'Neill, B. C.: The Jury is Still Out on Global Warming Potentials, Climatic Change, 44, 427-443, 10.1023/a:1005582929198, 2000.

Oeschger, H., Siegenthaler, U., Schotterer, U., and Gugelmann, A.: A box diffusion model to study the carbon dioxide exchange in nature, Tellus, 27, 170-192, 1975.

Olivie, D. J. L., and Peters, G. P.: The impact of model variation in CO_2 and temperature impulse response functions on emission metrics, Earth Syst. Dynam. Discuss., 3, 935-977, 10.5194/esdd-3-935-2012, 2012.

Orr, J.C., Najjar, R. G., Sabine, C., and Joos, F.: OCMIP-2 Abiotic-HOWTO: http://www.ipsl.jussieu.fr/OCMIP/phase2/simulations/Abiotic/HOWTO-Abiotic.html, access: 18 July 2012, 1999.

Orr, J. C., Fabry, V. J., Aumont, O., Bopp, L., Doney, S. C., Feely, R. A., Gnanadesikan, A., Gruber, N., Ishida, A., Joos, F., Key, R. M., Lindsay, K., Maier-Reimer, E., Matear, R., Monfray, P., Mouchet, A., Najjar, R. G., Plattner, G. K., Rodgers, K. B., Sabine, C. L., Sarmiento, J. L., Schlitzer, R., Slater, R. D., Totterdell, I. J., Weirig, M. F., Yamanaka, Y., and Yool, A.: Anthropogenic ocean acidification over the twenty-first century and its impact on calcifying organisms, Nature, 437, 681-686, 2005.

Palmer, J. R., and Totterdell, I. J.: Production and export in a global ocean ecosystem model, Deep Sea Research Part I: Oceanographic Research Papers, 48, 1169-1198, 2001.

Parekh, P., Joos, F., and Müller, S. A.: A modeling assessment of the interplay between aeolian iron fluxes and iron-binding ligands in controlling carbon dioxide fluctuations during Antarctic warm events, Paleoceanography, 23, PA4202, 4201-4214, 10.1029/2007PA001531, 2008.

Peters, G. P., Aamaas, B., Berntsen, T., and Fuglestvedt, J. S.: The integrated global temperature change potential (iGTP) and relationships between emission metrics, Environmental Research Letters, 6, 044021, 10.1088/1748-9326/6/4/044021, 2011.

Petoukhov, V., Claussen, M., Berger, A., Crucifix, M., Eby, M., Eliseev, A. V., Fichefet, T., Ganopolski, A., Goosse, H., Kamenkovich, I., Mokhov, I. I., Montoya, M., Mysak, L. A., Sokolov, A., Stone, P., Wang, Z., and Weaver, A. J.: EMIC Intercomparison Project (EMIP-CO2): comparative analysis of EMIC simulations of climate, and of equilibrium and transient responses to atmospheric CO_2 doubling, Climate Dynamics, 25, 363-385, 10.1007/s00382-005-0042-3, 2005.

Plattner, G.-K., Knutti, R., Joos, F., Stocker, T. F., von Bloh, W., Brovkin, V., Cameron, D., Driesschaert, E., Dutkiewicz, S., Eby, M., Edwards, N. R., Fichefet, T., Hargreaves, J. C., Jones, C. D., Loutre, M. F., Matthews, H. D., Mouchet, A., Mueller, S. A., Nawrath, S., Price, A., Sokolov, A., Strassmann, K. M., and Weaver, A. J.: Long-term climate commitments projected with climate - carbon cycle models, Journal of Climate, 21, 2721-2751, 2008.

Plattner, G.-K., Stocker, T., Midgley, P., and Tignor, M.: IPCC Expert Meeting on the Science of Alternative Metrics: Meeting Report, IPCC Working Group I, Technical Support Unit, Bern, Switzerland, 2009.

Plattner, G. K., Joos, F., Stocker, T. F., and Marchal, O.: Feedback mechanisms and sensitivities of ocean carbon uptake under global warming, Tellus Series B-Chemical and Physical Meteorology, 53, 564-592, 2001.

Portmann, F., Siebert, S., Bauer, C., and Döll, P.: Global Data Set of Monthly Growing Areas of 26 Irrigated Crops, Institute of Physical Geography, University of Frankfurt, Frankfurt am Main, Germany, 2008.

Prather, M. J.: Lifetimes and time-scales in atmospheric chemistry, Philosophical Transactions of the Royal Society of London Series A, 365, 1705-1726, 2007.

Prather, M. J., Penner, J. E., Fuglestvedt, J. S., Kurosawa, A., Lowe, J. A., Höhne, N., Jain, A. K., Andronova, N., Pinguelli, L., Pires de Campos, C., Raper, S. C. B., Skeie, R. B., Stott, P. A., van Aardenne, J., and Wagner, F.: Tracking uncertainties in the causal chain from human activities to climate, Geophys. Res. Lett., 36, L05707, 10.1029/2008gl036474, 2009.

Prather, M. J., and Hsu, J.: Coupling of Nitrous Oxide and Methane by Global Atmospheric Chemistry, Science, 330, 952-954, 2010.

Prather, M. J., Holmes, C. D., and Hsu, J.: Reactive greenhouse gas scenarios: Systematic exploration of uncertainties and the role of atmospheric chemistry, Geophys. Res. Lett., 39, L09803, 10.1029/2012gl051440, 2012.

Prentice, I. C., Farquhar, G. D., Fasham, M. J., Goulden, M. I., Heimann, M., Jaramillo, V. J., Kheshgi, H. S., LeQuéré, C., Scholes, R. J., and Wallace, D. W. R.: The carbon cycle and atmospheric CO_2, in: Climate Change 2001: The Scientific Basis. Contribution of Working Group I to the Third Assessment Report of the Intergovernmental Panel on Climate Change, edited by: Houghton, J. T., Ding, Y., Griggs, D. J., Noguer, M., van der Linden, P. J., Dai, X., Maskell, K., and Johnson, C. A., Cambridge University Press, Cambridge, United Kingdom and New York, NY, USA, 183-237, 2001.

Press, W. H., Teukolsky, S. A., Vetterling, W. T., and Flannery, B. P.: Numerical Recipes, Cambridge University Press, Cambridge UK, 1986.

Raddatz, T., Reick, C., Knorr, W., Kattge, J., Roeckner, E., Schnur, R., Schnitzler, K. G., Wetzel, P., and Jungclaus, J.: Will the tropical land biosphere dominate the climate–carbon cycle feedback during the twenty-first century?, Climate Dynamics, 29, 565-574, 10.1007/s00382-007-0247-8, 2007.

Randerson, J. T., Thompson, M. V., Conway, T. J., Fung, I. Y., and Field, C. B.: The contribution of terrestrial sources and sinks to trends in the seasonal cycle of atmospheric carbon dioxide, Global Biogeochemical Cycles, 11, 535-560, 1997.

Reader, M. C., and Boer, G. J.: The modification of greenhouse gas warming by the direct effect of sulphate aerosols, Climate Dynamics, 14, 593-607, 10.1007/s003820050243, 1998.

Reisinger, A., Meinshausen, M., Manning, M., and Bodeker, G.: Uncertainties of global warming metrics: CO_2 and CH_4, Geophys. Res. Lett., 37, L14707, doi:10.1029/2010GL043803, 2010.

Reisinger, A., Meinshausen, M., and Manning, M.: Future changes in global warming potentials under representative concentration pathways, Environmental Research Letters, 6, 024020, 2011.

Ridgwell, A., and Hargreaves, J. C.: Regulation of atmospheric CO2 by deep-sea sediments in an Earth system model, Global Biogeochem. Cycles, 21, GB2008, 10.1029/2006gb002764, 2007.

Ridgwell, A., Hargreaves, J. C., Edwards, N. R., Annan, J. D., Lenton, T. M., Marsh, R., Yool, A., and Watson, A.: Marine geochemical data assimilation in an efficient Earth System Model of global biogeochemical cycling, Biogeosciences, 4, 87-104, 2007.

Ritz, S. P., Stocker, T. F., and Joos, F.: A coupled dynamical ocean–energy balance atmosphere model for paleoclimate studies, Journal of Climate, 24, 349-375, 2011.

Roy, T., Bopp, L., Gehlen, M., Schneider, B., Cadule, P., Frölicher, T., Segschneider, J., Tjiputra, J., Heinze, C., and Joos, F.: Regional impacts of climate change and atmospheric CO_2 on future ocean carbon uptake:A multi-model linear feedback analysis, J. Climate, 24, 2300-2318, 10.1175/2010JCLI3787.1, 2011.

Sarmiento, J. L., Orr, J. C., and Siegenthaler, U.: A perturbation simulation of CO_2 uptake in an ocean general circulation model, Journal of Geophysical Research, 97, 3621-3645, 1992.

Sarmiento, J. L., Hughes, T. M. C., Stouffer, R. J., and Manabe, S.: Simulated response of the ocean carbon cycle to anthropogenic climate warming, Nature, 393, 245-249, 1998.

Schimel, D., Alves, D., Enting, I. G., Heimann, M., Joos, F., Raynaud, D., Wigley, T. M. L., Prather, M., Derwent, R., Ehhalt, D., Fraser, P., Sanhueza, E., Zhou, X., Jonas, P., Charlson, R., Rhode, H., Sadasivan, S., Shine, K. P., Fouquart, Y., Ramaswamy, V., Solomon, S., Srinivasan, J., Albritton, D., Derwent, R., Isaksen, I., Lal, M., and Wuebbles, D.: Radiative Forcing of Climate Change, in: Climate Change 1995: The Science of Climate Change. Contribution of WGI to the Second Assessment Report of the Intergovernmental Panel on Climate Change, edited by: Houghton, J. T., Meira Filho, L. G., Callander, B. A., Harris, N., Kattenberg, A., and Maskell, K., Cambridge University Press, New York, 65-131, 1996.

Schmittner, A., and Stocker, T. F.: The stability of the thermohaline circulation in global warming experiments, Journal of Climate, 12, 1117-1133, 1999.

Schmittner, A., and Galbraith, E. D.: Glacial greenhouse gas fluctuations controlled by ocean circulation changes, Nature, 456, 373-376, 10.1038/nature07531, 2008.

Shaffer, G., and Sarmiento, J. L.: Biogeochemical cycling in the global ocean 1. A new, analytical model with continuous vertical resolution and high-latitude dynamics, J. Geophys. Res., 100, 2659-2672, 10.1029/94jc01167, 1995.

Shaffer, G., Olsen, S. M., and Pedersen, J. O. P.: Presentation, calibration and validation of the low-order, DCESS Earth System Model (Version 1), Geosci. Model Dev., 1, 17-51, 2008.

Shine, K., Fuglestvedt, J., Hailemariam, K., and Stuber, N.: Alternatives to the Global Warming Potential for Comparing Climate Impacts of Emissions of Greenhouse Gases, Climatic Change, 68, 281-302, 10.1007/s10584-005-1146-9, 2005.

Shine, K.: The global warming potential-the need for an interdisciplinary retrial, Climatic Change, 467-472, 2009.

Shine, K. P., Derwent, R. G., Wuebbles, D. J., and Morcrette, J.-J.: Radiative Forcing of Climate, in: Climate Change: The IPCC Scientific Assessment, edited by: Houghton, J. T., Jenkins, G. J., and Ephraums, J. J., Cambridge University Press, Cambridge, United Kingdom and New York, NY, USA, 41-68, 1990.

Siegenthaler, U., and Oeschger, H.: Predicting future atmospheric carbon dioxide levels, Science, 199, 388-395, 1978.

Siegenthaler, U., and Oeschger, H.: Biospheric CO_2 emissions during the past 200 years reconstructed by deconvolution of ice core data, Tellus, 46B, 103-142, 1987.

Siegenthaler, U., and Joos, F.: Use of a Simple-Model for Studying Oceanic Tracer Distributions and the Global Carbon-Cycle, Tellus Series B-Chemical and Physical Meteorology, 44, 186-207, 1992.

Sitch, S., Smith, B., Prentice, I. C., Arneth, A., Bondeau, A., Cramer, W., Kaplan, J. O., Levis, S., Lucht, W., Sykes, M. T., Thonicke, K., and Venevsky, S.: Evaluation of ecosystem dynamics, plant geography and terrestrial carbon cycling in the LPJ dynamic global vegetation model, Global Change Biology, 9, 161-185, 2003.

Solomon, S., Qin, D., Manning, M., Alley, R., Berntsen, T., Bindoff, N. L., Chen, Z., Chidthaisong, A., Gregory, J., Hegerl, G., Heimann, M., Hewitson, B., Hoskins, B., Joos, F., Jouzel, J., Kattsov, V., Lohmann, U., Matsuno, T., Molina, M., Nicholls, N., Overpeck, J., Raga, G., Ramaswamy, V., Ren, J., Rusticucci, M., Somerville, R., Stocker, T. F., Stouffer, R. J., Whetton, P., Wood, R. A., and Wratt, D.: Technical Summary, in: Climate Change 2007: The Physical Science Basis. Contribution of Working Group I to the Fourth Assessment Report of the Intergovernmental Panel on Climate Change, edited by: Solomon, S., Qin, D., Manning, M., Chen, Z., Marquis, M., Averyt, K. B., Tignor, M., and Miller, H. L., Cambridge University Press, Cambridge United Kingdom and New York, NY, USA, 19-91, 2007.

Steinacher, M.: Modeling changes in the global carbon cycle-climate system, PhD, Philosophisch-naturwissenschaftliche Fakultät, University of Bern, Bern, 212 pp., 2011.

Steinacher, M., Joos, F., and Stocker, T. F.: Significantly lower allowable carbon emissions under multiple climate targets, Nature, submitted, 2012.

Stocker, B. D., Strassmann, K., and Joos, F.: Sensitivity of Holocene atmospheric CO_2 and the modern carbon budget to early human land use: analyses with a process-based model, Biogeosciences, 8, 69-88, 2011.

Stocker, T. F., Wright, D. G., and Mysak, L. A.: A Zonally Averaged, Coupled Ocean Atmosphere Model for Paleoclimate Studies, Journal of Climate, 5, 773-797, 1992.

Formatted: German (Switzerland)

Strassmann, K. M., Joos, F., and Fischer, G.: Simulating effects of land use changes on carbon fluxes: past contributions to atmospheric CO_2 increases and future commitments due to losses of terrestrial sink capacity, Tellus B, 60B, 583-603, 2008.

Strassmann, K. M., Plattner, G. K., and Joos, F.: CO_2 and non-CO_2 radiative forcing agents in twenty-first century climate change mitigation scenarios, Climate Dynamics, 33, 737-749, 2009.

Tanaka, K., Kriegler, E., Bruckner, T., Hooss, G., Knorr, W., and Raddatz, T.: Aggregated Carbon Cycle, Atmospheric Chemistry, and Climate Model (ACC2) – description of the forward and inverse modes, Max Planck Institute for Meteorology, Hamburg, 188, 2007.

Tanaka, K.: Inverse Estimation for the Simple Earth System Model ACC2 and Its Applications, Ph.D. , Universität Hamburg, Hamburg, 296 pp., 2008.

Tanaka, K., O'Neill, B., Rokityanskiy, D., Obersteiner, M., and Tol, R.: Evaluating Global Warming Potentials with historical temperature, Climatic Change, 96, 443-466, 10.1007/s10584-009-9566-6, 2009a.

Tanaka, K., Raddatz, T., O'Neill, B. C., and Reick, C. H. I.: Insufficient forcing uncertainty underestimates the risk of high climate sensitivity, Geophys. Res. Lett., 36, L16709, 10.1029/2009GL039642, 2009b.

Tanaka, K., Peters, G. P., and Fuglestvedt, J. S.: Policy Update: Multicomponent climate policy: why do emission metrics matter?, Carbon Management, 1, 191-197, 10.4155/cmt.10.28, 2010.

Tanaka, K., Berntsen, T., Fuglestvedt, J. S., and Rypdal, K.: Climate Effects of Emission Standards: The Case for Gasoline and Diesel Cars, Environmental Science & Technology, 46, 5205-5213, 10.1021/es204190w, 2012.

Tarnocai, C., Canadell, J. G., Schuur, E. A. G., Kuhry, P., Mayhitova, G., and Zimov, S.: Soil organic carbon pools in the northern circumpolar permafrost region, Global Biogeochem. Cycles, 23, 1-11, 2009.

Tol, R., Berntsen, T., O'Neill, B. C., Fuglestvedt, J. S., and Shine, K. P.: A unifying framework for metrics for aggregating the climate effect of different emissions, Environmental Research Letters, submitted, 2012.

Tschumi, T., Joos, F., and Parekh, P.: How important are Southern Hemisphere wind changes for low glacial carbon dioxide? A model study, Paleoceanography, 23, PA4208, doi:10.1029/2008PA001592, 2008.

Tschumi, T., Joos, F., Gehlen, M., and Heinze, C.: Deep ocean ventilation, carbon isotopes, marine sedimentation and the deglacial CO_2 rise, Clim. Past, 7, 771-800, 10.5194/cp-7-771-2011, 2011.

UNFCCC, FCCC/CP/1997/7 decision 4/CP.5, Guidelines for the preparation of national communications from Parties included in Annex I to the Convention. Secretary of the United Nations Framework Convention on Climate Change, Bonn, Germany: http://unfccc.int/resource/docs/cop5/07.pdf, 1997.

UNFCCC, FCCC/CP/1997/7/Add.1, Methodological issues related to the Kyoto Protocol, Secretary of the United Nations Framework Convention on Climate Change, Bonn, Germany: http://unfccc.int/resource/docs/cop3/07a01.pdf, 1998.

UNFCCC, FCCC/CP/2002/7/Add.2 Decision 17/CP.8, Guidelines for the preparation of national communications from Parties not included in Annex I to the Convention. Secretary of the United Nations Framework Convention on Climate Change, Bonn, Germany: http://unfccc.int/resource/docs/cop8/07a02.pdf#page=2, 2002.

UNFCCC, FCCC/KP/CMP/2011/10/Add.1, decision 4/CMP.7, Greenhouse gases, sectors and source categories, common metrics to calculate the carbon dioxide equivalence of anthropogenic emissions by sources and removals by sinks, and other methodological issues. Secretary of the United Nations Framework Convention on Climate Change, Bonn, Germany: http://unfccc.int/resource/docs/2011/cmp7/eng/10a01.pdf#page=23, 2011a.

UNFCCC, FCCC/CP/2011/9/Add.2, Decision 15/CP.17, Revision of the UNFCCC reporting guidelines on annual inventories for Parties included in Annex I to the Convention. Secretary of the United Nations Framework Convention on Climate Change, Bonn, Germany: http://unfccc.int/resource/docs/2011/cop17/eng/09a02.pdf#page=23, 2011b.

Van Vuuren, D. P., Meinshausen, M., Plattner, G.-K., Joos, F., Strassmann, K. M., Smith, S. J., Wigley, T. M. L., Raper, S. C. B., Riahi, K., de la Chesnaye, F., den Elzen, M., Fujino, J., Jiang, K., Nakicenovic, N., Paltsev, S., and Reilly, J. M.: Temperature increase of 21st century mitigation scenarios, Proc Natl Acad Sci USA, 105, 15258-15262, 2008.

Ver, L. M. B., Mackenzie, F. T., and Lerman, A.: Biogeochemical responses of the carbon cycle to natural and human perturbations; past, present, and future, American Journal of Science, 299, 762-801, 1999.

Wania, R., Ross, I., and Prentice, I. C.: Integrating peatlands and permafrost into a dynamic global vegetation model: 1. Evaluation and sensitivity of physical land surface processes, Global Biogeochem. Cycles, 23, GB3014, 10.1029/2008gb003412, 2009a.

Wania, R., Ross, I., and Prentice, I. C.: Integrating peatlands and permafrost into a dynamic global vegetation model: 2. Evaluation and sensitivity of vegetation and carbon cycle processes, Global Biogeochem. Cycles, 23, GB3015, 10.1029/2008gb003413, 2009b.

Weaver, A. J., Eby, M., Wiebe, E. C., Bitz, C. M., Duffy, P. B., Ewen, T. L., Fanning, A. F., Holland, M. M., MacFadyen, A., Matthews, H. D., Meissner, K. J., Saenko, O., Schmittner, A., H., W., and Yoshimori, M.: The UVic Earth System Climate Model: Model description, climatology and application to past, present and future climates, Atmosphere-Ocean, 39, 361-428, 2001.

Weaver, A. J., Sedlacek, J., Eby, M., Alexander, K., Fichefet, T., Joos, F., Kawamiya, M., Matsumoto, K., Steinacher, M., Tachiiri, K., Tokos, K., and Zickfeld, K.: Stability of the Atlantic Meridional Overturning Circulation: A Model Intercomparison, Geophys. Res. Lett., to be submitted, 2012.

Weyant, J. R., de la Chesnaye, F. C., and Blanford, G. J.: Overview of emf-21: Multigas mitigation and climate policy, Energy Journal, 27, 1-32, 2006.

Williamson, M. S., Lenton, T. M., Shepherd, J. G., and Edwards, N. R.: An efficient numerical terrestrial scheme (ENTS) for Earth system modelling, Ecological Modelling, 198, 362-374, 10.1016/j.ecolmodel.2006.05.027, 2006.

Wuebbles, D. J., Jain, A. K., Patten, K. O., and Grant, K. E.: Sensitivity of direct global warming potentials to key uncertainties, Climatic Change, 29, 265-297, 1995.

Zickfeld, K., Eby, M., Weaver, A. J., Crespin, E., Fichefet, T., Goosse, H., Edwards, N. R., Holden, P. B., Eliseev, A. V., Mokhov, I. I., Feulner, G., Kienert, H., Perrette, M., Schneider

von Deimling, T., Forest, C. E., Joos, F., Spahni, R., Steinacher, M., Kawamiya, M., Tachiiri, K., Kicklighter, D., Monier, E., Schlosser, A., Sokolov, A. P., Matsumoto, K., Tokos, K., Olsen, S. M., Pedersen, J. O. P., Shaffer, G., Ridgwell, A., Zeng, N., and Zhao, F.: Long-term Climate Change Commitment and Reversibility: An EMIC Intercomparison, Journal of Climate, submitted, 2012.

Table 1: Overview on main simulations. All simulations are started from a preindustrial state.

Simulation	Model setup
	PD100, standard impulse
run 1	Atmospheric CO2 prescribed to follow the historical evolution up to year 2010 and kept at 389 ppm thereafter. Compatible emissions are diagnosed. Non-CO_2 and land use forcing constant after 2010.
run 2	Model is forced with diagnosed emissions from run 1 and atmospheric CO_2 is computed. Other forcings as in run 1.
run 3	Setup as in run 2. An emission pulse of 100 GtC is added in 2015 AD
	PI100 and PI5000 preindustrial impulses
run 4~~5~~	Control simulation under preindustrial conditions and freely evolving CO_2
run 5~~6~~	As run 4~~5~~. An emission pulse of 100 GtC is added in year 10
run 6~~7~~	As run 4~~5~~. An emission pulse of 5000 GtC is added in year 10

Table 2: Characterization of the climate models: physical components, ΔT_{2x} denotes the equilibrium climate sensitivity for a nominal doubling of CO_2. ΔT_{2x} reported here for the Bern3D-LPJ, CLIMBER2, DCESS, LOVECLIM, MESMO1.0, UVic2.9 are those determined by doubling preindustrial CO_2 in a simulation over 1000 year (Eby et al., 2012).

Model	Atmosphere[a]	Ocean and Sea ice[b]	Land surface	ΔT_{2x} (Celsius)
ACC2	Land-ocean energy balance model	Diffusion model, simple sea-ice correction factor	Simple land surface albedo parameterization	4.04
Bern-SAR	1-box	upwelling-diffusion-entrainment model	n/a	n/a
Bern2.5D-LPJ (or Bern2.5CC)	1-dim (zonally and vertically averaged) energy moisture-balance model, 7.5° x 15°	2-d friction-geostrophic circulation model with thermodynamic sea ice; 3 ocean basins, connected in Southern Ocean, 7.5° x 15°, 14 vertical levels	n/a	3.2
Bern3D-LPJ	2-dim energy-moisture balance model; 10° x (3-19)°	3-d friction-geostrophic circulation model with sea ice; 10° x (3-19)°, 32 levels	1-layer soil temperature, no soil moisture storage, river routing	3.3
CLIMBER-2-LPJmL	3-dim statistical-dynamical model; 10° x 51°, 10 layers	2-d friction-geostrophic circulation model with sea ice; 2.5°, 21 levels	1-layer soil temperature, 2-layer soil hydrology, snow cover, river routing	3.0
DCESS	2-box energy-moisture balance model	2-box parameterized circulation and exchange, no explicit sea ice; 55 levels	No explicit soil temperature and moisture calculation	2.8
GENIE	2-dim energy-moisture balance model ; 10° x (3-19)°	3-d friction-geostrophic circulation model with sea ice; 10° x (3-19)°, 16 levels	1-layer soil temperature, bucket soil moisture model, river routing	4.0 ± 0.8
HADGEM2-ES	3D GCM, 38 vertical levels, N96 (1.25 x 1.875 degree) resolution	3-d ocean GCM, 1-degree, increasing to 1/3 degree at equator. 40 vertical levels	MOSES-2: tiled land-surface with 4-layer soil temperature and hydrology, river routing.	4.58
LOVECLIM 1.1	3-dim quasi-geostrophic circulation model ; 5.6° x 5.6°, 3 levels	3-d primitive equation circulation model with sea ice; 3° x 3°, 20 levels	1-layer soil temperature, bucket soil moisture model, river routing	1.5
MAGICC6	4-box energy-balance model.	2 hemispheric columns, upwelling-diffusion-entrainment, 50 levels, simple sea-ice correction factor.	Simple land surface albedo parameterization; soil temperature/moisture only parameterized for permafrost area.	1.9 to 5.7 (Average 2.88)
MESMO 1.0	2-dim energy-moisture balance model; 10° x (3-19)°	3-d friction-geostrophic circulation model with sea ice; 10° x (3-19)°, 16 levels	1-layer soil temperature, bucket soil moisture model, river routing	3.7
MPI-ESM	ECHAM6 3D GCM T63L47	MPIOM 3-d primitive equation GCM + sea ice GR15L40 grid	JSBACH: tiled land-surface, 5-layer soil temperature, 1-layer hydrology, HD river routing model	3.4
NCAR CSM1.4	CCM3 T31, L18	NCOM 3.6° lon 0.8-1.8° lat, 25 levels with sea ice	LSM T31	2.0
TOTEM	n/a	n/a	n/a	n/a
UVic 2.9	2-dim energy-moisture balance model ; 1.8° x 3.6°	3-d primitive equation circulation model with dynamic & thermodynamic sea ice 1.8° x 3.6°, 19 levels	1-layer soil temperature, complex soil moisture model, river routing	3.6

Table 3: Characterization of the carbon cycle models.

Model	Land Carbon Cycle	Land use (LU) (LU area data and anthropogenic LU classes	Marine Biogeochemistry & Ecosystem	Sediment / Weathering
ACC2	4-box, ß-factor (CO_2 fertilization) and Q10 temperature sensitivity of soil respiration)	n/a	4-box global atmosphere-ocean, temperature-sensitive carbonate chemistry	n/a
BernSAR	4-box, ß-factor (CO_2 fertilization)	n/a	n/a (perturbation approach)	n/a
Bern2.5D-LPJ (or Bern2.5CC)	Dynamic Vegetation Model, 9 Plant Functional Types, multiple-litter/soil pools, 3.75 ^{o} x 2.5^o	n/a	Prognostic export production, P, DIC, DOC, (POC), ALK, O_2, no ecosystem	n/a
Bern3D-LPJ	Dynamic Vegetation Model, 9 Plant Functional Types, multiple-litter/soil pools, 3.75 ^{o} x 2.5^o	Hyde 3.1 3 LU classes, products	Prognostic export production, P, Fe, Si, DIC, DOC,POC ALK, O_2, no ecosystem	yes / diagnosed
CLIMBER2-LPJmL	Dynamic Vegetation Model 9 Plant Functional Types, 12 Crop Functional Types, 0.5 ^{o} x 0.5^o	Landuse dataset 1700-2005 (Portman et al 2008, Fader et al. 2010)	Prognostic export production, P, DIC, DOC,POC, ALK, O_2, NPZD ecosystem	yes / yes
DCESS	4-box, ß-factor (CO_2 fertilization) and Q10 temperature sensitivity of soil respiration	n/a	Prognostic export production, P, O_2, POC PIC, DIC and ALK, no ecosystem	yes / yes
GENIE	Efficient Numerical Terrestrial Scheme (ENTS). 1 Plant Functional Type; 10° x (3-19) °	PMIP3 (800-1699), CMIP5 (1500-2005) 1 LU class	Prognostic export production, P, Fe, DIC, DOC, POC, ALK, O_2, no ecosystem	yes / diagnosed
HADGEM2-ES	TRIFFID Dynamic global vegetation model, with 5 PFTs. Half-hourly carbon fluxes from vegetation physiology and soil respiration. 4-pool soil carbon model.	Hurtt et al harmonized; Anthropogenic agricultural fraction	DiatHadOCC (Totterdell and Halloran)	n/a
LOVECLIM1.1	Dynamic Vegetation Model 2 Plant Functional Types; 5.6 ° x 5.6 °	n/a	Prognostic P, DIC, POC, DOC, ALK, O2, export production / no ecosystem	preservation /no
MAGICC6	4-box global carbon cycle model, calibrated towards 9 C4MIP carbon cycle model's pools and fluxes.	n/a.	n/a (perturbation approach)	n/a.
MESMO 1.0	Efficient Numerical Terrestrial Scheme (ENTS). 1 Plant Functional Type; 10° x (3-19) °	n/a	Prognostic export production, P, Fe, Si, N, DIC, DOC,POC, ALK, no ecosystem	n/a
MPI-ESM	JSBACH:, 3 living, 4 litter, 1 slow soil carbon pool, dynamical vegetation, 12 PFTs	Prescribed 1994 distribution of agricultural land	Full carbonate chemistry, NPZD type ecosystem, PO4, NO3, Fe colimitation of biological production	yes / diagnosed
NCAR CSM1.4	CASA, prescribed veg. distribution	n/a	Modified OCMIP-2 with prognostic epxort	n/a
TOTEM	Global carbon-nitrogen-phosphorus cycle model, explicit treatments of rivers, erosion, fertilizer appl.	n/a	Global carbon-nitrogen-phosphorus cycle model, explicit treatments of coastal zone	param./parameterized
UVic 2.9	Dynamic Vegetation Model, 5 Plant Functional Types, 3.6 ^{o} x 1.8^o, 3 carbon pools per PFT, 1 soil carbon pool	Hyde 3.1, 2 grass PFTs used for agriculture, LUC carbon split evenly to soil and atmosphere	NPZD, 2 nutrient and 2 phytoplankon classes, prognostic PO_4, NO_3, O_2, DIC, ALK, denitrification	yes / diagnosed

Table 4**:** Time-integrated airborne fraction for different time horizons in units of years and corresponding uncertainty ranges. Multiplication with 1.77 10^{-15} W m^{-2} kg-CO_2^{-1} yields the Absolute Global Warming Potential (AGWP) for CO_2. Values in parentheses for the Bern3D-LPJ, GENIE, and MAGICC6 ensembles represent median and 5% to 95% confidence range. The median for each of these models is included in the multi-model mean; reference setup of the Bern3D-LPJ is not included. The errors of the multi-model mean represent ± two standard deviations. Our best estimate for the mean is the value from the fit to the multi-model mean and the best estimate for the 5 to 95% confidence range is the average range from the different methods centered at the mean.

Time Horizon	20 yr	50 yr	100 yr	500 yr	1000 yr
			time-integrated IRF_{CO2} (yr)		
NCAR CSM1.4	13.8	27.8	46.6	n/a	n/a
HadGEM2-ES	14.7	30.9	53.3	n/a	n/a
MPI-ESM	14.5	29.2	48.8	n/a	n/a
Bern3D-LPJ (reference)	15.4	34.3	61.9	241	417
Bern3D-LPJ ensemble	15.1	32.7	57.6	205	n/a
	(14.0-16.0)	(28.9-36.0)	(48.9-65.6)	(160-265)	n/a
Bern2.5D-LPJ	13.9	29.7	51.1	163	283
CLIMBER2-LPJ	13.0	26.8	49.2	181	306
DCESS	14.6	31.8	56.3	199	329
GENIE ensemble	13.6	28.9	50.5	173	n/a
	(10.9-17.6)	(21.7-41.4)	(38.3-77.9)	(143.68-271)	n/a
LOVECLIM	13.5	27.9	45.3	170	280
MESMO	15.1	33.6	61.1	238	410
UVic2.9	13.7	29.5	53.0	209	376
ACC2	13.7	27.9	46.5	151	252
Bern-SAR	14.0	29.0	48.9	161	270
MAGICC6 ensemble	14.0	29.6	51.8	199	nan
	(12.0-16.1)	(23.6-35.7)	(40.0-64.2)	(148-233)	n/a
TOTEM2	16.9	38.3	66.6	180	281
multi-model mean	14.3±1.8	30.2±5.7	52.4±11.3	186±48	308±94
			Uncertainty ranges (yr)		
multi-model range	3.6	11.3	22.6	96	189
Bern3D-LPJ	2.1	7.2	16.7	105	n/a

GENIE	6.7	19.8	39.5	128	172
MAGICC6	4.1	12.1	24.2	85	n/a
Linear Progamming	n/a	n/a	24.0	n/a	n/a
Average of ranges	4.1	12.6	25.8	103	180
in % of multi-model mean	28.8	41.6	49.1	56	58
	Best estimates for time-integrated IRF_{CO2} (yr)				
mean	14.2~~3~~	30.3~~2~~	52.4	18~~46~~	310~~08~~
5-95% confidence range	(12.1~~2~~-16.2~~3~~)	(24~~3~~.09-36.6~~5~~)	(39.5~~6~~-65.3)	(132~~4~~-235~~7~~)	(2201~~8~~-400~~398~~)
	Best estimates forAGWP of CO_2 (10^{-15} yr W m^{-2} kg-CO_2^{-1})				
mean	25.2	53.5~~4~~	92.5~~7~~	324~~8~~	548~~6~~
5-95% confidence range	(20.8-29.6)	(41.2~~1~~-65.9~~8~~)	(68~~8.1~~-117)	(227~~31~~-421~~5~~)	(378~~6~~-715~~3~~)

Table 5: Coefficients to fit multi-model mean responses to a pulse emission of 100 GtC following Equation 11 in the main text and for 0< *t* <1000 yr. The mean relative error of the fit is given in percent. The error is calculated from annual values as the average of the absolute differences between fit (*f*) and multi-model mean (*m*) divided by the multi-model mean ($1/N \sum(m-f)/m$)). Multiplication by (12/(100 x 44 x 10^{12}) yields the change per kg-CO_2 for ocean and land carbon storage, surface air temperature (SAT), time-integrated SAT (iSAT), steric sea level rise (SSLR), and ocean heat content (OHC). The timescales τ_i are given in years and units of a_i are indicated in parentheses in the first column.

	rel. error	a_0	a_1	a_2	a_3	τ_1	τ_2	τ_3
IRF_{CO2}	0.6	0.2173	0.2240	0.2824	0.2763	394.4	36.54	4.304
Ocean (GtC)	0.6	60.29	-26.48	-17.45	-16.35	390.5	100.5	4.551
Land (GtC)	1.3	17.07	332.1	-334.1	-15.09	74.76	70.31	6.139
SAT (°C)	1.8	0.1383	0.05789	-0.06729	-0.1289	264.0	5.818	0.8062
iSAT (° C yr)	1.8	3934	-4432	777.7	-280.0	16080	2294	1144
SSLR (cm)	1.5	5.259	-3.789	-0.9351	-0.5350	581.7	75.71	5.963
OHC(10^{22} J)	1.0	42.63	-32.86	-6.589	-3.182	420.4	54.82	6.340

Formatted: Font: Italic

Formatted: Font: Italic

Formatted: Font: Italic

Formatted: Font: Italic

Table 6~~5~~: Response in global mean surface air temperature to an emission pulse of 100 GtC added to an atmospheric concentration of 389 ppm.

Time Horizon	20 yr	50 yr	100 yr	500 yr	1000 yr
			temperature response (^{o}C)		
NCAR CSM1.4	0.10	0.14	0.01	n/a	n/a
HadGEM2-ES	0.31	0.18	0.59	n/a	n/a
MPI-ESM	0.27	0.09	0.10	n/a	n/a
Bern3D-LPJ (reference)	0.26	0.26	0.24	0.23	0.17
Bern3D-LPJ ensemble	0.18	0.18	0.17	0.14	n/a
	(0.10-0.27)	(0.10-0.30)	(0.09-0.33)	(0.06-0.39)	n/a
Bern2.5D-LPJ	0.18	0.17	0.17	0.13	0.13
CLIMBER2-LPJ	0.16	0.17	0.18	0.12	0.11
DCESS	0.21	0.22	0.21	0.15	0.12
GENIE ensemble	0.22	0.23	0.22	0.16	n/a
	(0.17-0.35)	(0.17-0.46)	(0.15-0.49)	(0.12-0.29)	n/a
LOVECLIM	0.09	0.06	0.13	0.07	0.08
MESMO	0.26	0.27	0.28	0.23	0.2
UVic2.9	0.19	0.19	0.18	0.19	0.19
ACC2	0.23	0.21	0.18	0.12	n/a
Bern-SAR	n/a	n/a	n/a	n/a	n/a
MAGICC6 ensemble	0.19	0.17	0.16	0.13	n/a
	(0.14-0.26)	(0.12-0.27)	(0.10-0.26)	(0.09-0.26)	n/a
TOTEM2	n/a	n/a	n/a	n/a	n/a
multi-model mean	0.20+0.12	0.17+0.11	0.20+0.26	0.14+0.08	0.14+0.08
			Uncertainty ranges (^{o}C)		
Multi-model range	0.24	0.21	0.52	0.17	0.16
Bern3D-LPX	0.17	0.21	0.25	0.33	n/a
GENIE	0.18	0.28	0.34	0.16	0.13
MAGICC6	0.12	0.15	0.16	0.17	n/a
Average of ranges	0.18	0.21	0.32	0.21	0.14
in % of multi-model mean	90	123	160	144	101
			Best estimates for temperature response (^{o}C)		

mean	0.192	0.197	0.182	0.154	0.14
5-95% confidence range	(0.101-0.289)	(0.097-0.3028)	(0.024-0.346)	(0.054-0.265)	(0.07-0.21)
	Best estimates for AGTP of CO_2 (10^{-15} °C kg-CO_2^{-1})				
mean	0.525	0.5146	0.4955	0.4038	0.38
5-95% confidence range	0.2730-0.769	0.2419-0.8176	0.0511-0.928	0.131-0.7068	0.19-0.57

Table 7: Response in time-integrated global mean surface air temperature to an emission pulse of 100 GtC added to an atmospheric concentration of 389 ppm.

Formatted: Not Highlight

Time Horizon	20 yr	50 yr	100 yr	500 yr	1000 yr
	time-integrated temperature response (°C yr)				
NCAR CSM1.4	2.53	7.36	10.6	n/a	n/a
HadGEM2-ES	4.24	12.4	30.3	n/a	n/a
MPI-ESM	3.83	8.84	19.1	n/a	n/a
Bern3D-LPJ (reference)	4.11	12.1	24.5	121	219
Bern3D-LPJ ensemble	3.20	8.61	17.3	79.7	n/a
	(2.1-4.6)	(5.1-13.5)	(9.5-29.3)	(38-175)	n/a
Bern2.5D-LPJ	3.15	8.40	17.1	71.0	133
CLIMBER2-LPJ	3.05	7.96	16.5	74.2	134
DCESS	3.38	9.96	20.6	89.8	158
GENIE ensemble	3.77	10.54	21.6	96.6	n/a
	(3.0-5.2)	(8.2-17.5)	(17-42)	(76 -195)	n/a
LOVECLIM	0.22	3.46	7.83	36.8	80.8
MESMO	4.41	12.5	26.0	129	236.
UVic2.9	3.40	9.17	18.5	94.8	189.
ACC2	3.99	10.55	20.0	76.9	n/a

Bern-SAR	n/a	n/a	n/a	n/a	n/a
MAGICC6 ensemble	3.64	8.96	17.2	74.4	n/a
	(2.7-4.7)	(6.6-12.7)	(12-26)	(49-129)	n/a
TOTEM2	n/a	n/a	n/a	n/a	n/a
multi-model mean	3.29+2.03	9.13+4.45	18.7+11.1	82.2+44.5	158+91
	Uncertainty ranges (^{o}C yr)				
Multi-model range	4.06	8.9	22.1	89.1	182
Bern3D-LPX	2.52	8.34	19.8	137	n/a
GENIE	2.13	9.27	24.7	119	184
MAGICC6	2.00	6.11	14.4	80.4	n/a
Average of ranges	2.68	8.16	20.3	106	183
in % of multi-model mean	81.4	89.3	108	130	116
	Best estimates for time-integrated temperature response (^{o}C yr)				
mean	3.31	8.67	17.4	82.2	155
5-95% confidence range	(2.2-4.8)	(4.8-13.5)	(7.3-27.5)	(29-135)	(64-247)
	Best estimates for time-integrated AGTP of CO_2 (10^{-15} ^{o}C yr kg-CO_2^{-1})				
mean	9.03	23.6	47.6	224	424
5-95% confidence range	5.38-13.2	12.5-34.7	19.0-75.2	79.0-369	174-673

Formatted: English (U.S.)

Formatted: English (U.S.)

Formatted: English (U.S.)

Formatted: English (U.S.)

Formatted: English (U.S.)

Formatted: English (U.S.)

Table 8~~6~~: Response in ocean heat content and steric sea level rise to an emission pulse of 100 GtC added to an atmospheric concentration of 389 ppm. Multiplication by (12 / (100 x 44 x10^{12}) yields the change per kg-CO_2.

Time Horizon	20 yr	50 yr	100 yr	500 yr	1000 yr
	Best estimates for steric sea level rise (cm)				
mean	0.86~~7~~	1.30~~28~~	1.81~~75~~	3.65~~58~~	4.58~~5~~
5-95% confidence range	(0.37~~8~~-1.35~~6~~)	(0.46~~4~~-2.15~~3~~)	(0.58~~2~~-3.03~~2.97~~)	(1.17~~0~~-6.14~~07~~)	(0.99~~6~~-8.18~~5~~)
	Best estimates for ocean heat content change (10^{22} J)				
mean	6.59~~78~~	10.8~~6~~	15.7~~4~~	32.6~~2~~	39.6~~3~~
5-95% confidence range	(4.07~~26~~-9.49~~30~~)	(5.20~~5~~-16.3~~1~~)	(6.30~~0~~-25.2~~4.9~~)	(12.2~~1.8~~-52.9~~5~~)	(13.58-65.3~~0~~)

Table 9~~7~~: Sensitivity of GWP on the time horizon *TH* and the perturbation life time of a gas.

Gas/*TH*		20 yr	50 yr	100 yr	500 yr	1000 yr
	life time (yr)	*ratio of GWP(TH) to GWP(TH*=100)				
CH_4	12	2.98~~7~~	1.71	1.00	0.28	0.17
N_2O	114	1.01	1.05	1.00	0.48	0.29
SF_6	3200	0.74	0.87	1.00	1.33	1.48

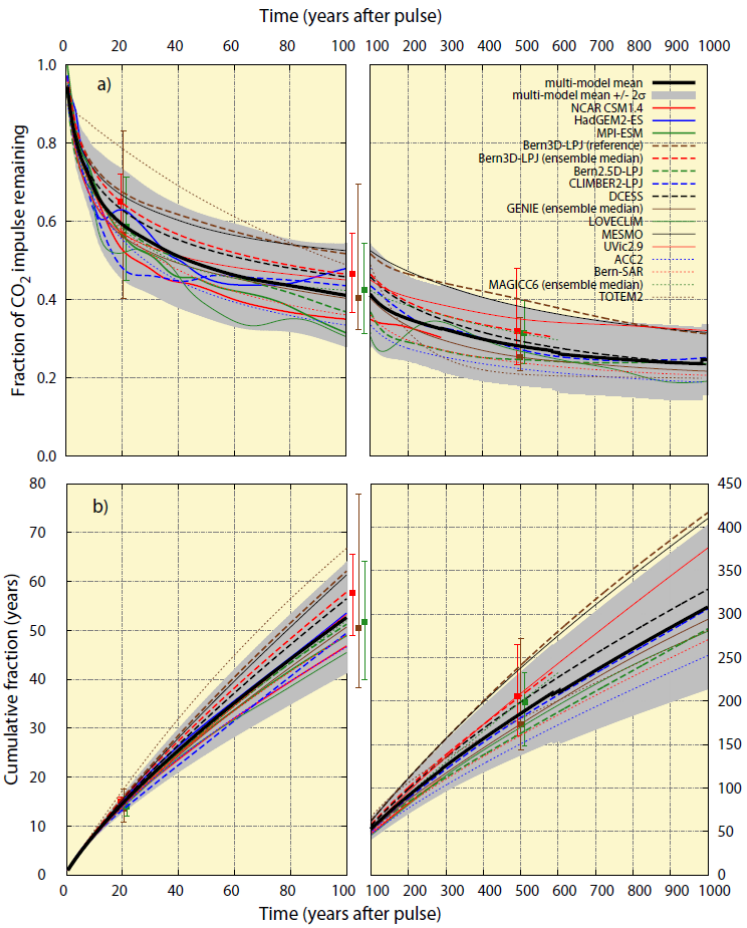

Figure 1: a) The evolution of the impulse response function for CO_2, IRF_{CO2}, for an emission pulse of 100 GtC added to an atmospheric background concentration of 389 ppm (PD100) for a range of Earth System Models (thick solid), EMICs (dashed and thin solid), and reduced-form models (dotted). The multi-model mean, computed by giving each available model equal weight, and the corresponding ± two standard deviation range is shown by the black solid line and the grey shading. Note that not all models were run to year 1000 and thus the number of models included in the average changes with time. For three models, Bern3D-LPJ (red), GENIE (brown) and MAGICC (green), an ensemble of simulations is available and the ensemble median and 5 to 95% confidence intervals are given by error bars for year 20, 100, and 500. Only the ensemble medians are included in the multi-model mean and range. b) Same as a) but for the time-integrated IRF_{CO2}.

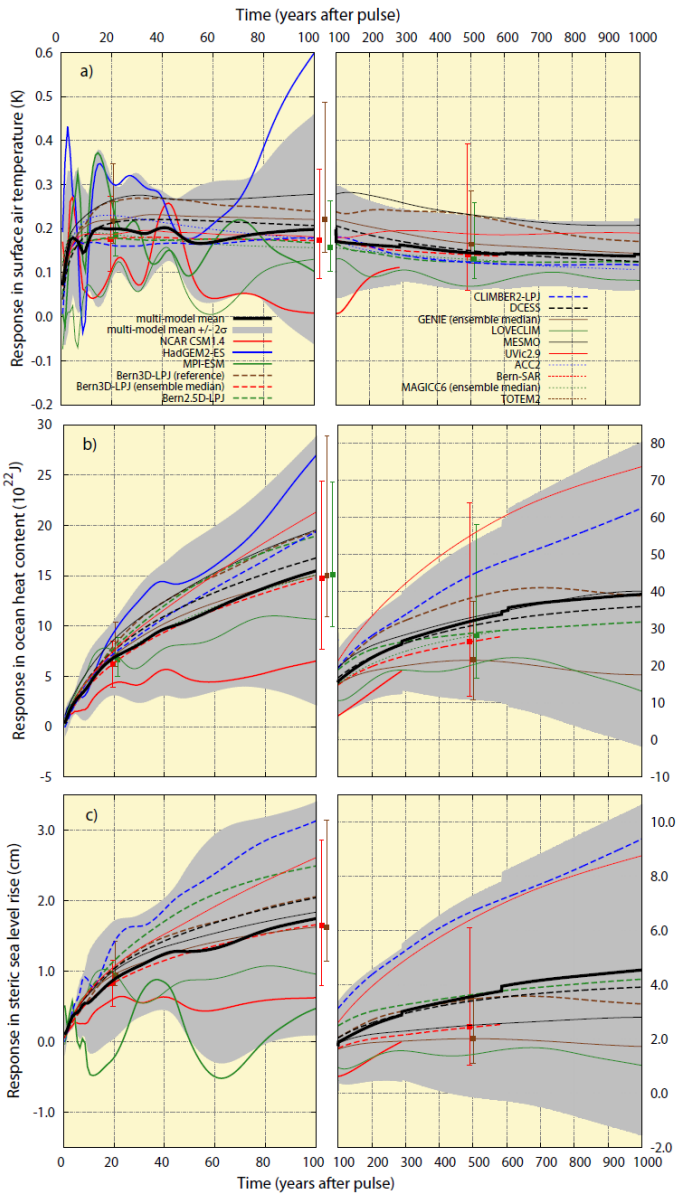

Figure 2: As figure 1 but for the perturbation in global mean surface air temperature (a), in ocean heat content (b), and in steric sea level rise (c). Results are for a CO_2 emission pulse of 100 GtC added to a current CO_2 concentration of 389 ppm (PD100). We note that the signal-to-noise ratio is small for the models that feature a dynamic atmosphere (HadGEM2-ES, MPI-ESM, NCAR-CSM1.4, and LOVECLIM) and the plotted evolutions for these models represent both the forced response and a contribution from the models' internal (unforced) climate variability. Small abrupt changes in the multi-model mean and confidence range arise from a change in the number of model simulations; different groups run their model over different periods, pending on CPU availability.

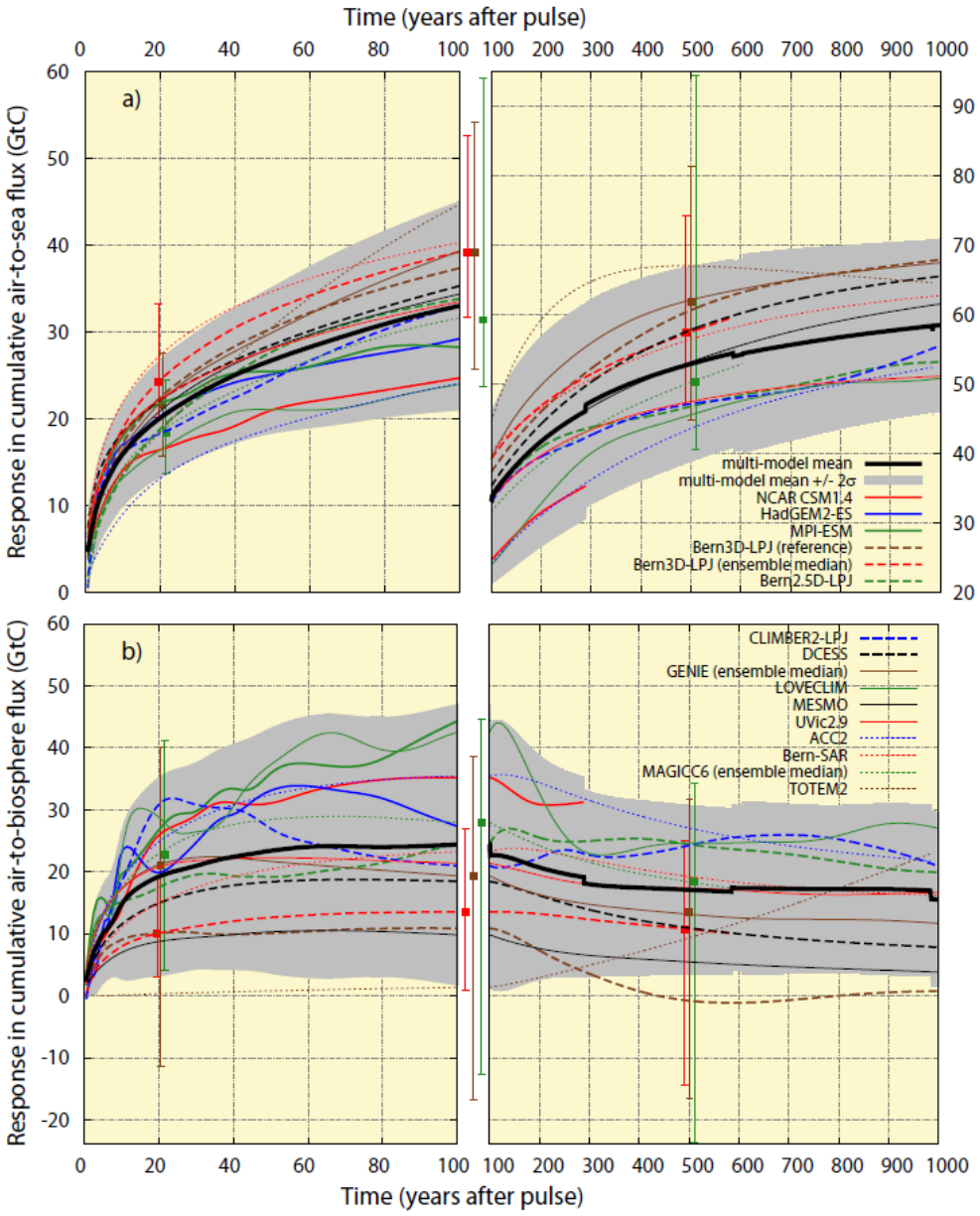

Figure 3: as figure 1, but for the time-integrated perturbation in air-to-sea (a) and air-to-land biosphere carbon fluxes (b). Results are for a CO_2 emission pulse of 100 GtC added to a present day CO_2 concentration of 389 ppm (PD100).

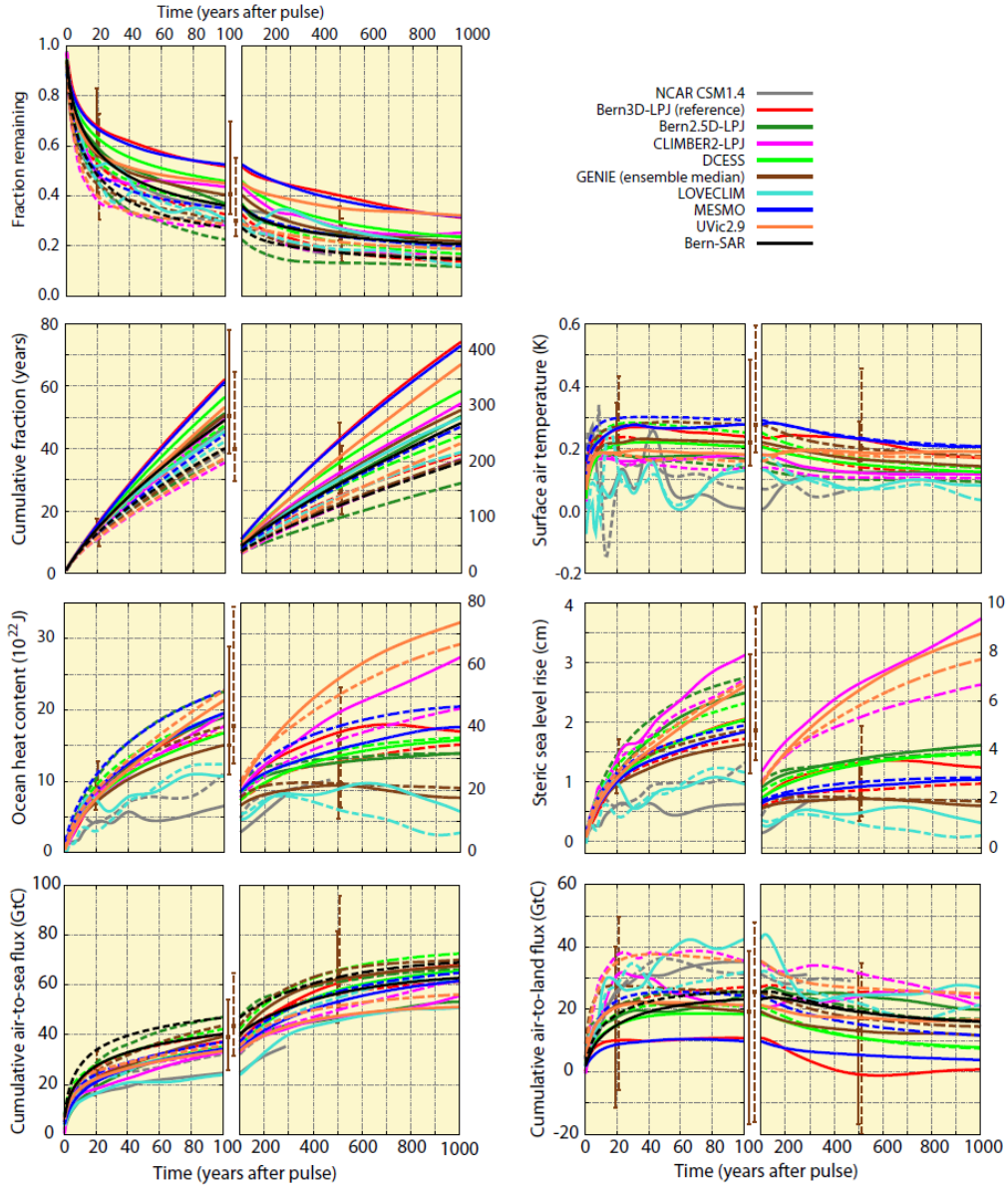

Figure 4: Influence of the background conditions on the climate-carbon cycle response to a pulse emission of 100 GtC into the atmosphere. Solid lines are for current conditions ($CO_{2,\ ref}$ =389 ppm, PD100) and dashed lines for preindustrial conditions ($CO_{2,\ ref}$ ~280 ppm, PI100).

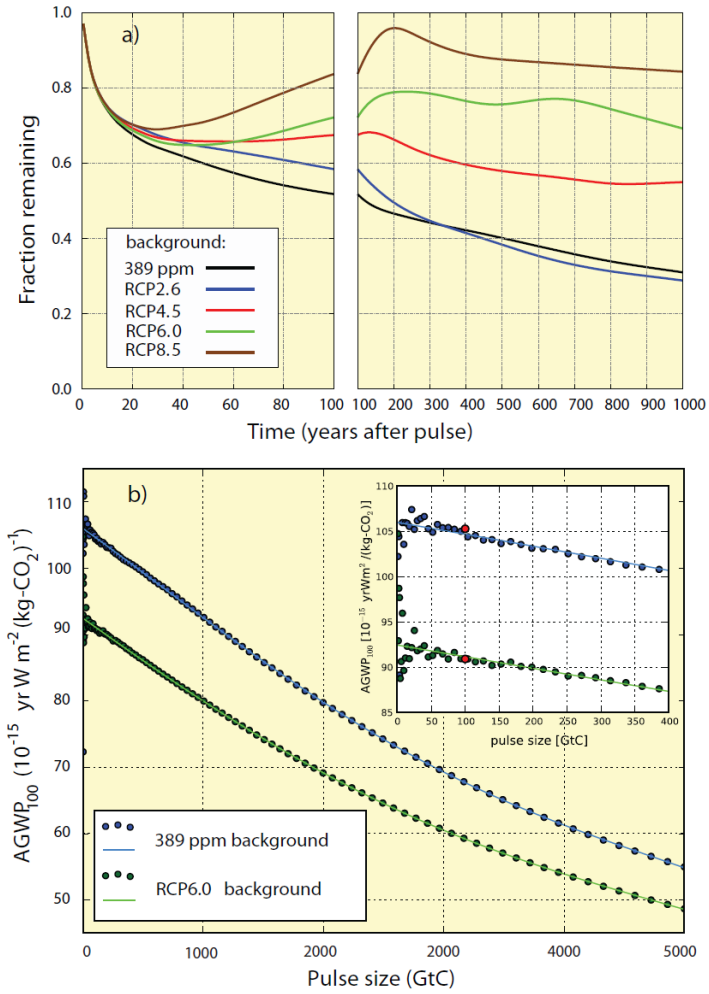

Figure 5: **(a)** IRF_{CO2} for different background conditions as simulated with the Bern3D-LPJ model (reference). Carbon emissions and emissions of other agents, and land use maps are prescribed following those of the Representative Concentration Pathways. In the runs without pulse, atmospheric CO_2 is projected to reach 421, 538, 670, 936 ppm by 2100 and 360, 543, 752, 1962 ppm by year 3000 and for RCP2.6, RCP4.5, RCP6, and RCP8.5 respectively. The IRF_{CO2} for the standard setup with a constant CO_2 background of 389 ppm is shown by the black line. (b) $AGWP_{CO2}$ versus pulse size for two different background conditions. Circles represent results from individual simulations and the lines fits through the results. The standard pulse size of 100 GtC is indicated by red circles.

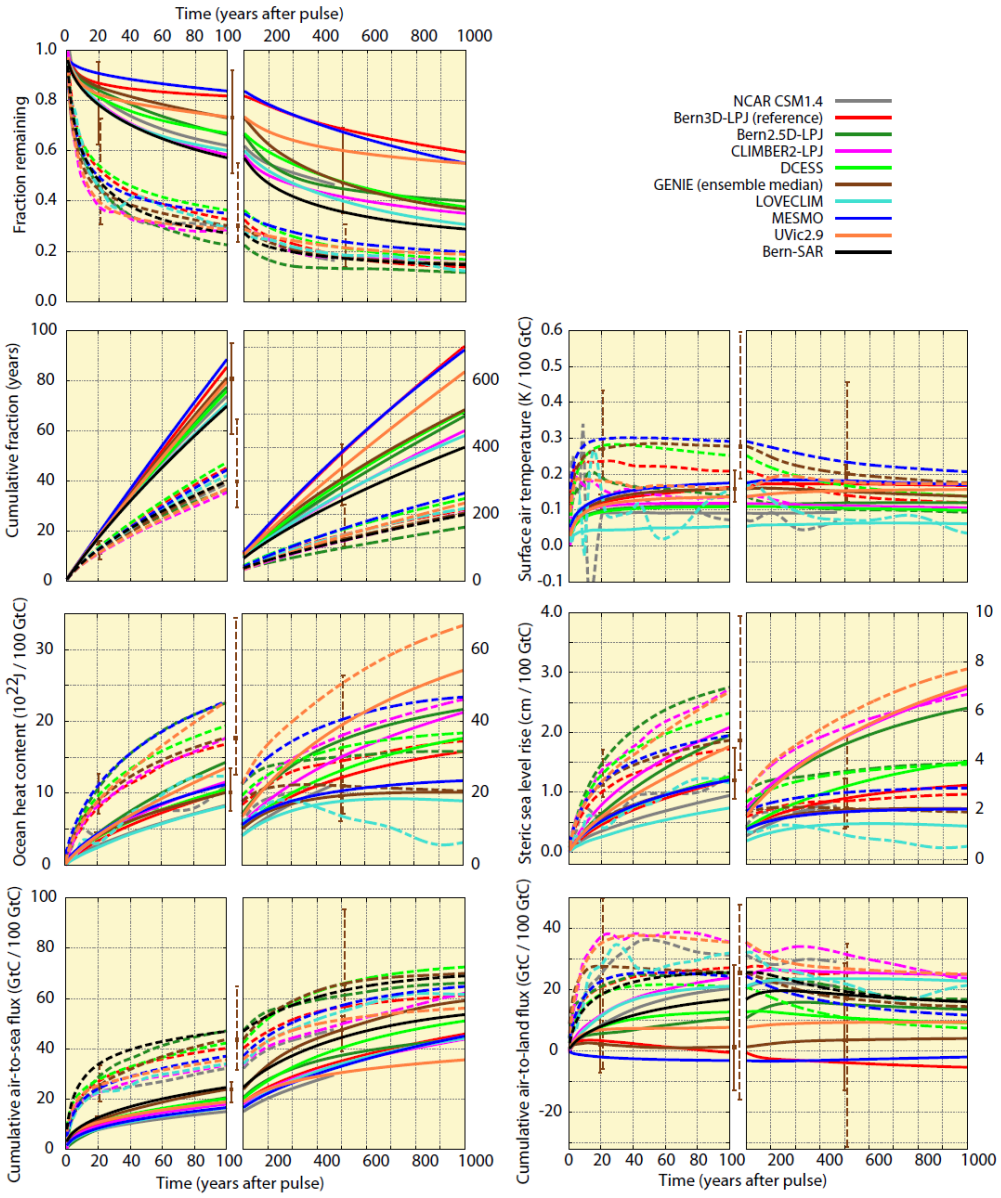

Figure 6~~5~~: Response of the carbon cycle-climate system to a pulse emission of 5000 GtC (solid, PI5000) and 100 GtC (dashed, PI100) added to the atmosphere under preindustrial conditions. The responses in surface air temperature, ocean heat content, steric sea level rise, and in carbon fluxes for PI5000 are scaled by a factor of 50 for a better comparison with the 100 GtC pulse.

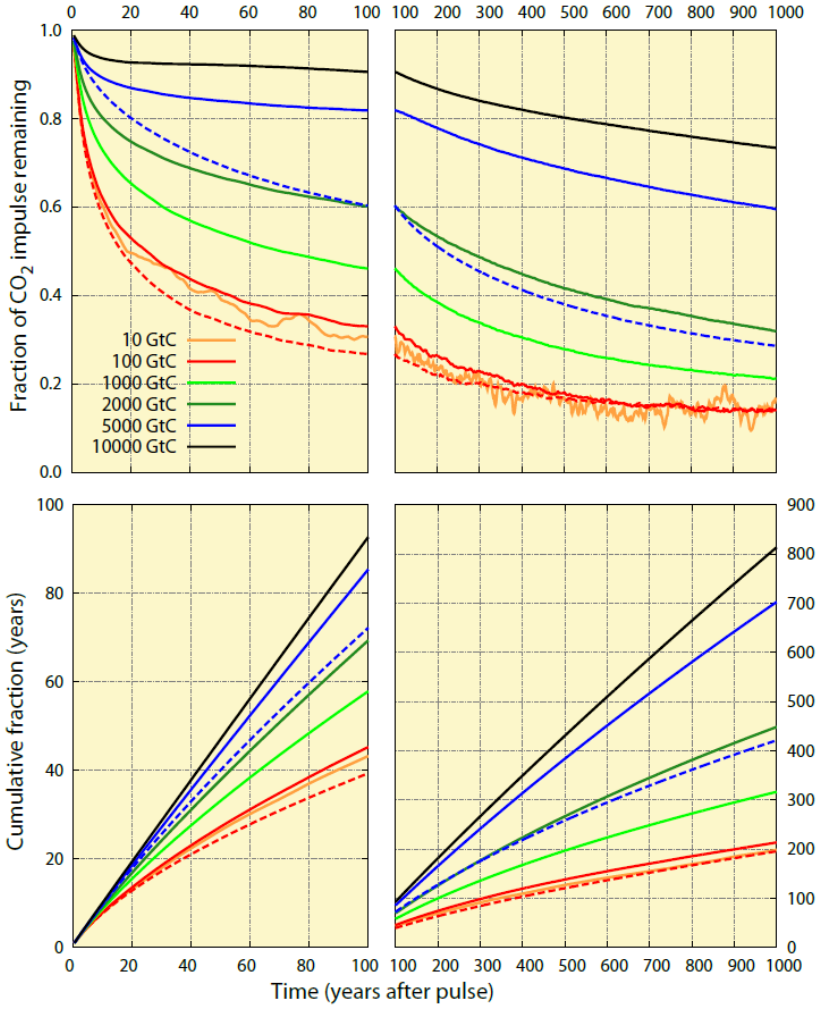

Figure 7~~6~~: Influence of pulse size and climate-carbon cycle feedback on the response in atmospheric CO_2 and the time-integrated IRF_{CO2} as simulated with the Bern3D-LPJ model (standard setup). Pulse emissions, ranging from 10 to 10,000 GtC in the individual simulations, are added to the atmosphere under preindustrial conditions. Dashed lines represent simulations where climate was kept constant in the model.

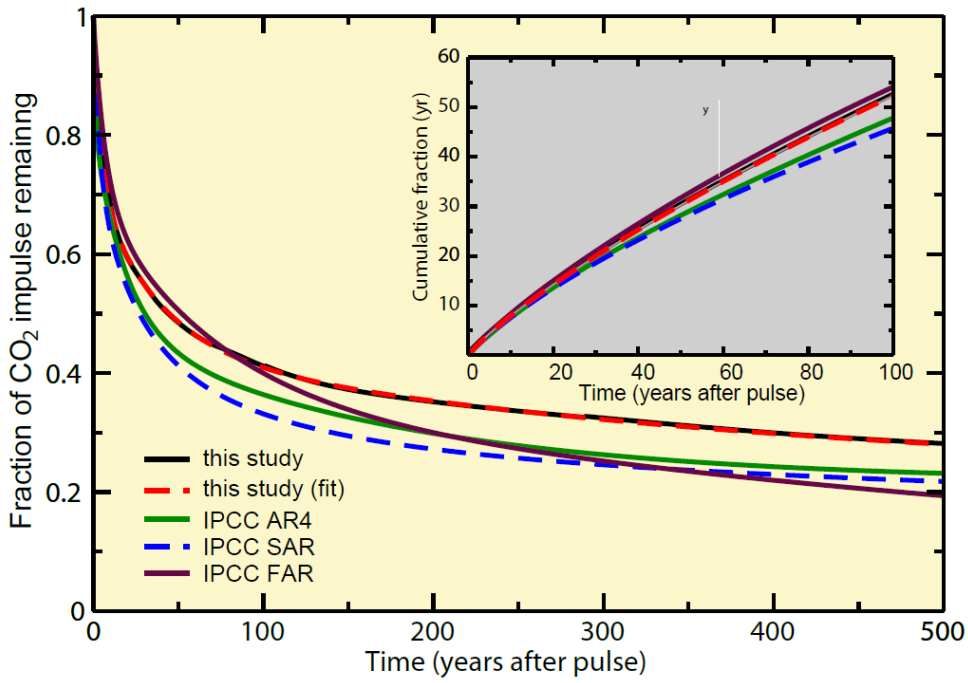

Figure 8~~7~~: The impulse response function for CO_2 (IRF_{CO2}) as used to compute GWP in the IPCC First (FAR), Second (SAR) and Fourth (AR4) Assessment Report and from this study. The red curve is a fit to the multi-model mean shown in black. The inset shows the time-integrated IRF_{CO2} for the first 100 years after the emission pulse.

Impulse response function of climate-carbon cycle models: a model intercomparison study

Protocol V1.1

Fortunat Joos, Raphael Roth
Physics Institute, Climate and Environmental Physics and Oeschger Centre for Climate Change Research, University of Bern, Bern, Switzerland; , joos@climate.unibe.ch, roth@climate.unibe.ch

Jan Fuglestvedt, Glen Peters
Center for International Climate and Environmental Reseach - Oslo (CICERO), Norway; j.s.fuglestvedt@cicero.uio.no, glen.peters@cicero.uio.no

Documents and updates are available online: http://www.climate.unibe.ch/~joos/IRF_Intercomparison

Global warming potentials (GWP) of different gases are used as a metric to compare emissions of various greenhouse gases in the Kyoto Basket approach. The response in atmospheric CO_2 to an instantaneous release of carbon into the atmosphere, the atmospheric CO_2 impulse response function (IRF), is used for the computation of global warming potentials (GWP) and global temperature change potential (GTP) (Shine et al., 2005).

The goal of this exercise is to determine the atmospheric CO_2 impulse response function (IRF) by a suite of carbon-cycle climate models to explore model-model differences. Results will be written up for publication in a peer-reviewed journal in spring 2012 (IPCC AR5 WG1 deadline is summer 2012) in order to be available for calculations of GWPs in IPCC AR5. The results will also be useful for metrics and simplified climate models in other contexts.

Model requirements

The model must be able to compute the redistribution of anthropogenic carbon among the principal carbon reservoirs atmosphere, land biosphere, and ocean. Further compartments such as ocean sediments may also be included. Preferentially, the model simulates changes in climate in response to CO_2 radiative forcing and includes a representation of the relevant carbon cycle-climate feedbacks.

Model runs: overview

The scenario setup is inspired by the calculation of the IRF function as done for the Second Assessment Report (SAR) and as used in the Kyoto GWP with the Bern SAR model version and as repeated in preparation of the Fourth Assessment. The setup relies on that described in Enting, Wigley, Heimann, CSIRO Division of Atmospheric Research. Technical Paper No 31, 1994:

Three simulations are performed:
(a) The model is forced with historical concentration up to a reference year (here t_{ref}=2010) and then concentration are kept fixed thereafter at a constant value (here $CO_{2,ref}$=389 ppm). The allowed emission are calculated from the change in total inventory (prescribed atmospheric change plus modelled ocean and terrestrial uptake)
(b) A simulation with prescribed emissions from (a)
(or concentration prescribed up to the reference year and emissions prescribed thereafter)
(c) same as (b) but an impulse of carbon, here of 100 GtC, added instantaneously to the atmosphere five years after the reference year (here in 2015).

The normalised IRF is then approximately:

$IRF(t=t_{model}-2015.0) = (CO_2(t_{model})-CO_{2,ref})/(100\ GtC/2.123GtC/ppm)$ for $t_{model} > 2015$

Model runs: detailed description

A) CO_2 *background concentration of* 389 *ppm*

1. PresCO2_389ppm: The simulation starts from preindustrial conditions. Atmospheric CO_2 is prescribed and compatible emissions (=change in all carbon reservoirs) diagnosed. Atmospheric CO_2 is prescribed to follow the historical evolution up to year 2010. After 2010, the concentration is kept fixed at the value of 389.0 ppm. The diagnosed emissions should be written frequently (at least annually); these will be used to drive the model in run 2 and 3. An input file with the historical concentrations is provided
   (file name: co2ccn_irf_850_2010_v1.0.dat).
   A restart file may be written in 2010 to start simulation 2 and 3 in 2010
2. PresEmiss_389ppm: run 2 may either start in 2010 as a continuation of run 1 or at the same preindustrial initial conditions used in run 1. Atmospheric CO_2 is evolving freely. Diagnosed emissions from run PresCO2_389ppm are used to force the model. (Expected result: the computed CO_2 evolution should be close to the evolution prescribed in run PresCO2_389ppm, see Figure 1).
3. PresEmiss100_389ppm: Atmospheric CO_2 is evolving freely. Diagnosed emissions from run PresCO2_389ppm are used to force the model as in run PresEmiss_389ppm. In addition, 100 GtC are released <u>at the beginning</u> of year 2015. (Expected results: Atmospheric CO_2 will increase by 47.1032 ppm above the background concentration (~389 ppm) in 2015 and then slowly decline over the coming decades, see Figure 1)

Remarks:

- It is crucial that the carbon pulse will be added to a constant background concentration of 389 ppm for comparability (roughly 2010 value).
- run 1 (PresCO2_389ppm): An existing run or setup from the CMIP or EMIC Intercomparison projects may be used up to a concentration of 389 ppm.
- run 3 (PresEmiss100_389ppm): The atmospheric CO_2 concentration should be increased at the beginning of year 2015 by 47.1032 ppm (100 GtC/2.123 GtC/ppm) in all atmospheric grid cells.
- non-CO_2 forcing agents should be included to the extent possible. Non-CO_2 forcing should be kept constant at 2010 level after 2010 (or at the year at which 389 ppm CO_2 is reached).
- land use and land use changes should be included to the extent possible. Land use area should be kept constant at 2010 level after 2010.
- If CPU time is an issue and if a group is sure that CO_2 remains at a constant value with the emissions diagnosed in run #1, run#2 may be skipped. This may only apply to ESMs and it is strongly recommended to perform run #2 to avoid problems with model drift.

B) Preindustrial Set

Runs 4 to 5 start from preindustrial conditions

4. CTRL: Control simulation with constant boundary conditions and freely evolving atm. CO_2
5. PI100: Freely evolving atm. CO_2. 100 GtC are released into the atmosphere during year 10 of the control simulation and then continued. (Expected result: atm CO_2 will increase from the preindustrial value of around 280 ppm by about 45 ppm to 325 ppm in year 10. Afterwards, the CO_2 concentration will then decrease due to uptake by the ocean and the land biosphere).
6. PI5000: as PI100, but 5000 GtC are released instead of 100 GtC

Remark: an available control simulation may be used to minimize work

Resulting IRFs

We will use your results to compute impulse response functions for CO_2 and other variables:

a) IRF_100GtC_389ppm: The difference in atm. CO_2 of run PresEmiss100_389ppm and PresEmiss_389ppm divided by the pulse size of 47 ppm will yield the (normalized) IRF for a background concentration of 389 ppm and a pulse size of 100 GtC (see Figure 2)
b) IRF_100GtC_PI: The difference in atm. CO_2 of run PI100 and CTRL will yield the IRF for preindustrial background conditions and a pulse size of 100 GtC
c) IRF_5000GtC_PI: The difference in atm. CO_2 of run PI5000 and CTRL will yield the IRF for preindustrial background conditions and a pulse size of 5000 GtC

Duration of runs

Preferentially, simulations are run for 2000 years after the pulse release until a complete equilibrium between atmosphere-ocean-land biosphere is re-established. If this is not feasible, runs of shorter duration are also welcome. Usually models are close to equilibrium after 1000 years. Global Warming Potentials for which the IRFs will be used were tabulated in past IPCC reports for 500, 100, and 20 years. A time horizon of 100 years is used in the Kyoto protocol.

A minimum of 100 years after the pulse release is requested.

Models that include ocean sediments and/or weathering and that are cost-efficient enough may also be run over many millennia (e.g. 100 ka).

Priority of runs

The *top priority* is to get results needed to compute the IRF for a background concentration of 389 ppm (IRF_100GtC_389ppm). For this, *runs 1, 2, and 3* are required.
Alternative: If computing requirements are too high for run 1 to 3, please provide at least results for runs 4 and 5 (PI100, CTRL).

Conversion factor GtC to ppm

Please use a conversion factor of 2.123 GtC per ppm

Preindustrial condition

It is up to the researcher to define the exact preindustrial state and the exact evolution how to reach the 2010 atmospheric CO_2 value of 389 ppm. However, model runs should start before 1900 AD and concentration should be kept fixed at a value of 389 ppm a few years before and during the pulse release. The idea is that the carbon pulse is added for the same background concentration of 389 ppm in all models.

Other forcings

Non-CO_2 forcings and land use are preferentially included in run 1 to 3; keep non-CO_2 forcing and land use area constant after 2010 at the level of year 2010. A suitable set of forcing is provided by the EMIC Intercomparison Project (http://climate.uvic.ca/EMICAR5/forcing).

Output

Ascii files with global mean values, provide at least 5 significant digits for each run.

a) File name: RUNNAME_MODELNAME_Modelversion_startyear_endyear.dat, e.g. "PresCO2_2010_Bern3DLPX_v1.0_1750_4015.dat" for run 1 with the Bern3DLPX model, version 1.0 and simulation starting at 1750 AD and ending at 4015
b) Header:
   - start each comment line with: #
   - indicate run name
   - provide contact address,
   - indicate model name and version and model components included,
   - indicate climate sensitivity of model
   - conversion factor used to convert GtC into ppm and/or pulse size in ppm
   - description of non-CO_2 forcing applied
   - indicate whether tabulated data show annual averages or instantaneous values
   - column headers with units

c) Tabulated data including year, global mean values of atmospheric CO_2 in ppm (CO2atm), global mean net air-to-sea carbon flux in GtC per year (Fas,net), global mean net air-to-land carbon flux in GtC per year (Fab,net), global mean surface temperature in Celsius (T) , global mean sea level rise in cm (SLR), ocean heat content in Joule (Heat)
   # year CO2atm [ppm] Fas,net [GtC/yr] Fab,net [GtC/yr] T [deg Celsius] SLR[cm] Heat[J]

A text file in ascii describing the model, model resolution, model components, climate sensitivity, and appropriate references. File name: MODELNAME_Modelversion_description.txt. Include contact address.

It is assumed that group will store more output individually than just the few global numbers that we ask for as output. It is anticipated that the runs may be very useful to diagnose response patterns for a wide range of variables. In additions to IRFs for CO_2, temp, and sea level, one may also want to analyze pH, precip, etc.

Deadlines

Please let us know by *15 December 2011* whether you plan to contribute and submit the runs until **15 February 2012** to joos@climate.unibe.ch and roth@climate.unibe.ch

Further Reading

Section 2.10, page 210 ff in:

Forster, P., et al. (2007), Changes in Atmospheric Constitutents and in Radiative Forcing, in *Climate Change 2007: The Physical Science Basis. Contribution of Working Group I to Fourth Assessment Report of the Intergovernmental Panel on Climate Change*, edited by S. Solomon, D. Qin, M. Manning, Z. Chen, M. Marquis, K. B. Averyt, M. Tignor and H. L. Miller, pp. 129-234, Cambridge United Kingdom and New York, NY, USA, New York, NY, USA.

Enting, I.G., Wigley, T.M.L., Heimann, M., 1994. Future Emissions and Concentrations of Carbon Dioxide: Key Ocean/Atmosphere/Land Analyses. CSIRO Division of Atmospheric Research Technical Paper no. 31.

Shine, K., Fuglestvedt, J., Hailemariam, K., and Stuber, N.: Alternatives to the Global Warming Potential for Comparing Climate Impacts of Emissions of Greenhouse Gases, Climatic Change, 68, 281-302, 10.1007/s10584-005-1146-9, 2005

Results obtained with the Bern3D-LPJ model for a CO_2 background of 389 ppm (R. Roth)

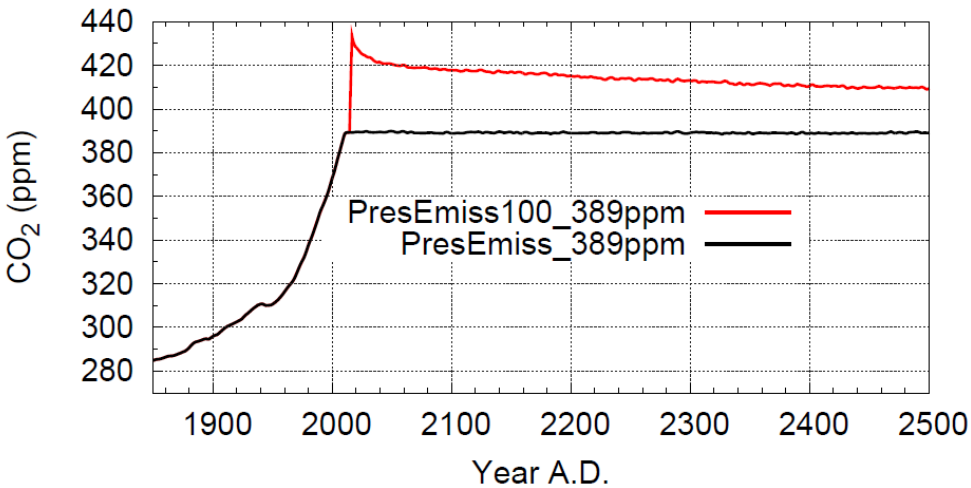

Figure 1: Simulated evolution of atmospheric CO_2 for runs 2 and 3 (PresEmiss_389ppm PresEmiss100_389ppm). 100 GtC are instantaneously released at the beginning of year 2015 in simulations PresEmiss100_389ppm (red) in addition to the emissions prescribed in run PresEmiss_389ppm (black). Prescribed emissions were diagnosed from a run in which atmospheric CO_2 was prescribed to follow the observed evolution until 2010 and kept constant at 389 ppm after 2010.

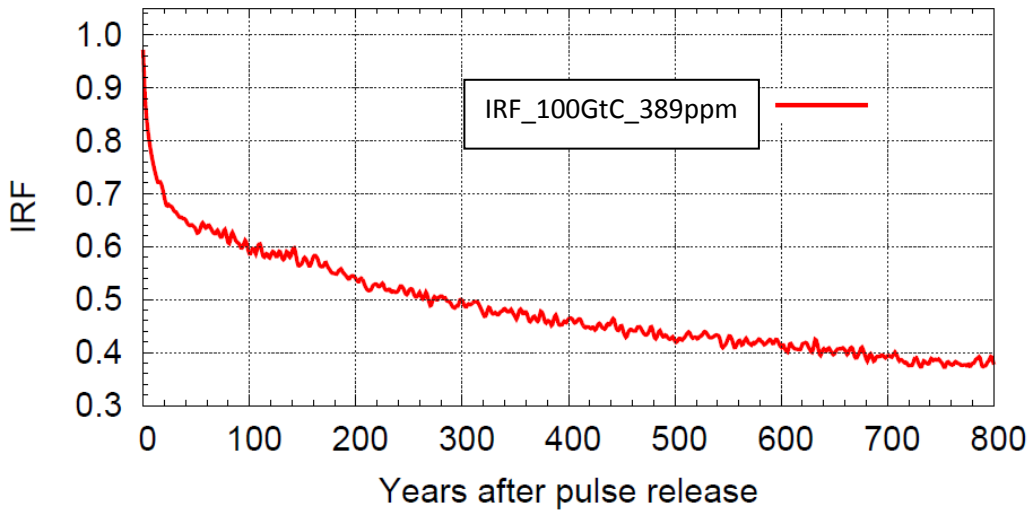

Figure 2: CO_2 impulse response function (IRF) as obtained from the difference of the runs shown in figure 1. The IRF is normalised by the size of the pulse input. Time is shifted such that year 0 corresponds to the time when the pulse of 100 GtC was released into the atmosphere.

Results of sensitivity runs with the Bern3D-LPJ model (Raphael Roth)

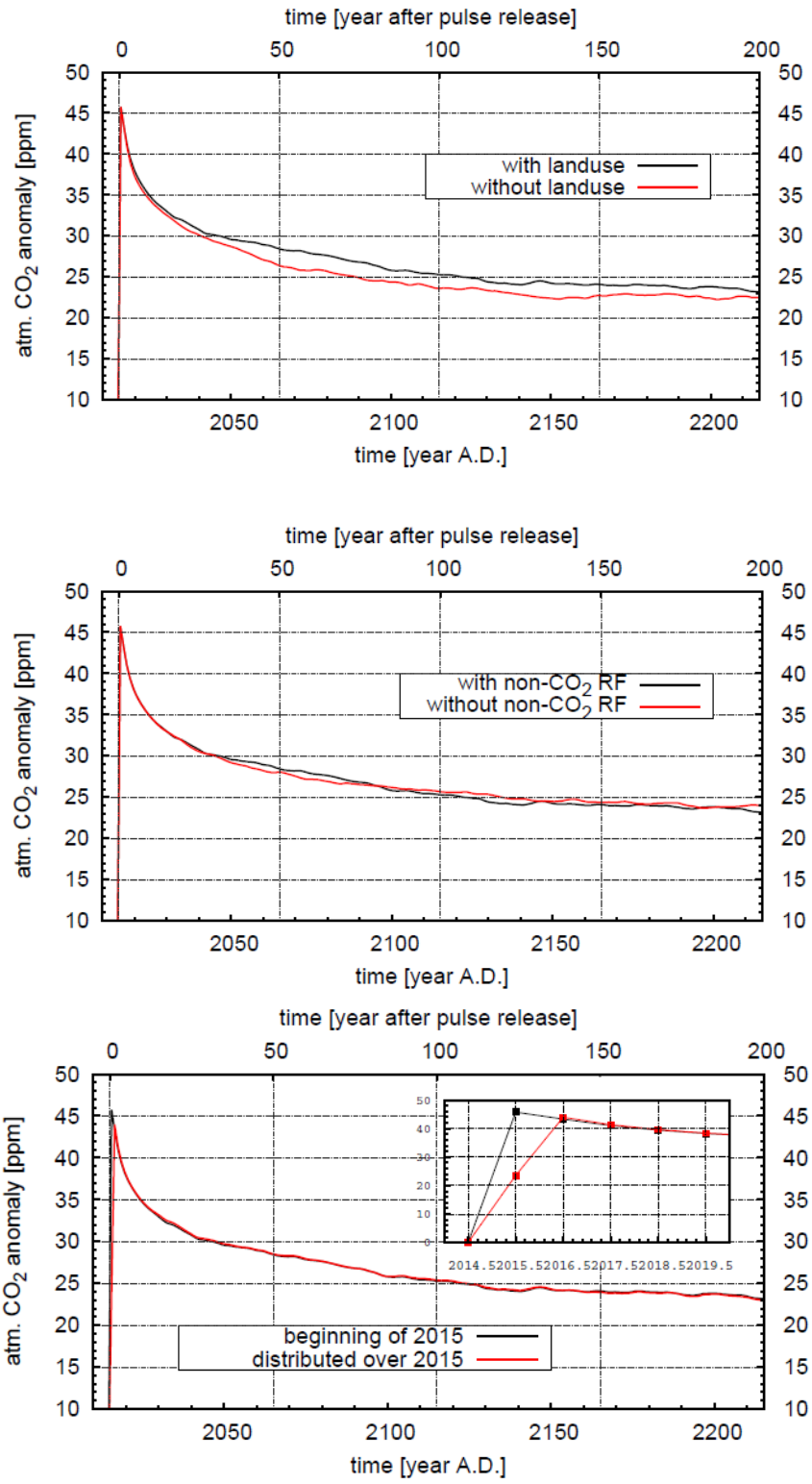

Differences in Impulse Response Function computed with the Bern3D-LPX model for different model setups. Top: Results from simulations with and without anthropogenic land use. Middle: Results from simulations with and without non-CO2 forcings. Bottom: release of pulse emissions at the beginning of the year versus a release of 100 GtC over one year. Note that the Bern3D-LPX model considers CO_2 to be well mixed in the atmosphere. Thus differences in IRF may be larger for models that feature atmospheric carbon transport.

```
# ------------------------------------------------------------

# midyear CO2 concentrations 850-2010
# to be used for the IRF intercomparison experiment "PresCO2_389ppm"
#

# author: Raphael Roth, roth@climate.unibe.ch
# date:   24/11/2011
# ------------------------------------------------------------
#
# data used:
# from 850 - 2005 EMIC AR5 forcing was used
(http://climate.uvic.ca/EMICAR5/data/UVic_data/co2ccn_850-2005.nc.gz)
#     -->PMIP3 CO2 concentration (850 to 1800) and the CMIP5 historical
CO2 concentration (1765 to 2005).
#     -->The data sets were linearly blended between 1765 and 1800.
#
# from 2005-2010, RCP6.0 midyear CO2-concentration
#                 (value from 2010.5 of 389.072 was rounded to 389.00)
# from 2010-      constant value of 389.00 ppm
#
#
#
# year  co2 [ppm]
#
 850.5  279.266
 851.5  279.272
 852.5  279.277
 853.5  279.281
 854.5  279.284
 855.5  279.286
 856.5  279.287
 857.5  279.287
 858.5  279.285
 859.5  279.283
 860.5  279.279
 861.5  279.274
 862.5  279.268
 863.5  279.261
 864.5  279.254
 865.5  279.245
 866.5  279.236
 867.5  279.226
 868.5  279.216
 869.5  279.204
 870.5  279.193
 871.5  279.181
 872.5  279.169
 873.5  279.156
 874.5  279.143
 875.5  279.130
 876.5  279.117
 877.5  279.103
 878.5  279.090
 879.5  279.077
 880.5  279.064
 881.5  279.051
 882.5  279.038
 883.5  279.026
```

884.5	279.014
885.5	279.002
886.5	278.991
887.5	278.980
888.5	278.970
889.5	278.961
890.5	278.953
891.5	278.945
892.5	278.938
893.5	278.932
894.5	278.927
895.5	278.923
896.5	278.920
897.5	278.919
898.5	278.918
899.5	278.919
900.5	278.921
901.5	278.924
902.5	278.928
903.5	278.932
904.5	278.938
905.5	278.945
906.5	278.952
907.5	278.960
908.5	278.968
909.5	278.977
910.5	278.987
911.5	278.996
912.5	279.007
913.5	279.017
914.5	279.027
915.5	279.038
916.5	279.048
917.5	279.059
918.5	279.069
919.5	279.079
920.5	279.089
921.5	279.099
922.5	279.108
923.5	279.116
924.5	279.124
925.5	279.132
926.5	279.139
927.5	279.145
928.5	279.150
929.5	279.154
930.5	279.157
931.5	279.160
932.5	279.161
933.5	279.161
934.5	279.159
935.5	279.157
936.5	279.153
937.5	279.147
938.5	279.140
939.5	279.132
940.5	279.121
941.5	279.109
942.5	279.095
943.5	279.079

944.5	279.062
945.5	279.042
946.5	279.020
947.5	278.997
948.5	278.973
949.5	278.947
950.5	278.920
951.5	278.893
952.5	278.865
953.5	278.837
954.5	278.809
955.5	278.781
956.5	278.754
957.5	278.727
958.5	278.701
959.5	278.677
960.5	278.654
961.5	278.633
962.5	278.613
963.5	278.596
964.5	278.581
965.5	278.568
966.5	278.559
967.5	278.552
968.5	278.549
969.5	278.549
970.5	278.553
971.5	278.560
972.5	278.570
973.5	278.584
974.5	278.600
975.5	278.620
976.5	278.642
977.5	278.666
978.5	278.694
979.5	278.724
980.5	278.755
981.5	278.790
982.5	278.826
983.5	278.864
984.5	278.904
985.5	278.946
986.5	278.989
987.5	279.034
988.5	279.080
989.5	279.128
990.5	279.176
991.5	279.226
992.5	279.276
993.5	279.328
994.5	279.379
995.5	279.432
996.5	279.484
997.5	279.538
998.5	279.591
999.5	279.644
1000.5	279.697
1001.5	279.750
1002.5	279.803
1003.5	279.856

1004.5	279.907
1005.5	279.959
1006.5	280.009
1007.5	280.059
1008.5	280.107
1009.5	280.154
1010.5	280.199
1011.5	280.243
1012.5	280.285
1013.5	280.325
1014.5	280.363
1015.5	280.398
1016.5	280.431
1017.5	280.461
1018.5	280.488
1019.5	280.513
1020.5	280.533
1021.5	280.551
1022.5	280.564
1023.5	280.574
1024.5	280.580
1025.5	280.581
1026.5	280.579
1027.5	280.573
1028.5	280.565
1029.5	280.556
1030.5	280.549
1031.5	280.544
1032.5	280.543
1033.5	280.546
1034.5	280.557
1035.5	280.575
1036.5	280.603
1037.5	280.641
1038.5	280.691
1039.5	280.752
1040.5	280.822
1041.5	280.901
1042.5	280.987
1043.5	281.081
1044.5	281.180
1045.5	281.283
1046.5	281.391
1047.5	281.500
1048.5	281.612
1049.5	281.724
1050.5	281.836
1051.5	281.947
1052.5	282.055
1053.5	282.160
1054.5	282.260
1055.5	282.355
1056.5	282.444
1057.5	282.526
1058.5	282.599
1059.5	282.662
1060.5	282.717
1061.5	282.764
1062.5	282.802
1063.5	282.833

1064.5	282.857
1065.5	282.874
1066.5	282.885
1067.5	282.891
1068.5	282.891
1069.5	282.886
1070.5	282.877
1071.5	282.863
1072.5	282.847
1073.5	282.827
1074.5	282.805
1075.5	282.781
1076.5	282.755
1077.5	282.728
1078.5	282.701
1079.5	282.673
1080.5	282.645
1081.5	282.618
1082.5	282.592
1083.5	282.567
1084.5	282.545
1085.5	282.525
1086.5	282.508
1087.5	282.494
1088.5	282.484
1089.5	282.478
1090.5	282.476
1091.5	282.478
1092.5	282.483
1093.5	282.491
1094.5	282.502
1095.5	282.516
1096.5	282.533
1097.5	282.552
1098.5	282.573
1099.5	282.597
1100.5	282.622
1101.5	282.649
1102.5	282.678
1103.5	282.708
1104.5	282.739
1105.5	282.772
1106.5	282.805
1107.5	282.838
1108.5	282.872
1109.5	282.907
1110.5	282.943
1111.5	282.978
1112.5	283.014
1113.5	283.050
1114.5	283.086
1115.5	283.123
1116.5	283.159
1117.5	283.195
1118.5	283.231
1119.5	283.267
1120.5	283.302
1121.5	283.337
1122.5	283.372
1123.5	283.406

1124.5	283.439
1125.5	283.472
1126.5	283.504
1127.5	283.535
1128.5	283.565
1129.5	283.594
1130.5	283.622
1131.5	283.649
1132.5	283.674
1133.5	283.698
1134.5	283.721
1135.5	283.743
1136.5	283.763
1137.5	283.781
1138.5	283.797
1139.5	283.812
1140.5	283.826
1141.5	283.838
1142.5	283.849
1143.5	283.858
1144.5	283.867
1145.5	283.874
1146.5	283.880
1147.5	283.886
1148.5	283.891
1149.5	283.895
1150.5	283.898
1151.5	283.901
1152.5	283.904
1153.5	283.906
1154.5	283.908
1155.5	283.910
1156.5	283.911
1157.5	283.913
1158.5	283.915
1159.5	283.917
1160.5	283.919
1161.5	283.922
1162.5	283.925
1163.5	283.928
1164.5	283.931
1165.5	283.935
1166.5	283.938
1167.5	283.942
1168.5	283.946
1169.5	283.949
1170.5	283.953
1171.5	283.956
1172.5	283.959
1173.5	283.962
1174.5	283.965
1175.5	283.967
1176.5	283.969
1177.5	283.970
1178.5	283.971
1179.5	283.972
1180.5	283.972
1181.5	283.972
1182.5	283.970
1183.5	283.969

1184.5	283.966
1185.5	283.963
1186.5	283.958
1187.5	283.953
1188.5	283.948
1189.5	283.941
1190.5	283.933
1191.5	283.924
1192.5	283.914
1193.5	283.903
1194.5	283.891
1195.5	283.877
1196.5	283.862
1197.5	283.845
1198.5	283.827
1199.5	283.807
1200.5	283.786
1201.5	283.763
1202.5	283.737
1203.5	283.709
1204.5	283.680
1205.5	283.648
1206.5	283.613
1207.5	283.576
1208.5	283.537
1209.5	283.495
1210.5	283.451
1211.5	283.404
1212.5	283.355
1213.5	283.305
1214.5	283.254
1215.5	283.200
1216.5	283.146
1217.5	283.090
1218.5	283.034
1219.5	282.977
1220.5	282.919
1221.5	282.862
1222.5	282.804
1223.5	282.746
1224.5	282.688
1225.5	282.631
1226.5	282.575
1227.5	282.519
1228.5	282.464
1229.5	282.410
1230.5	282.358
1231.5	282.308
1232.5	282.259
1233.5	282.212
1234.5	282.167
1235.5	282.124
1236.5	282.084
1237.5	282.046
1238.5	282.012
1239.5	281.980
1240.5	281.952
1241.5	281.927
1242.5	281.905
1243.5	281.887

1244.5	281.874
1245.5	281.864
1246.5	281.858
1247.5	281.858
1248.5	281.861
1249.5	281.866
1250.5	281.874
1251.5	281.883
1252.5	281.892
1253.5	281.900
1254.5	281.906
1255.5	281.909
1256.5	281.909
1257.5	281.904
1258.5	281.893
1259.5	281.876
1260.5	281.854
1261.5	281.826
1262.5	281.794
1263.5	281.758
1264.5	281.718
1265.5	281.676
1266.5	281.630
1267.5	281.583
1268.5	281.534
1269.5	281.484
1270.5	281.434
1271.5	281.384
1272.5	281.334
1273.5	281.285
1274.5	281.238
1275.5	281.193
1276.5	281.150
1277.5	281.110
1278.5	281.073
1279.5	281.040
1280.5	281.009
1281.5	280.982
1282.5	280.958
1283.5	280.937
1284.5	280.920
1285.5	280.907
1286.5	280.897
1287.5	280.892
1288.5	280.889
1289.5	280.891
1290.5	280.897
1291.5	280.907
1292.5	280.921
1293.5	280.940
1294.5	280.962
1295.5	280.990
1296.5	281.021
1297.5	281.058
1298.5	281.099
1299.5	281.144
1300.5	281.195
1301.5	281.250
1302.5	281.311
1303.5	281.376

1304.5	281.447
1305.5	281.523
1306.5	281.605
1307.5	281.691
1308.5	281.783
1309.5	281.879
1310.5	281.977
1311.5	282.078
1312.5	282.180
1313.5	282.281
1314.5	282.382
1315.5	282.481
1316.5	282.577
1317.5	282.669
1318.5	282.757
1319.5	282.838
1320.5	282.913
1321.5	282.979
1322.5	283.037
1323.5	283.086
1324.5	283.123
1325.5	283.148
1326.5	283.161
1327.5	283.161
1328.5	283.145
1329.5	283.114
1330.5	283.066
1331.5	283.001
1332.5	282.919
1333.5	282.823
1334.5	282.712
1335.5	282.591
1336.5	282.458
1337.5	282.316
1338.5	282.167
1339.5	282.012
1340.5	281.852
1341.5	281.689
1342.5	281.524
1343.5	281.359
1344.5	281.196
1345.5	281.035
1346.5	280.878
1347.5	280.727
1348.5	280.583
1349.5	280.448
1350.5	280.323
1351.5	280.210
1352.5	280.106
1353.5	280.013
1354.5	279.930
1355.5	279.856
1356.5	279.791
1357.5	279.735
1358.5	279.687
1359.5	279.647
1360.5	279.614
1361.5	279.588
1362.5	279.569
1363.5	279.556

1364.5	279.549
1365.5	279.547
1366.5	279.551
1367.5	279.558
1368.5	279.570
1369.5	279.586
1370.5	279.605
1371.5	279.627
1372.5	279.651
1373.5	279.678
1374.5	279.707
1375.5	279.736
1376.5	279.767
1377.5	279.798
1378.5	279.829
1379.5	279.860
1380.5	279.891
1381.5	279.920
1382.5	279.948
1383.5	279.973
1384.5	279.997
1385.5	280.017
1386.5	280.035
1387.5	280.049
1388.5	280.059
1389.5	280.065
1390.5	280.066
1391.5	280.062
1392.5	280.053
1393.5	280.039
1394.5	280.022
1395.5	280.001
1396.5	279.977
1397.5	279.951
1398.5	279.924
1399.5	279.895
1400.5	279.866
1401.5	279.837
1402.5	279.809
1403.5	279.782
1404.5	279.757
1405.5	279.734
1406.5	279.714
1407.5	279.698
1408.5	279.686
1409.5	279.678
1410.5	279.676
1411.5	279.680
1412.5	279.690
1413.5	279.707
1414.5	279.730
1415.5	279.760
1416.5	279.796
1417.5	279.839
1418.5	279.888
1419.5	279.944
1420.5	280.006
1421.5	280.074
1422.5	280.149
1423.5	280.230

1424.5	280.318
1425.5	280.412
1426.5	280.512
1427.5	280.619
1428.5	280.731
1429.5	280.850
1430.5	280.975
1431.5	281.098
1432.5	281.213
1433.5	281.316
1434.5	281.409
1435.5	281.491
1436.5	281.563
1437.5	281.624
1438.5	281.675
1439.5	281.715
1440.5	281.745
1441.5	281.765
1442.5	281.775
1443.5	281.775
1444.5	281.764
1445.5	281.745
1446.5	281.715
1447.5	281.675
1448.5	281.626
1449.5	281.568
1450.5	281.500
1451.5	281.424
1452.5	281.340
1453.5	281.250
1454.5	281.155
1455.5	281.056
1456.5	280.954
1457.5	280.849
1458.5	280.745
1459.5	280.640
1460.5	280.536
1461.5	280.435
1462.5	280.338
1463.5	280.245
1464.5	280.158
1465.5	280.077
1466.5	280.004
1467.5	279.941
1468.5	279.887
1469.5	279.844
1470.5	279.814
1471.5	279.796
1472.5	279.789
1473.5	279.795
1474.5	279.810
1475.5	279.837
1476.5	279.872
1477.5	279.917
1478.5	279.970
1479.5	280.032
1480.5	280.100
1481.5	280.176
1482.5	280.258
1483.5	280.345

1484.5	280.438
1485.5	280.535
1486.5	280.637
1487.5	280.742
1488.5	280.849
1489.5	280.959
1490.5	281.071
1491.5	281.184
1492.5	281.298
1493.5	281.412
1494.5	281.525
1495.5	281.638
1496.5	281.749
1497.5	281.857
1498.5	281.963
1499.5	282.066
1500.5	282.165
1501.5	282.260
1502.5	282.349
1503.5	282.434
1504.5	282.513
1505.5	282.588
1506.5	282.658
1507.5	282.723
1508.5	282.784
1509.5	282.840
1510.5	282.892
1511.5	282.940
1512.5	282.983
1513.5	283.023
1514.5	283.059
1515.5	283.092
1516.5	283.121
1517.5	283.147
1518.5	283.169
1519.5	283.188
1520.5	283.204
1521.5	283.217
1522.5	283.228
1523.5	283.236
1524.5	283.241
1525.5	283.244
1526.5	283.245
1527.5	283.244
1528.5	283.240
1529.5	283.235
1530.5	283.228
1531.5	283.219
1532.5	283.209
1533.5	283.196
1534.5	283.182
1535.5	283.165
1536.5	283.147
1537.5	283.126
1538.5	283.103
1539.5	283.077
1540.5	283.049
1541.5	283.018
1542.5	282.985
1543.5	282.949

1544.5	282.909
1545.5	282.867
1546.5	282.822
1547.5	282.774
1548.5	282.722
1549.5	282.667
1550.5	282.609
1551.5	282.547
1552.5	282.483
1553.5	282.419
1554.5	282.355
1555.5	282.292
1556.5	282.232
1557.5	282.176
1558.5	282.125
1559.5	282.080
1560.5	282.042
1561.5	282.013
1562.5	281.992
1563.5	281.978
1564.5	281.970
1565.5	281.966
1566.5	281.965
1567.5	281.967
1568.5	281.969
1569.5	281.971
1570.5	281.972
1571.5	281.969
1572.5	281.963
1573.5	281.951
1574.5	281.933
1575.5	281.907
1576.5	281.871
1577.5	281.824
1578.5	281.764
1579.5	281.690
1580.5	281.599
1581.5	281.491
1582.5	281.364
1583.5	281.216
1584.5	281.045
1585.5	280.850
1586.5	280.630
1587.5	280.383
1588.5	280.107
1589.5	279.800
1590.5	279.467
1591.5	279.112
1592.5	278.741
1593.5	278.358
1594.5	277.963
1595.5	277.562
1596.5	277.156
1597.5	276.748
1598.5	276.342
1599.5	275.939
1600.5	275.543
1601.5	275.156
1602.5	274.781
1603.5	274.421

1604.5	274.080
1605.5	273.758
1606.5	273.461
1607.5	273.190
1608.5	272.948
1609.5	272.739
1610.5	272.565
1611.5	272.429
1612.5	272.331
1613.5	272.268
1614.5	272.240
1615.5	272.243
1616.5	272.275
1617.5	272.334
1618.5	272.418
1619.5	272.525
1620.5	272.652
1621.5	272.798
1622.5	272.960
1623.5	273.136
1624.5	273.323
1625.5	273.521
1626.5	273.725
1627.5	273.935
1628.5	274.148
1629.5	274.361
1630.5	274.574
1631.5	274.784
1632.5	274.991
1633.5	275.193
1634.5	275.390
1635.5	275.581
1636.5	275.764
1637.5	275.939
1638.5	276.105
1639.5	276.259
1640.5	276.403
1641.5	276.534
1642.5	276.652
1643.5	276.759
1644.5	276.853
1645.5	276.936
1646.5	277.008
1647.5	277.069
1648.5	277.119
1649.5	277.159
1650.5	277.189
1651.5	277.210
1652.5	277.221
1653.5	277.224
1654.5	277.220
1655.5	277.207
1656.5	277.188
1657.5	277.163
1658.5	277.132
1659.5	277.096
1660.5	277.056
1661.5	277.011
1662.5	276.963
1663.5	276.911

1664.5	276.858
1665.5	276.802
1666.5	276.745
1667.5	276.688
1668.5	276.630
1669.5	276.572
1670.5	276.515
1671.5	276.460
1672.5	276.406
1673.5	276.355
1674.5	276.307
1675.5	276.263
1676.5	276.222
1677.5	276.186
1678.5	276.156
1679.5	276.131
1680.5	276.113
1681.5	276.101
1682.5	276.097
1683.5	276.100
1684.5	276.110
1685.5	276.126
1686.5	276.148
1687.5	276.173
1688.5	276.202
1689.5	276.234
1690.5	276.267
1691.5	276.301
1692.5	276.336
1693.5	276.370
1694.5	276.403
1695.5	276.435
1696.5	276.466
1697.5	276.496
1698.5	276.525
1699.5	276.553
1700.5	276.581
1701.5	276.607
1702.5	276.634
1703.5	276.660
1704.5	276.686
1705.5	276.712
1706.5	276.738
1707.5	276.764
1708.5	276.790
1709.5	276.818
1710.5	276.845
1711.5	276.874
1712.5	276.903
1713.5	276.934
1714.5	276.965
1715.5	276.998
1716.5	277.032
1717.5	277.068
1718.5	277.106
1719.5	277.145
1720.5	277.187
1721.5	277.230
1722.5	277.276
1723.5	277.324

1724.5	277.374
1725.5	277.425
1726.5	277.474
1727.5	277.521
1728.5	277.563
1729.5	277.600
1730.5	277.630
1731.5	277.651
1732.5	277.661
1733.5	277.659
1734.5	277.644
1735.5	277.614
1736.5	277.571
1737.5	277.518
1738.5	277.457
1739.5	277.390
1740.5	277.320
1741.5	277.250
1742.5	277.181
1743.5	277.117
1744.5	277.058
1745.5	277.005
1746.5	276.957
1747.5	276.912
1748.5	276.871
1749.5	276.832
1750.5	276.796
1751.5	276.761
1752.5	276.727
1753.5	276.695
1754.5	276.665
1755.5	276.638
1756.5	276.614
1757.5	276.595
1758.5	276.582
1759.5	276.575
1760.5	276.576
1761.5	276.585
1762.5	276.604
1763.5	276.634
1764.5	276.675
1765.5	276.728
1766.5	276.830
1767.5	276.943
1768.5	277.067
1769.5	277.202
1770.5	277.344
1771.5	277.493
1772.5	277.648
1773.5	277.809
1774.5	277.974
1775.5	278.143
1776.5	278.319
1777.5	278.501
1778.5	278.689
1779.5	278.882
1780.5	279.077
1781.5	279.275
1782.5	279.478
1783.5	279.685

1784.5	279.897
1785.5	280.115
1786.5	280.338
1787.5	280.565
1788.5	280.793
1789.5	281.016
1790.5	281.232
1791.5	281.440
1792.5	281.638
1793.5	281.828
1794.5	282.009
1795.5	282.180
1796.5	282.341
1797.5	282.494
1798.5	282.638
1799.5	282.773
1800.5	282.899
1801.5	283.007
1802.5	283.111
1803.5	283.211
1804.5	283.307
1805.5	283.400
1806.5	283.490
1807.5	283.578
1808.5	283.661
1809.5	283.735
1810.5	283.797
1811.5	283.847
1812.5	283.889
1813.5	283.926
1814.5	283.963
1815.5	284.001
1816.5	284.043
1817.5	284.086
1818.5	284.129
1819.5	284.167
1820.5	284.198
1821.5	284.223
1822.5	284.244
1823.5	284.263
1824.5	284.281
1825.5	284.300
1826.5	284.320
1827.5	284.340
1828.5	284.360
1829.5	284.380
1830.5	284.400
1831.5	284.385
1832.5	284.280
1833.5	284.125
1834.5	283.975
1835.5	283.825
1836.5	283.675
1837.5	283.525
1838.5	283.425
1839.5	283.400
1840.5	283.400
1841.5	283.425
1842.5	283.500
1843.5	283.600

1844.5	283.725
1845.5	283.900
1846.5	284.075
1847.5	284.225
1848.5	284.400
1849.5	284.575
1850.5	284.725
1851.5	284.875
1852.5	285.000
1853.5	285.125
1854.5	285.275
1855.5	285.425
1856.5	285.575
1857.5	285.725
1858.5	285.900
1859.5	286.075
1860.5	286.225
1861.5	286.375
1862.5	286.500
1863.5	286.625
1864.5	286.775
1865.5	286.900
1866.5	287.000
1867.5	287.100
1868.5	287.225
1869.5	287.375
1870.5	287.525
1871.5	287.700
1872.5	287.900
1873.5	288.125
1874.5	288.400
1875.5	288.700
1876.5	289.025
1877.5	289.400
1878.5	289.800
1879.5	290.225
1880.5	290.700
1881.5	291.200
1882.5	291.675
1883.5	292.125
1884.5	292.575
1885.5	292.975
1886.5	293.300
1887.5	293.575
1888.5	293.800
1889.5	294.000
1890.5	294.175
1891.5	294.325
1892.5	294.475
1893.5	294.600
1894.5	294.700
1895.5	294.800
1896.5	294.900
1897.5	295.025
1898.5	295.225
1899.5	295.500
1900.5	295.800
1901.5	296.125
1902.5	296.475
1903.5	296.825

1904.5	297.200
1905.5	297.625
1906.5	298.075
1907.5	298.500
1908.5	298.900
1909.5	299.300
1910.5	299.700
1911.5	300.075
1912.5	300.425
1913.5	300.775
1914.5	301.100
1915.5	301.400
1916.5	301.725
1917.5	302.075
1918.5	302.400
1919.5	302.700
1920.5	303.025
1921.5	303.400
1922.5	303.775
1923.5	304.125
1924.5	304.525
1925.5	304.975
1926.5	305.400
1927.5	305.825
1928.5	306.300
1929.5	306.775
1930.5	307.225
1931.5	307.700
1932.5	308.175
1933.5	308.600
1934.5	309.000
1935.5	309.400
1936.5	309.750
1937.5	310.000
1938.5	310.175
1939.5	310.300
1940.5	310.375
1941.5	310.375
1942.5	310.300
1943.5	310.200
1944.5	310.125
1945.5	310.100
1946.5	310.125
1947.5	310.200
1948.5	310.325
1949.5	310.500
1950.5	310.750
1951.5	311.100
1952.5	311.500
1953.5	311.925
1954.5	312.425
1955.5	313.000
1956.5	313.600
1957.5	314.225
1958.5	314.848
1959.5	315.500
1960.5	316.272
1961.5	317.075
1962.5	317.795
1963.5	318.397

1964.5	318.925
1965.5	319.647
1966.5	320.647
1967.5	321.605
1968.5	322.635
1969.5	323.902
1970.5	324.985
1971.5	325.855
1972.5	327.140
1973.5	328.677
1974.5	329.742
1975.5	330.585
1976.5	331.747
1977.5	333.272
1978.5	334.848
1979.5	336.525
1980.5	338.360
1981.5	339.728
1982.5	340.793
1983.5	342.198
1984.5	343.783
1985.5	345.283
1986.5	346.797
1987.5	348.645
1988.5	350.737
1989.5	352.487
1990.5	353.855
1991.5	355.017
1992.5	355.885
1993.5	356.777
1994.5	358.128
1995.5	359.837
1996.5	361.462
1997.5	363.155
1998.5	365.323
1999.5	367.348
2000.5	368.865
2001.5	370.467
2002.5	372.522
2003.5	374.760
2004.5	376.813
2005.5	378.813
2006.5	380.828
2007.5	382.777
2008.5	384.800
2009.5	386.935
2010.5	389.000
999999.	389.000

Supplementary Information: Part B

Responses in CO_2 for the 100 GtC emission pulse added to a constant background of 389 ppm (PD100 case) are fitted by a sum of exponentials:

$$IRF_{\mathrm{CO2}}(t) = a_0 + \sum_{i=1}^{3} a_i \cdot \exp\left(\frac{-t}{\tau_i}\right) \qquad \text{for } 0 \le t \le nryears \quad . \tag{S1}$$

For IRF_{CO2} the conditions is applied that the sum of the coefficients a_i equals 1. Note that the fits only apply for the period from 0 to *nryears*, where *nryears* is the number of available output years.

The mean relative error, *mre*, in permil is calculated from annual values:

$$mre = \frac{1}{nryears} \sum_{i=1}^{nryears} \frac{|f_i - m_i|}{m_i} \cdot 1000\text{permil} \ , \tag{S2}$$

where f_i are the annual data from the fit and m_i from the model output.

Table S1: Coefficients to fit model responses in CO_2 (IRF_{CO2}) for the PD100 case. The mean relative error (mre) is given in permil.

model	*nryears*	*mre*	a_0	a_1	a_2	a_3	τ_1	τ_2	τ_3
NCAR CSM1.4	289	11	2.935E-07	3.665E-01	3.542E-01	2.793E-01	1.691E+03	2.836E+01	5.316E+00
HadGEM2-ES	101	40	4.340E-01	1.973E-01	1.889E-01	1.798E-01	2.307E+01	2.307E+01	3.922E+00
MPI-ESM	101	16	1.252E-07	5.864E-01	1.826E-01	2.310E-01	1.781E+02	9.039E+00	8.989E+00
Bern3D-LPJ (reference)	1000	5	6.345E-10	5.150E-01	2.631E-01	2.219E-01	1.955E+03	4.583E+01	3.872E+00
Bern3D-LPJ (ensemble)	585	3	2.796E-01	2.382E-01	2.382E-01	2.440E-01	2.762E+02	3.845E+01	4.928E+00
Bern2.5D-LPJ	1000	9	2.362E-01	9.866E-02	3.850E-01	2.801E-01	2.321E+02	5.850E+01	2.587E+00
CLIMBER2-LPJ	1000	20	2.318E-01	2.756E-01	4.900E-01	2.576E-03	2.726E+02	6.692E+00	6.692E+00
DCESS	1000	4	2.159E-01	2.912E-01	2.410E-01	2.518E-01	3.799E+02	3.631E+01	3.398E+00
GENIE (ensemble)	1000	5	2.145E-01	2.490E-01	1.924E-01	3.441E-01	2.701E+02	3.932E+01	4.305E+00
LOVECLIM	1000	58	8.539E-08	3.606E-01	4.503E-01	1.891E-01	1.596E+03	2.171E+01	2.281E+00
MESMO	1000	1	2.848E-01	2.938E-01	2.382E-01	1.831E-01	4.543E+02	2.500E+01	2.014E+00
UVic2.9	1000	4	3.186E-01	1.748E-01	1.921E-01	3.145E-01	3.046E+02	2.656E+01	3.800E+00
ACC2	985	4	1.779E-01	1.654E-01	3.796E-01	2.772E-01	3.862E+02	3.689E+01	3.723E+00
Bern-SAR	1000	3	1.994E-01	1.762E-01	3.452E-01	2.792E-01	3.331E+02	3.969E+01	4.110E+00
MAGICC6 (ensemble)	604	1	2.051E-01	2.533E-01	3.318E-01	2.098E-01	5.961E+02	2.197E+01	2.995E+00
TOTEM2	984	2	7.177E-06	2.032E-01	6.995E-01	9.738E-02	8.577E+04	1.118E+02	1.583E-02
multi-model mean	1000	6	2.173E-01	2.240E-01	2.824E-01	2.763E-01	3.944E+02	3.654E+01	4.304E+00

Table S2: Coefficients to fit model responses in CO_2 (IRF_{CO2}) for the PI100 case with and without climate feedbacks and for the Bern3D-LPJ(reference). The mean relative error (mre) is given in permil.

	nryears	*mre*	a_0	a_1	a_2	a_3	τ_1	τ_2	τ_3
With climate feedback	1000	4	1.266E-01	2.607E-01	2.909E-01	3.218E-01	3.028E+02	3.161E+01	4.240E+00
Without climate feedback	1000	3	1.332E-01	1.663E-01	3.453E-01	3.551E-01	3.133E+02	2.999E+01	4.601E+00

Figure S1: Responses in IRF_{CO2} from individual models (black) and corresponding fits (red).